Exploration of strategies to alter the meiotic recombination landscape in barley (*Hordeum vulgare*)

Dissertation

zur Erlangung des

Doktorgrades der Naturwissenschaften (Dr. rer. nat.)

der

Naturwissenschaftlichen Fakultät III

Agrar- und Ernährungswissenschaften,

Geowissenschaften und Informatik

Martin-Luther-Universität Halle-Wittenberg

vorgelegt von

Herrn Mohammad Abdelmordy Mohammad Ayoub

Gutachter:

Prof. Dr. Andreas Houben

Prof. Dr. Mónica Pradillo Orellana

Tag der öffentlichen Verteidigung: 23 October 2023, Halle (Salle).

Acknowledgments

First, I would like to thank my supervisor Stefan Heckmann for giving me the chance to perform this work in his lab. Your critical thinking, advice and patience were always inspiring. My gratitude is to Andreas Houben and Monica Pradillo for accepting to review this work.

I would like also to thank all lab technicians: Jana Lorenz, Franziska Hartmann, Franziska Backhaus and Marius Dölling. Most of this work would not have been done without your enormous help. Also, my thanks go to the lab members (Stefan Steckenborn, Yun-Jae Ahn, Maria Cuacos, Suriya Amutha and Chao Feng) for the amazing time we spent together either discussing science or at social events. I am thankful to my students Moammar Hossain and Hanaa Ibrahim for their input and their short stays. I enjoyed supervising you – it was a learning process for me too.

I thank colleagues and collaborators: Veit Schubert, Jörg Fuchs, Ingo Schubert, Jochen Kumlehn, Götz Hensel, Nils Stein, Jacqueline Pohl, James Higgins and Abdellah Barakate for great discussions and fruitful collaborations.

I express my gratitude to Britt Leps and Bianka Jacobi for their support and for making any paperwork for non-German speakers much easier than ever. I am sure you are doing help above your duties. Thank you!

I thank my professors and mentors from Cairo University (Naglaa Abdallah, Ebtissam Hussein, Reda Moghaieb, Abdelhadi Abdallah, Mohamed El Soda and Ahmed Abdelsamad) whom I have learned much and without their knowledge and support, I would have not reached this point.

I deeply thank my friends: Ali Elhakeem, Mohannad Dardidy, Mohammad Omar, Yahia Ata, Mohamed Yahia, Rasha Tarawneh, Diaa Daghma, Helmy Youssef, Ahmad Alqudah, Dalia Alamri and Omar Heleil for their continuous support. My heartful gratitude to Abdollah Arkan and Rebeka Arkan-Kovács for the amazing time we spent together that kept me cheerful. As I always say, I wish I knew you earlier.

I am extremely grateful to be surrounded with such an amazing family: my dad, Abdelmordy Ayoub, my mom, Nagwa Elattar, my sister, Nahla Ayoub and my brother Ahmed Ayoub, to whom I will always be indebted. Thank you for your unconditional love and support.

Words cannot express my love and gratitude to my wife Hanaa. I am deeply indebted to you for your enormous sacrifice and for giving me an endless support and trust that I can finish this thesis. To my little angel, Hana, you always put a smile on my face even in difficult times. Thanks for being my friend and daughter. Finally, and before all, all praise is due to Allah the merciful, all-wise and all-knowing.

Table of Contents

List of Abbreviations

AA	Amino Acid
AE	Axial Elements
bp	Base pairs
CR	Central Region
CRISPR	clustered regularly interspaced short palindromic repeats
CDS	Coding sequence
Col-0	Columbia-0
crRNA	CRISPR RNA
CO	Crossover
cv	Cultivar
DAPI	DAPI: 4',6-diamidino-2-phenylindole
DNA	Deoxyribonucleic acid
DK	Diakinesis
DP	Diplotene
D-loops	Displacements loops
DSB	DNA double-strand break
dHJ	Double Holiday Junctions
GBS	Genotyping-by-sequencing
GP	Golden Promise
gRNA	guide RNA
HR	Homologous recombination
hyperrec	Hyper-recombination
I_2-KI	Iodine potassium iodide solution
JMs	Joint Molecules
Ler	Landsberg *erecta*
LE	Lateral Elements
LP	Leptotene
MMS	Methyl methanesulfonate
MCN	Minimum chiasma numbers
MMC	Mitomycin C
NCO	Noncrossover
PQ	Pachytene
PMC	Pollen mother cell
PCR	Polymerase chain reaction
RNA	Ribonucleic acid
SNP	Single nucleotide polymorphism
SC	Synaptonemal Complex
SDSA	Synthesis-dependent strand assembly
TILLING	Targeting Induced Local Lesions IN Genomes
tracrRNA	Trans-activating RNA
WT	Wild-type
ZY	Zygotene

List of Figures

1 Introduction

1.1 Meiosis – the key event for sexual reproduction

Traditional breeding harnesses the natural genetic variation that arises during meiosis. Meiosis is a specialized cell division that leads to the formation of haploid cells giving rise to the gametes from diploid cells to maintain somatic diploidy after the fusion of male and female gametes and it also creates new combinations of parental alleles (Fig 1). Unlike mitosis, during meiosis a single DNA replication phase (S-phase) is followed by two successive rounds of chromosome segregation, meiosis I and meiosis II. In meiosis I, a reductional division causes a disjunction of homologous chromosomes (also called "homologs") to opposite poles without separation of sister chromatids, reducing chromosome number by half. Whereas in meiosis II, an equational division results in the segregation of sister chromatids to opposite poles. The first meiotic division is characterized by three events that do neither occur during meiosis II nor mitosis (Marston & Amon, 2004). (i) Homologous recombination (HR) and independent assortment of homologs assures genetic diversity. HR also ensures faithful homologous chromosome segregation during meiosis I by physically connecting homologs. (ii) Monopolar spindle fiber attachments enable sister chromatid segregation to the same pole during meiosis I while segregating homologs to opposite poles. (iii) Step-wise loss of cohesin i.e., cleavage of cohesin rings along chromosome arms during metaphase I protecting centromeric cohesion until metaphase II, to allow sister chromatids to segregate only during meiosis II (Fig 3).

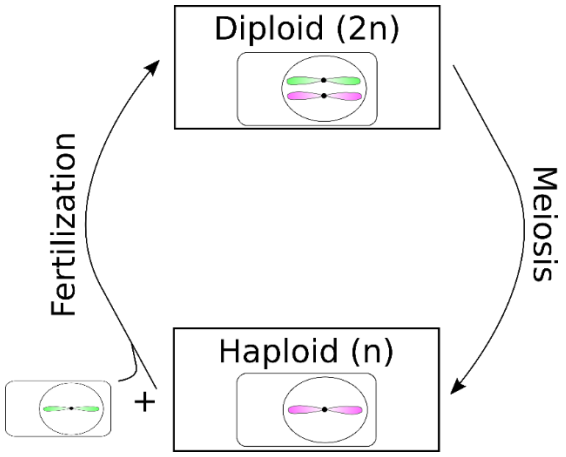

Figure 1 The significance of meiosis for sexual reproduction is two-fold.

Chromosome number reduction, to maintain somatic diploidy after fusion of male and female gametes, and genetic diversity, based on HR and random assortment of homologous chromosomes.

Meiosis I is characterized by a prolonged prophase I during which crucial and unique phenomena take place. It is divided into five substages: leptotene, zygotene, pachytene, diplotene and diakinesis (Fig 2). Most eukaryotic species follow a fixed order of events that must occur one after another with few exceptions. First, '*pairing*' between homologous chromosomes occurs by their physical co-alignment in leptotene (Fig 2) (Padmore et al., 1991). Co-alignment is typically dependent on programmed DNA double-strand breaks (DSBs) catalyzed by SPO11 during leptotene (Zickler & Kleckner, 2015). Meiotic DSBs enable reciprocal DNA exchange or 'crossover'. Second, '*synapsis*' is a tight bond between structural axes of homologous chromosomes (for details see below 1.3) initiated by the formation of the so-called Synaptonemal Complex (SC) (Fig 2). Third, '*crossing over*' (CO) assures reciprocal genetic exchange between homologous chromosomes, which also physically connects homologous chromosomes allowing their faithful segregation during meiosis I (Fig 2). This canonical prophase I program is found in most sexually reproducing eukaryotes.

1.2 Key steps during prophase I

To initiate SC and CO formation, chromosomes need to find their homologous partner. Hence, spatial co-alignment between homologous chromosomes occurs facilitated by different mechanisms. The highly conserved SPO11 protein catalyzes the formation of meiotic DSBs. *A. thaliana* encodes for two meiosis-specific homologs of *SPO11, AtSPO11-1* and *AtSPO11-2*, that are both required for meiotic DSB formation (Grelon et al., 2001; Hartung, Wurz-Wildersinn, et al., 2007; Stacey et al., 2006). In addition to SPO11-1/2, also MTOPVIB, PRD1/2/3 and DFO are required for SPO11-dependent meiotic DSB induction in plants (A. de Muyt et al., 2007, 2009; Robert et al., 2016; Vrielynck et al., 2016; Z. Xue et al., 2016; C. Zhang et al., 2012). In Arabidopsis, MTOPVIB forms a heterotetrameric complex consisting of a SPO11-1/SPO11-2 heterodimer and a MTOPVIB homodimer essential for meiotic DSB formation (Fig 4C). After catalyzing DSB formation, SPO11 remains covalently bound to the 5′ end of each broken DNA strand until liberated by MRE11 endonuclease cleavage. Then, the Mre11-Rad50-Nbs1/Xrs2 (MRN or MRX) complex resects some nucleotides of the 5′ end to generate 3′ single-stranded DNA molecules (3′ overhangs) (Neale et al., 2005). These 3′ overhangs are loaded with the RecA recombinases RAD51 and the meiosis-specific DMC1 generating single-stranded nucleofilaments that search for homologous sequences as repair template (Fig 4D) (Bishop et al., 1992; Sung & Robberson, 1995). This homology search results either in invading homologous chromatids (Fig 4E) or sister chromatids (Fig 4I-J). The former is likely the major cause of the juxtaposition of homologous chromosomes (pairing or

co-alignment). This preference of invading homologous chromatids is known as ‘inter-homolog bias’. If the single-stranded nucleofilament invades the sister chromatid, the repair outcome cannot be traced genetically due to identical sequences between sisters.

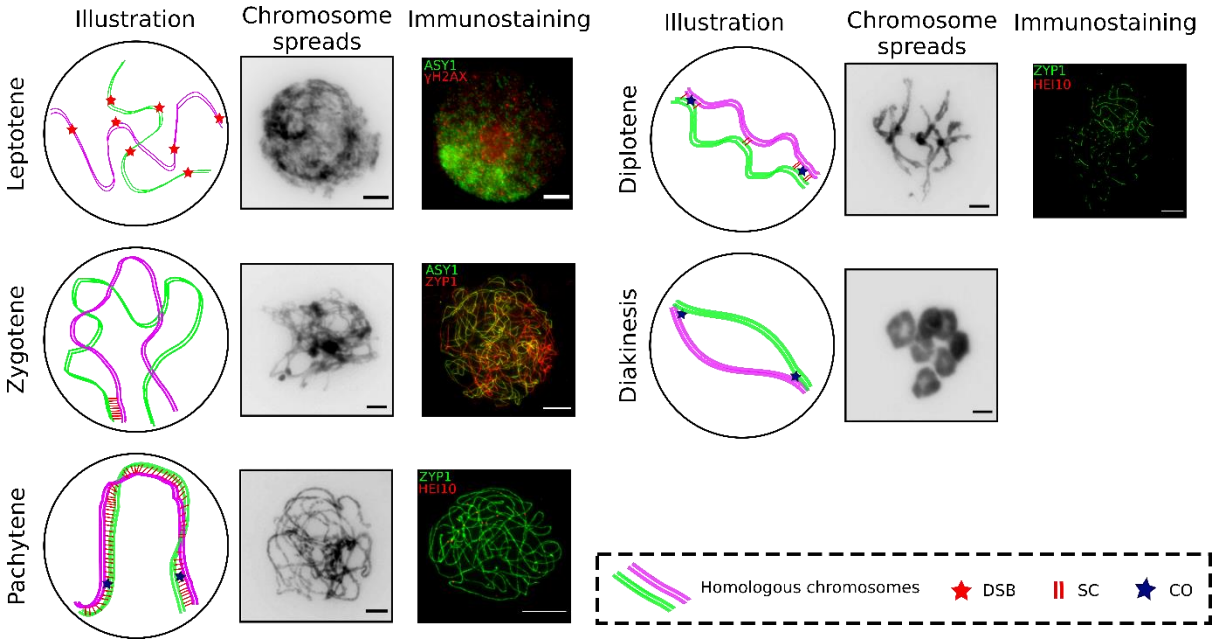

Figure 2 Stages of meiotic prophase I in barley.

An illustration (left) of only one pair of homologous chromosomes (for simplification) through all substages of prophase I (Leptotene, Zygotene, Pachytene, Diplotene and Diakinesis). DAPI-stained meiotic chromosomes (middle) and immunostaining of key meiotic proteins throughout prophase I (right). Scale bar represents 5 µm.

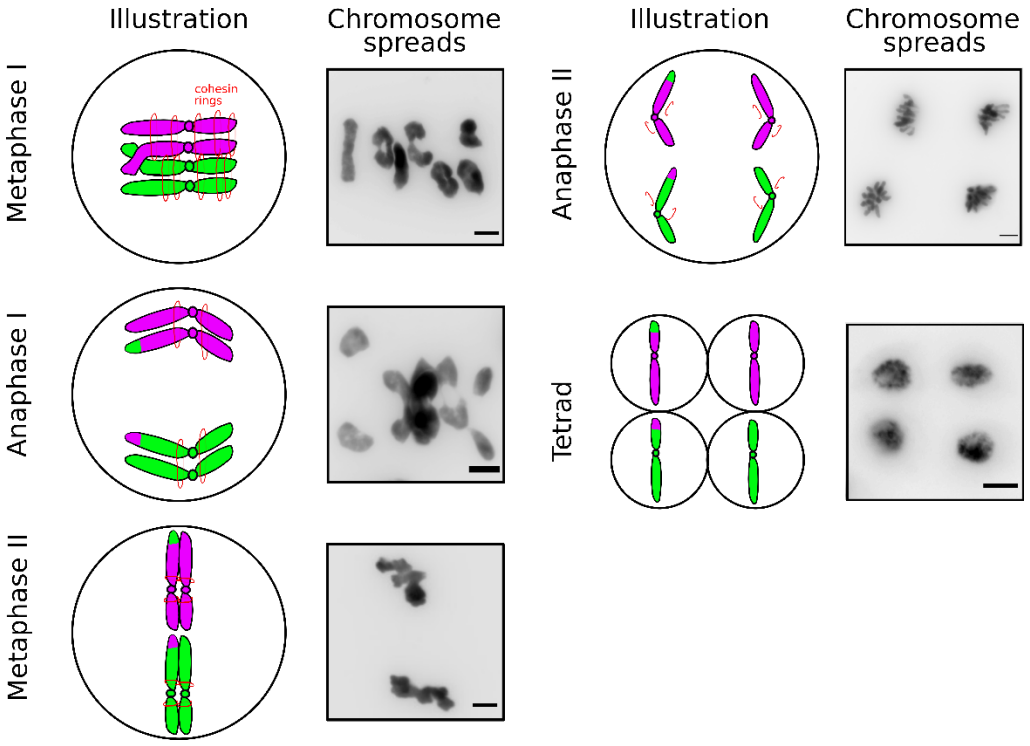

Figure 3 Metaphase I until tetrad stage of meiosis in barley.

Only a pair of homologous chromosomes is illustrated (for simplification) through the remaining stages of meiosis I (metaphase I and anaphase I) and meiosis II stages (metaphase II, anaphase II and tetrad) (left). Examples of DAPI-stained meiotic chromosomes in the respective stages next to an illustration (right). Scale bar represents 5 µm.

Crossovers (CO) or **non-crossovers (NCO)** are two potential outcomes of inter-homolog repair. A **CO** is defined as a reciprocal exchange of DNA segments between homologous pairs, while a **NCO** is either a meiotic DSB repaired on the sister chromatid or a non-reciprocal exchange of short DNA segments between homologous chromosomes. Cytologically, a CO manifests as **'chiasma'**, while a NCO cannot be visualized. It is unclear how and when the decision between CO or NCO is taken; however, there are some indications for a very early decision at leptotene/zygotene transition (A. D. Muyt et al., 2014; L. Zhang et al., 2014; Zickler & Kleckner, 2015). CO are divided into two subgroups: class I CO and class II CO. The pathway forming class I CO depends on a group of proteins collectively called ZMM proteins (Zip1, Zip2, Zip3, Zip4, Mer3, Msh4 and Msh5), identified first in budding yeast (Börner et al., 2004). In plants, proteins were classified as ZMM due to functional similarities to yeast ZMM such as SHOC1/Zip2 (Macaisne et al., 2011), HEI10/Zip3 (Chelysheva et al., 2012), PTD (Wijeratne et al., 2006), MER3 (Mercier et al., 2005) or MSH4/5 (Higgins et al., 2004, 2008) in Arabidopsis, ZIP4, MER3 and HEI10 in rice (Mao et al., 2021; Shen et al., 2012; K. Wang et al., 2009, 2012) or MSH4 and MSH5 in wheat (Desjardins et al., 2020).

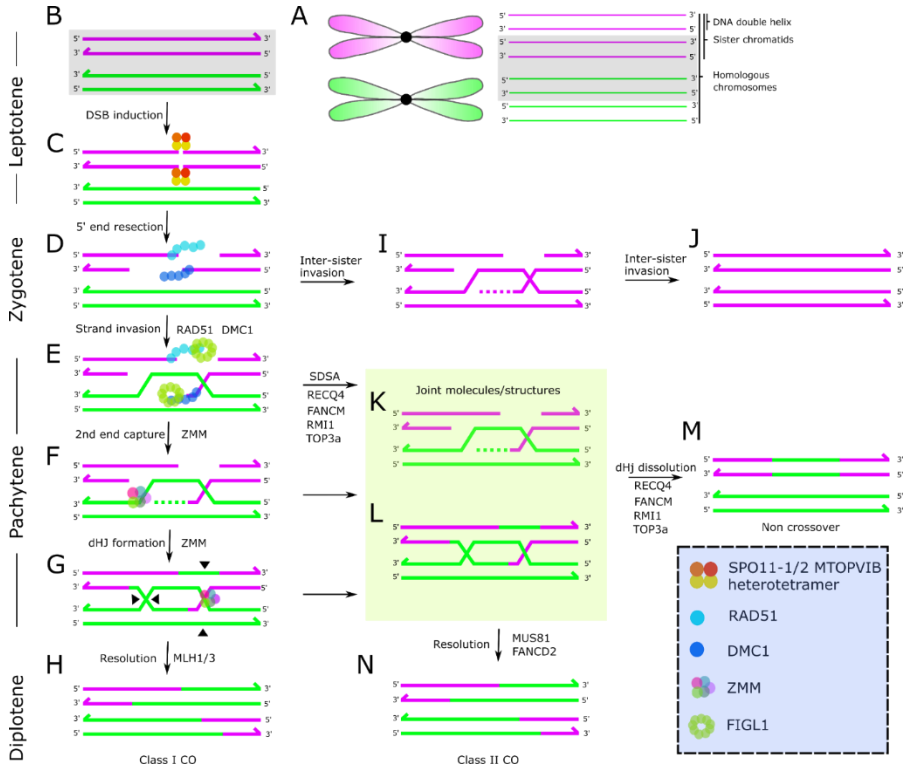

Figure 4 Illustration of the meiotic recombination process in *A. thaliana*.

(A) A pair of homologous chromosomes after S-phase: parental chromosomes are depicted in purple and green (left) as well as the corresponding DNA double helix, sister chromatids and homologous chromosomes (right). **(B-N)** For simplicity, only non-sister chromatids are shown. **(C)** The formation of meiotic DSBs is catalyzed by the heterotetrameric SPO11-1/-2//MTOPVIB complex during leptotene. **(D)** Resection at the 5' end of the DSB results in a 3' single-stranded DNA overhang that is bound by the recombinases RAD51 and DMC1 during zygotene. These nucleofilaments can either **(I-J)** invade the sister chromatid as a template for repair or **(E)** due to inter-homolog bias invade the homologous chromosome for homology search forming a D-loop. **(F)** Second end capture, DNA synthesis and ligation lead to the formation of a double Holliday junction (dHJ). **(G) A** dHJ can be resolved into the ZMM-dependent class I CO **(H)**. **(N)** The second category of CO, called class II CO, can form upon the function of MUS81 and FANCD2 resolving recombination intermediates in a ZMM-independent fashion. **(K-M)** Some joint molecules mature into class II CO resolved by MUS81 and/or FANCD2. Non-crossover (NCO) can arise by synthesis-dependent strand annealing (SDSA). **(L-M)** NCO can also form by dissolution of the dHJ or joint molecules.

Class I CO are interference-sensitive [see below 1.4.2]. ZMM proteins stabilize inter-homolog strand invasion intermediates and catalyze formation and resolution of double Holiday Junctions (dHJ) (Fig 4F-G). The number of CO are severely reduced (~15% residual CO compared to wild-type (WT)) in either single or double *zmm* mutants in Arabidopsis (Chelysheva et al., 2007, 2012; Higgins et al., 2004, 2008; Macaisne et al., 2011; Mercier et al., 2015). Thus, the majority of CO are ZMM-dependent class I CO (Fig 4H).

In barley, an exonic deletion in *MLH3*, also called *DES10*, resulted in the loss of ~50% of chiasmata and of 63% of MLH3 foci compared to WT. In Arabidopsis *mlh3* and *mlh1*, chiasmata numbers were reduced by 60% and by 70%, respectively (Dion et al., 2007; Jackson et al., 2006). In barley *mlh3*, the obligate CO was lost (Colas et al., 2016) and ZYP1 signals

were punctuated instead of linear as in WT, despite pairing between axes being similar to WT (Colas et al., 2016; Phillips et al., 2013). Moreover, EdU (incorporated into newly-replicating DNA) pulse-labeling indicated that zygotene was delayed and prolonged in *mlh3*, indicating likely defective synapsis (Colas et al., 2016) while Arabidopsis MutL complex components (MLH1-MLH3) and mouse MLH3 were not reported to affect synapsis (Dion et al., 2007; Jackson et al., 2006; Lipkin et al., 2002). Hence, studying meiosis in diverse organisms can expand our knowledge on the regulation of key meiotic events.

In *A. thaliana*, a minor type of CO is the class II CO, that is in part MUS81- and/or FANCD2-dependent (Fig 4N) and is interference-insensitive i.e., no interference occurs between class II CO (Berchowitz et al., 2007). In Arabidopsis, *mus81* led to a 10% reduction in total CO numbers (Berchowitz et al., 2007) while FANCD2 was required for ~14% of CO (Kurzbauer et al., 2018). Interestingly, limited residual CO were formed in *msh4 mus81 fancd2* (Kurzbauer et al., 2018). Thus, some CO are dependent on yet unknown candidates. Moreover, while class II CO are interference-sensitive, in tomato interference was not only detected between class I CO but also between class I and class II CO (Anderson et al., 2014). In a nutshell, class II CO represent approximately 10-20% of the total CO in Arabidopsis.

Information on the contribution of class I CO and class II CO on the recombination landscape in crops is limited. In rice, class I CO represent 70-92% of the total CO (K. Wang et al., 2012; L. Zhang et al., 2014). In barley, the only *zmm* mutant studied so far, *mlh3*/*des10*, had a reduction of 50% of WT chiasma numbers (Colas et al., 2016). However, the reported mutation was an exonic in-frame deletion, likely being hypomorphic and thus observed chiasmata numbers might be an overestimate due to possibly residual MLH3 function. In the tetraploid durum wheat, a reduction of 85% of chiasma numbers was observed in *msh4ab* and *msh5ab* compared to WT (Desjardins et al., 2020).

Together, two independent classes of CO are formed in plants. Interfering class I CO depending on ZMM proteins represent the majority of CO events, while non-interfering class II CO represent a minor fraction and are in part MUS81- and FANCD2-dependent. However, data on the contribution of class I and class II CO on the recombination landscape in crops is limited.

1.3 Synaptonemal complex – the mediator between chromosome partners

The SC is a tripartite zipper-like proteinaceous structure that is critical for physically linking homologs mediating and stabilizing meiotic inter-homolog recombination. The SC consists of three layers; one inner layer representing the central region (CR) flanked by two outer layers representing axial elements (AE), that link chromatin loops between non-sister chromatids of a homolog (Fig4) (Cahoon & Hawley, 2016). Across species, the central region consists mainly of transverse filaments of dimers of the large coiled-coil ZIPPER1 (Zip1 in yeast, ZEP1 in rice and maize and ZYP1 in Arabidopsis and barley). This central region is flanked by AE proteins. In Arabidopsis, among AE proteins identified are ASY1 (Armstrong et al., 2002), ASY3 (Ferdous et al., 2012) and ASY4 (Chambon et al., 2018) or cohesins, e.g., REC8 (Mercier et al., 2005). In early leptotene, SC assembly starts with the accumulation of AE proteins along chromosomes. These AE proteins work as docking sites where numerous other proteins important for cell cycle regulation and HR interact. For example, AE proteins interact with cohesin proteins that keep sister chromatids together. By zygotene, two AE co-align along with each homolog (Gray & Cohen, 2016). At that moment, AE are referred to as 'Lateral Elements' (LE). During pachytene, synapsis occurs as the SC is assembled via integration of transverse filaments (ZYP1) connecting two lateral elements (axes). By the end of pachytene, all chromosomes are synapsed and recombination intermediates are repaired. SC disassembly occurs in diplotene (Fig 5). SC components start falling off from chromosomes in an asymmetric manner. Subsequently, a chromosome is moving away from its homolog until being only linked via chiasma sites during diakinesis (Fig 5). An interesting feature was observed in barley (Higgins et al., 2012) and wheat (Osman et al., 2021) which is the spatiotemporal asymmetry of events of chromosome pairing, synapsis and chiasma distribution towards distal rather than proximal regions. One reason for this polarization is likely that distal regions are first to be replicated prior proximal regions, and therefore enter the meiotic program earlier. The ultrastructure of the SC is conserved among almost all eukaryotes. While SC components share little amino acid sequence homology, they share a similar secondary protein structure. Central region proteins share the coiled-coil domain (e.g., ZYP1) enabling protein-protein interactions with other SC proteins.

The SC has different roles in meiosis. First, it is required for CO formation/maturation in many species. In yeast, Zip1 is required for the resolution of recombination intermediates (i.e., dHJ) into CO. Similarly, *zyp1* knockdown barley lines show a reduction in CO numbers by ~72%

(Barakate et al., 2014). A few species including *A. thaliana* can undergo meiotic recombination even without the SC leading to altered meiotic recombination landscapes (more CO and weaker interference [see below 1.4.2]) in *zyp1a zyp1b* (Capilla-Pérez et al., 2021; France et al., 2021). Similarly, in rice chiasma frequency in a specific chromosomal region increased 3-4 fold in *zep1* compared to WT (M. Wang et al., 2010). Second, the SC may stabilize chromatin regions around CO sites. Certain changes in the structure of axes called axis exchange or local separation of sister chromatids surrounding a recombination nodule are accompanied by CO formation and thus the SC may play an important role in stabilizing those regions until CO are formed (Martinez-Perez et al., 2008; Storlazzi et al., 2008). Third, SC's axes play an important role in DSB induction. Chromatin loops are ultimately tethered to the SC's axes during pairing. SPO11 accessory proteins bind to chromatin loops at DSB hot spots, together with Spo11 they are translocated to axes where SPO11 is functionally inducing the cut (Panizza et al., 2011). In a nutshell, the SC is a characteristic meiotic feature that is conserved in almost all eukaryotes. The role of the SC is not only restricted to physically mediating the exchange of DNA molecules during meiotic HR but the SC is also important for DSB induction and stabilizing CO sites.

1.4 CO formation is tightly regulated

CO formation is tightly controlled due to (but not exclusively) three phenomena (1) the obligate CO, (2) CO interference and (3) CO homeostasis (Fig 6).

1.4.1 Obligate CO

A mechanism assuring that each bivalent receives at least one CO necessary to ensure faithful homologous chromosome disjunction during meiosis I (Fig 6B). This rule exists typically in most sexually reproducing organisms. Several pieces of evidence implied that the obligatory CO relies on class I CO formation. In *C. elegans*, each bivalent formed one single class I CO (Yokoo et al., 2012). In mice, each bivalent received also at least one class I CO (Cole et al., 2012). Taken together, likely class I assure the obligate CO formation.

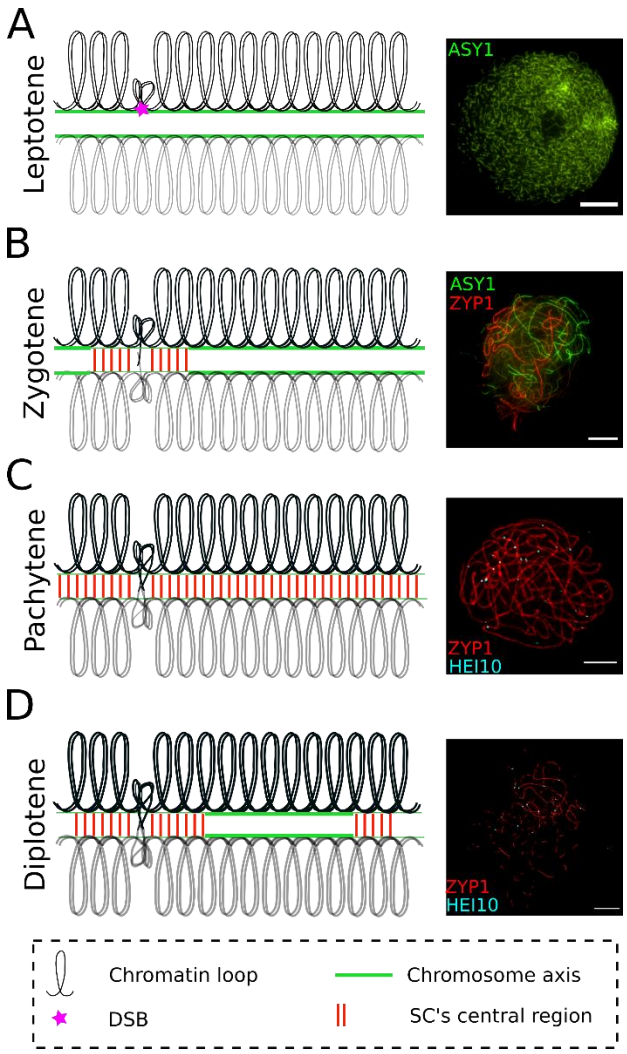

Figure 5 Simplified illustration of the SC structure during early prophase I and immunostaining images of ASY1, ZYP1 and HEI10 during SC assembly and disassembly in barley in prophase I substages.

(A) Leptotene, **(B)** zygotene, **(C)** pachytene and **(D)** diplotene. Scale bar represents 10 µm.

1.4.2 CO interference

CO interference implies an inhibitory effect generated by one CO disfavoring the formation of a nearby CO along a bivalent (Fig 6C). In yeast, sumoylated Red1 (yeast homolog of plant ASY3) and Topoisomerase II (TOPOII) are necessary for CO interference (L. Zhang et al., 2014). Interference distance was reduced by around 60% without a functional TOPO II. Subsequently, CO numbers were increased due to weaker interference (L. Zhang et al., 2014). The exact underlying mechanisms of CO interference across species are still unclear, however recent articles suggested that the SC and HEI10 are likely involved in CO interference regulation (Durand et al., 2022; Morgan et al., 2021). However, various models were proposed to explain CO interference (Foss et al., 1993; Fujitani et al., 2002; King & Mortimer, 1990; Kleckner et al., 2004; Morgan et al., 2021; L. Zhang et al., 2014).

1.4.3 CO homeostasis

Typically, there is no positive correlation between the number of DSBs and the number of CO as long as a minimum number of DSBs forms. If the number of DSBs is decreased but not abolished, CO numbers are not affected (Fig 6A). In *A. thaliana*, upon increased numbers of DSBs, no increase in CO numbers was found (Varas et al., 2015). However, in *Z. mays*, CO homeostasis seems not active given a direct relationship between the number of DSBs and CO (more DSBs resulted in more CO) (Sidhu et al., 2015). Interestingly, in *A. thaliana*, a hypomorphic allele of *spo11* led to less formed DSBs and proportional, albeit lesser, reductions in CO numbers (M. Xue et al., 2018). Hence, whether CO homeostasis is a universal feature of meiosis in plants needs further investigation. It might be possible that homeostasis is only effective in the case of increased DSBs (resulting in no increase in CO rates).

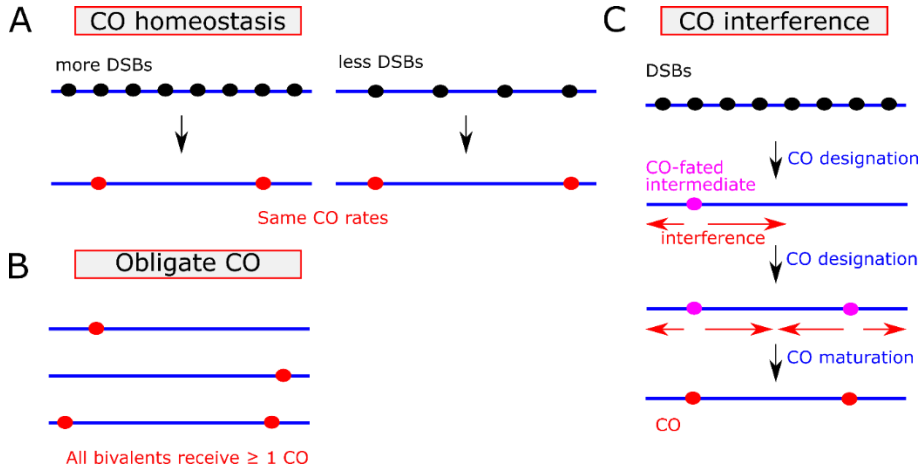

Figure 6 A simplified illustration of three major phenomena assuring a tight regulation of meiotic recombination in eukaryotes.

(A) CO homeostasis; similar CO rates (red dots) independent of DSB numbers (black dots) as long as a minimum number of DSBs is formed, **(B)** Obligate CO; all bivalents receive at least one CO and **(C)** CO interference; CO-fated intermediate is likely exerting a force of interference lowering the probability of another CO to be formed in close proximity.

1.5 DSBs hotspots – where DSBs like to form

Typically, SPO11-catalyzed meiotic DSBs are not randomly placed along the genome. Certain genomic regions tend to acquire more DSBs than others. These regions of commonly few kilobases are called DSB hotspots. DSBs do not occur exclusively within these regions, however, they are more frequently induced within those hotspots compared to other so-called coldspot regions (Pan et al., 2011; Tock & Henderson, 2018). DSB hotspots are found in genes and repetitive sequences in Arabidopsis (Choi & Henderson, 2015) and maize (Blary & Jenczewski, 2019; He et al., 2017). In yeast, mice, Arabidopsis and maize, DSB hotspots are

also located in nucleosome-depleted (e.g., gene promoters) and hypomethylated DNA regions (He et al., 2017; Lambing & Heckmann, 2018).

1.6 CO hotspots – where CO are densely located along chromosomes

CO also tend to form at non-random genomic regions called CO hotspots with centromeres being typically repressed for CO formation. In barley (Higgins et al., 2012; Phillips et al., 2013), wheat (Choulet et al., 2014; Osman et al., 2021), maize (X. Li et al., 2015) and tomato (Demirci et al., 2017), CO distribution is further skewed towards distal sub-telomeric regions. However, in Arabidopsis, CO are distributed in almost all genomic regions except at centromeres (Salomé et al., 2012). Chromatin structure affects CO landscapes. In Arabidopsis, heterochromatin regions enriched for H3K9me2 are negatively correlated with CO (Yelina et al., 2015). CO preferentially occur in regions enriched for typical euchromatin marks such as H2A.Z and H3K4me3 (Choi & Henderson, 2015) or are devoid in repetitive regions such as regions enriched for transposons. In large cereal genomes like maize and barley (Wicker et al., 2017), transposons represent over 80% of the genome, while in Arabidopsis only 20% of its genome comprises transposons. Transposons are highly enriched for DNA methylation. These links with chromatin could be a major factor for variations in CO landscapes across different plants (Lambing et al., 2017). In wheat, a positive correlation was found between CO regions at distal chromosomal sites and high levels of DMC1, ASY1 and the gene-associated histone mark H3K27me3 (Tock et al., 2021).

1.7 Factors affecting the CO landscape

Meiotic recombination is plastic in nature. In plants, many environmental factors have a direct impact on CO rates, like temperature (Bomblies et al., 2015; Higgins et al., 2012; Lloyd et al., 2018; Modliszewski et al., 2018; Phillips et al., 2015; Storme & Geelen, 2020), nutrient availability (Bennett & Rees, 1970; Fedak, 1973; Law, 1963), DNA-damaging agents (Lawrence, 1961; Sanchez-Moran et al., 2007), pathogen infection (Andronic, 2012; Kovalchuk et al., 2003) and plant's age (F. Li et al., 2017). Moreover, epigenetic modifications (Underwood et al., 2018; Yelina et al., 2015) and genetic factors can also impact meiotic recombination landscapes.

1.7.1 Identification of Anti-CO factors (anti-recombinases) – the brakes of CO formation

Although many DSBs are formed, few (2-10%) are repaired into CO e.g., in barley 250-450 DSBs are formed while only ~15-22 are repaired as CO. The repair of DSBs into CO is restrained by so-called anti-CO factors in Arabidopsis (Crismani et al., 2012). Identification of anti-CO factors was carried out by screening for suppressors of class I CO-defective plants' phenotype with restored fertility and restored CO upon EMS mutagenesis. Three major complementation groups were identified, which are (i) FANCM (Crismani et al., 2012) and its associated cofactors MHF1 and MHF2 (Girard et al., 2014), (ii) the BTR complex of RECQ4A/B, TOP3α and RMI1 (Séguéla-Arnaud et al., 2015) and (iii) FIGL1 (Girard et al., 2015) and its associated cofactor FLIP (Fernandes, Duhamel, et al., 2018).

1.7.1.1 FANCM

The first identified anti-CO factor group was the Arabidopsis homolog of the helicase human Fanconi anaemia complementation group M (FANCM) and its two DNA-binding cofactors MHF1 and MHF2 (Crismani et al., 2012; Girard et al., 2014). Fertility was restored in *zmm fancm* compared to *zmm.* Helicases have a vital role in meiosis by binding to and unwinding D-loops promoting NCO formation via SDSA. Meiotic fidelity was restored by increased CO numbers (hyper-recombination phenotype or *hyperrec*) compared to *zmm* (Crismani et al., 2012). Interestingly, additional CO in the double mutant *zmm fancm* are MUS81-dependent interference-insensitive class II CO. This suggests that FANCM interferes with the class II CO pathway converting recombination intermediates into NCO. In Arabidopsis, CO numbers were increased by 2- to 3-fold in *fancm zip4* compared to *zip4* (Crismani et al., 2012). In inbreds, *fancm* causes a 3-fold increase in CO rates, while it has almost no effect on CO rates in hybrids (Col/Ler) (Fernandes, Séguéla-Arnaud, et al., 2018). In Arabidopsis, FANCM limits class II CO promoting NCO formation. However, when combined with *recq4* or *figl1* recombination rates were subtly increased but still lesser than in *recq4 figl1*. However, *fancm* has no impact on changing the meiotic recombination landscape in Col/Ler hybrid background, it causes an increase in CO rates in hybrids of different crops like Brassica, rice and pea, but not in wheat. In crop species, *fancm* causes a 2- to 3-fold increase in CO numbers in Brassica (Blary & Jenczewski, 2019), rice and pea hybrids (Mieulet et al., 2018). However, in wheat hybrids, knocking down FANCM did not cause any change in recombination rates of chromosome 1A (Raz et al., 2021). Nonetheless, in a recent study (Desjardins et al., 2022) in tetraploid and hexaploid wheat, null mutant alleles showed a reduction in chiasma numbers and the loss of

the obligate CO together resulting in reduced fertility, consistent with studies in lettuce (X. Li et al., 2021). Interestingly, FANCM was shown to suppress the class II CO pathway (similar to Arabidopsis) in addition to being required for the class I CO pathway revealing a complex role for FANCM in wheat (Desjardins et al., 2022). Hence, FANCM has an evolutionary divergent role between studied species in regulating CO numbers.

1.7.1.2 RECQ4

The second complementation group consists of RECQ4 helicase, TOP3α and RMI1, collectively named RTR complex. Similar to *fancm*, mutations in individual RTR components complement a *zmm* phenotype by increasing bivalent numbers and thus restoring fertility (Séguéla-Arnaud et al., 2015).

Arabidopsis encodes two copies of *RECQ4* (*RECQ4A* and *RECQ4B*). RECQ4A is one of seven identified RECQ Arabidopsis proteins related to the human BLM complex. RECQ helicases are evolutionarily conserved (Hartung & Puchta, 2006). In the Landsberg *erecta* (Ler) ecotype of *A. thaliana,* two mutations in *AtRECQ4A* were detected in two *msh4* suppressors. *RECQ4B* in Ler carries a natural loss-of-function mutation and thus in Ler only one functional copy (RECQ4A) is found (Séguéla-Arnaud et al., 2015). Restoring CO/bivalent formation and fertility was found only after combining mutations in *msh4* and *recq4a/b* in Col-0. Six-fold increase in CO numbers was found in the double mutant line *recq4a recq4b*. So far, this is the strongest increase in CO numbers upon depleting a single anti-CO factor described. *top3α, top3α recq4a* and *recq4a recq4b* mutants restored fertility and bivalent formation in a *zmm* (Séguéla-Arnaud et al., 2015). Importantly, this increase in meiotic CO upon knocking out single or double anti-CO factor genes is not causing any dramatic meiotic aberrations. *recq4a/b* plants grow normally and are fully fertile. Thus, a *hyperrec* phenotype does not interfere with meiotic fidelity. However, *top3α recq4a recq4b* plants exhibited a meiotic catastrophe and thus resulted in sterility. Chromosome spreads showed irregular bivalents, chromosome missegregation and chromatin bridges during anaphase I. Surprisingly, an earlier study showed that *recq4a* causes non-homologous telomeric chromatin bridges in meiosis I and therefore reduction in fertility. In *recq4a msh4*, no obvious change/increase in CO rates were found compared to *msh4* (Higgins et al., 2011). Only when both RECQ4 copies are mutated in a *zmm* background (i.e., *recq4a/b msh4*), CO rates increased significantly compared to *msh4* (Séguéla-Arnaud et al., 2015). In summary, *recq4a recq4b* rescued a *zmm* phenotype by increasing CO numbers without affecting meiotic fidelity or plant fertility.

RECQ4 function has been studied also in barley, tomato, pea, rice and wheat (Arrieta et al., 2021; Gardiner et al., 2019; Maagd et al., 2020; Mieulet et al., 2018). CRISPR/Cas has been applied to F_1 interspecific hybrids from a cross between S*olanum lycopersicum* and *S. pimpinellifolium* to generate *recq4* mutants. Cytological analysis has shown a slight increase in CO numbers by a factor of 1.5 and genome-wide recombination maps showed around an 1.8-fold increase in meiotic recombination compared to WT F_1 hybrids (Maagd et al., 2020). A higher increase in CO numbers i.e., 2.7-fold, was observed in F_1 intraspecific tomato hybrids (Mieulet et al., 2018). Notably, CO rates were only measured in chromosomes 4 and 7. In pea hybrids, *recq4* plants showed the highest increase in CO numbers (4.7-fold) compared to WT (Mieulet et al., 2018), while their fertility dropped significantly. However, rice *recq4* hybrids showed a 3.2-fold increase in CO numbers in selfed F_2 hybrids compared to WT siblings. Surprisingly, knockouts of three wheat homeologous candidates homologs to *AtRECQ4A/B* lead to -statistically not significant- reduction in CO numbers (Gardiner et al., 2019). In rice and tomato hybrids fertility was unaffected in *recq4* (Mieulet et al., 2018). However, in pea *recq4* hybrids, fertility was reduced 4-fold compared to WT (Mieulet et al., 2018). In a recent study in barley (Arrieta et al., 2021), a single amino acid substitution mutation restored fertility in the background of *des10* (*Hvmlh3*). This mutation caused recombination rates to increase 2-fold compared to WT or 4-fold in *mlh3 recq4* compared to *mlh3*. So far, no report showed the null effect of *recq4* in barley. Whether a null allele of *recq4* has a similar or a different phenotype (in terms of recombination rates and distribution) needs further investigation.

The other RTR complex members have been functionally studied as well. *top3a* showed an elevated number of CO by 1.5-fold compared to WT. However, *top3α* also causes early plant lethality or stunted growth, mitotic and meiotic chromosome fragmentation and plant fertility problems (Hartung et al., 2008; Séguéla-Arnaud et al., 2015). RMI1 prevents extra CO in Arabidopsis (Séguéla-Arnaud et al., 2015). Importantly, a complete knockout of *top3α* causes plant lethality and of *rmi1* causes a meiotic catastrophe rendering them not suitable candidates for application to crops (Séguéla-Arnaud et al., 2015). However, hypomorphic alleles of both *top3a* and *rmi* caused an increase in meiotic CO rates while undergoing faithful meiotic segregations leading to normal plant fertility (Séguéla-Arnaud et al., 2015). To sum up, RECQ4 has a vital role in somatic and meiotic recombination repair. Loss-of-function mutations in *RECQ4* cause different influences on CO rates in different crop species.

1.7.1.3 FIGL1

The third *zmm* complementation group identified includes FIGL1 and its cofactor FLIP. FIGL1 is a conserved member of the AAA-ATPase FIDGETIN family (Mercier et al., 2015). Several mutations were identified in *AtFIGL1* and the vast majority of the mutants rescued a *zmm* phenotype (Girard et al., 2015). Intriguingly, FIGL1 likely acts independently of FANCM or RECQ4, given an additive effect in surplus CO observed in the double *figl1 fancm* mutant compared to either single mutant (Girard et al., 2015). The highest CO increase was found in *recq4 figl1* double mutants (~9-fold compared to WT) (Fernandes, Séguéla-Arnaud, et al., 2018). FIGL1 limits the temporal localization of the recombinases DMC1 and RAD51 and acts upstream of strand invasion during HR (Girard et al., 2015). In contrast to Arabidopsis, FIGL1 is essential for meiosis and plant fertility in rice (P. Zhang et al., 2017), pea and tomato (Mieulet et al., 2018). In other crops such as barley it is unclear whether FIGL1 is essential for meiosis and fertility or whether *figl1* can be harnessed to improve breeding.

FIGL1 cofactor FLIP also negatively regulates class II CO formation in Arabidopsis. FIGL1 and FLIP directly interact with each other (Fernandes, Duhamel, et al., 2018). Fertility was restored upon mutating *FLIP* in *zmm*. The double mutant *figl1 flip* showed no further CO increase compared to either single mutant (Fernandes, Duhamel, et al., 2018), suggesting that both are acting in the same pathway. Additional CO arise via the class II CO pathway in *flip*. These data support a functional role of a FIGL1-FLIP complex in limiting class II CO by interfering with strand invasion during meiotic HR. FIGL1 also has an important role in somatic DNA repair. *figl1* plants are hypersensitive to Mitomycin C (MMC), which is a DNA damaging agent that induces mostly DNA inter-strand crosslinks (Kumar et al., 2019).

Interestingly, comparing different combinations of double or triple mutants of *recq4*, *figl1* and *fancm*, showed that all three anti-CO factors mutants increased CO rates to a different extent in inbreds or Col/Ler hybrids, except *fancm* that does not lead to a change in CO numbers in Col/Ler hybrids (Fernandes, Séguéla-Arnaud, et al., 2018). There is an increase in CO rates in any double mutant compared to the relevant single mutants in inbred and hybrid backgrounds, except for *recq4 fancm* in the hybrid background (Fernandes, Séguéla-Arnaud, et al., 2018). This implies that all three groups of anti-CO factors are likely acting independently of each other, while possibly RECQ4 and FANCM work in the same pathway. Pollen viability was decreased to almost 50% in *recq4 figl1* and *recq4 figl1 fancm* in Col-0 and slightly decreased in almost all tested mutants in Col/Ler hybrids. Furthermore, there was no reduction in seed setting in all tested mutants in a hybrid background, while only in *recq4* full seed set was found in a Col-0 background (Fernandes, Séguéla-Arnaud, et al., 2018). *figl1* causes opposite effects

on fertility between Arabidopsis and the studied crops so far (rice, pea and tomato). It is unknown whether this is a common phenotype for cereal species. Therefore, studying the effect of *figl1* across cereals is required to possibly unlock its potential in particular when combined with *recq4*, leading to a massive increase in CO numbers in Arabidopsis.

1.7.2 Pro-CO factor: HEI10 – the accelerator of CO formation

All these above-mentioned anti-CO factors are acting in the MUS81-dependent CO pathway preventing class II CO formation. However, some proteins also limit, e.g. MSH2 (Emmanuel et al., 2006) or HCR1 (Nageswaran et al., 2021a), or promote, HEI10 (Ziolkowski et al., 2017), interference-sensitive class I CO formation.

HEI10 is a member of the Zip3/Hei10 family that includes two major categories: (1) the HEI10 family and (2) the Zip3/RNF212 family (Chelysheva et al., 2012). Organisms differ in either the presence or absence of proteins from each of those two categories. Plants and Sordaria encode only a HEI10 family member (Chelysheva et al., 2012; A. D. Muyt et al., 2014; K. Wang et al., 2012), budding yeast and worms encode only a Zip3 family member (Agarwal & Roeder, 2000; Bhalla et al., 2008; Jantsch et al., 2004) and mammals encode one member of each category (Qiao et al., 2014; Reynolds et al., 2013; Strong & Schimenti, 2010; Toby et al., 2003; Ward et al., 2007). HEI10 is an E3 ligase essential for class I CO maturation/formation, containing a RING protein domain (Chelysheva et al., 2012; Reynolds et al., 2013). RING is a zinc-binding domain that recruits the ubiquitin-charged E2 stimulating ubiquitin transfer to a substrate protein (Morreale & Walden, 2016). Arabidopsis and rice HEI10 are likely functional homologs of yeast Zip3 and *C. elegans* ZHP-3 (Chelysheva et al., 2012; K. Wang et al., 2012). Zip3 and ZHP-3 are classified as SUMO E3 ligases, while human HEI10 acts in the ubiquitination pathway (Rao et al., 2017; Toby et al., 2003; Vujin & Zetka, 2017).

Despite HEI10 interacting with a poly-complex of ZMM proteins (ZYP4, SHOC1, MSH5 and PTD) in rice (J. Zhang et al., 2019), direct substrates of the E3 ligase HEI10 in plants are unknown. Whether any of these interactors is a substrate of HEI10 is unclear. CO-fated DSBs (CO designation) are defined in early prophase (zygotene) and the dynamics of HEI10 are likely linked to CO designation (Lambing et al., 2015; A. D. Muyt et al., 2014). HEI10 appears as foci throughout prophase I and exists in numerous numbers in early prophase I (until zygotene). As prophase I progresses, HEI10 foci gradually decrease in number (from pachytene until diakinesis), until most of the final HEI10 foci colocalize with the late class I CO marker MLH1 in Arabidopsis. In Sordaria, Arabidopsis and rice, a limited number of HEI10 foci in late prophase I becomes brighter and bigger in diameter, relative to early HEI10 foci, reflecting

the CO designation process of class I CO-fated recombination intermediates (Chelysheva et al., 2012; A. D. Muyt et al., 2014; K. Wang et al., 2012; L. Zhang et al., 2014). In *A. thaliana*, levels of HEI10 likely regulate CO interference. Increased (overexpression) or decreased doses (heterozygous *hei10*) of HEI10 correlated with weaker or stronger CO interference, respectively (Morgan et al., 2021). HEI10 involvement in CO interference/positioning has been assumed following a coarsening model where many close small HEI10 foci grow and diffuse with nearby HEI10 foci creating less -in number- bigger foci which are evenly spaced. This diffusion-mediated coarsening continues until formation of a few (~1-3 foci per bivalent) large HEI10 foci by the end of pachytene (Morgan et al., 2021).

The absence of HEI10 caused a drastic reduction in CO rates in Arabidopsis (85-90%) and rice (70%); representing the loss of class I CO. Due to the severe reduction in chiasma numbers, fertility was severely affected, too. In rice, no seeds formed in *hei10*, even when *hei10* plants were pollinated with WT pollen, suggesting that both male and female meiosis were defective (K. Wang et al., 2012). No pairing or synapsis defects were observed in *hei10* mutants in Arabidopsis and rice (Chelysheva et al., 2012; K. Wang et al., 2012).

Notably, additional CO in *HEI10* OE lines occurred mainly in euchromatic subtelomeric regions, but also to a limited extent in pericentromeric regions (Kim et al., 2022; Ziolkowski et al., 2017). CO rates in Col/Ler hybrids increased up to 3.7-fold when *HEI10* was overexpressed in *recq4a/b* compared to WT Col/Ler hybrids (Serra et al., 2018). This effect was additive being greater than only overexpressing HEI10 (2.7-fold increase) or mutating *recq4a*/*b* (3.3-fold increase). No obvious difference in fertility was found in *recq4a*/*b* or *HEI10* OE lines compared to WT, while a significant decrease was found in pollen viability and in the number of formed seeds in *HEI10 recq4a/b* (Serra et al., 2018). In a nutshell, dosage of HEI10 regulates the number of class I CO in Arabidopsis. Whether *HEI10* overexpression can be harnessed to alter recombination landscapes also in cereals is unclear.

2 Aims of this thesis

Plant breeding towards superior varieties relies on selection of novel allelic combinations after creating genetically diverse materials. Meiosis assures novel allelic combinations through meiotic recombination. However, in cereal crops such as barley (*Hordeum vulgare*) meiotic recombination events are limited in their number and in their distribution being skewed towards chromosome ends.

This thesis aims to translate knowledge from *Arabidopsis thaliana* into the crop *Hordeum vulgare*, to possibly modify the meiotic recombination landscape (number and distribution of meiotic recombination events) in a cereal crop. In *A. thaliana*, mutations in *RECQ4* or *FIGL1* (so-called anti-CO factors) result in increased meiotic recombination rates. In mid-2017, at the beginning of my PhD work, no data on the function of anti-CO factors in large-genome crops were available and it was unclear whether they could be harnessed to alter meiotic recombination landscapes in crops. Moreover, in barley no information on the function of the pro-CO factor HEI10, as a major ZMM protein critical for CO formation and regulating dosage-dependent CO numbers in *A. thaliana*, was available.

Hence, the overarching aim of this thesis is:

The functional dissection of the pro-CO factor HEI10 and the anti-CO factors RECQ4 and FIGL1 during meiosis in barley and their role for the barley recombination landscape, in particular the isolation of corresponding mutants and their cytological characterization.

3 Materials & Methods

3.1 Plant material

3.1.1 Barley plant material and growing conditions

H. vulgare cv GP and Barke as well as all mutant plants (except *HvmtopVIB* (Steckenborn et al., 2023)) were grown in a greenhouse under long day conditions (16 h light/8 h dark) at 19°C/16°C day/night temperatures under supplementary light (~180 µmol/m^2s) and 60-70% humidity. Segregating *HvmtopVIB-1* plants were grown in a greenhouse under long day conditions (16 h light/8 h dark) at 18°C/15°C day/night temperatures under supplementary light (~136 µmol/m^2s) and 60-70% humidity. Grains were germinated on a wet filter paper in a petri dish at RT on a window bench for around 4-5 days and then transferred to soil (two parts self-made compost, two parts 108 substrate two (Klassmann-Deilmann), one-part sand) in small pots (6 cm in diameter). Re-potting into big pots (diameter of 16 cm) occurred one week later. At the three-leaf stage, Plantacote depot 4 m granulate (ICL) was added once to the soil and fertilizer (1% Hakaphos blau, COMPO EXPERT) was applied once per week. At the flowering stage, fertilizer (1% Hakaphos rot, COMPO EXPERT) was applied once per week.

3.1.2 Barley crossing

Barley crossing was performed according to (Y.-J. Ahn et al., 2020). Eight-week-old barley cv. Barke WT or mutant plants were emasculated by creating a small cut at one side of each spikelet and removing the three green immature anthers without touching the female organ. Two days later, fully mature yellow-colored anthers were collected from nine-week-old Barke or 10-11-week-old GP or mutant plants in a petri dish in the morning. Two to three anthers were inserted using forceps inside each female spikelet of the emasculated plant. The crossed spike was put back into the leaf layer and covered with a glassine bag with a label. Two weeks later, the glassine bag was removed and the success of the cross was evaluated based on presence of an embryo. Mature grains were harvested 30-40 days later.

3.1.3 Fertility measurements – grain counts and pollen viability

Barley grain numbers were counted manually from the first five mature tillers/spikes per plant. Pollen viability was assessed using Alexander's stain (Alexander, 1969) or 1% Iodine potassium iodide solution (I_2-KI) (Fu et al., 2016). Anthers before pollen shedding were put in a drop of Alexander stain or I_2-KI on a microscopic slide. A cover slip was added and pressed

gently. More staining solution was added to keep the sample surrounded by the stain. The slide was incubated at 50°C on a hot plate for 5-15 min and stored at 4°C overnight. On the next day 1,000 pollen were analysed under a binocular microscope. In case of Alexander's staining, pollen was counted viable when being roundish and red-coloured, while differently sized, shrunken and colourless or light pink pollen was considered not viable. In case of I_2-KI staining, pollen was counted viable when being roundish and purple-coloured, while differently sized, shrunken, and pale yellow-coloured pollen was considered not viable.

3.1.4 Root growth sensitivity assay to DNA damaging agents

Five or six surface-sterilized barley grains (see 3.1.6.1) were transferred to a petri dish (diameter of 145 mm) containing two sterilized filter papers (diameter of 125 mm) soaked with 7 mL of ddH_2O and stored at 4°C for 3 days in darkness. Three independent plates were used per genotype per treatment. Plates were then transferred to a plant growth chamber (PolyKlima) (16 h light/8 h dark at 19°C day/16°C night under supplementary light of ~180 µmol/m^2s and 60% humidity) for two days. Zeocin (100 µg/mL), MMC (3 µg/mL) or water was added to the plates under a laminar hood and plates were put back to the plant growth chamber. After 2 days, plates were washed with water and brought back to the plant growth chamber for one day. All plantlets were put on a black paper and photographed with a scale. The longest three roots per plant were measured by length using ImageJ. At least three independent experiments were performed. P values were determined using unpaired Student's t-test.

3.1.5 Barley grain surface sterilization

Barley grains were surface sterilized by shaking them in 70% Ethanol followed by shaking in 4% sodium hypochlorite solution (NaClO) and washed twice with ddH_2O each for 5 min.

3.2 Molecular methods

3.2.1 Identification of *HvHEI10, HvRECQ4* and *HvFIGL1*

Sequences of AtHEI10 (AT1G53490), AtRECQ4A (AT1G10930), or AtFIGL1 (AT3G27120) were used as query against the barley Morex protein database (https://webblast.ipk-gatersleben.de/barley_ibsc/). The identified barley HEI10 homolog (6HG0481560.1) was PSI-blasted to find further plant orthologous HEI10 sequences.

3.2.2 TILLING

A barley cv. Barke population (~11,000 M3 plants) of Targeting Induced Local Lesions IN Genomes (TILLING) (Gottwald et al., 2009) was screened for mutations within *RECQ4* and *FIGL1*. Two regions in each candidate were selected in order to identify SNPs either close to the beginning of the ORF or within the functional domain. Primers to amplify area one and two within *HvRECQ4* were MA-58 + MA-57 and MA-94 + MA-95, respectively. Primers for area one and two within *HvFIGL1* were MA-142 + MA-143 and MA-102 + MA-103, respectively. All amplicons were in the range of 1 - 1.5 kb. After PCR and clean-up (see 3.2.8.1 and 3.2.8.2), the dsDNA cleavage kit (Advanced Analytical) was used to cleave DNA fragments carrying a mismatch (SNP). A working solution of dsDNA cleavage enzyme was prepared by diluting the stock dsDNA cleavage enzyme 1:125 in T-digest buffer. Two µL of working solution were added to 2 µL of cleaned-up PCR product. The mixture was incubated at four different conditions, at 45°C for 15, 30 and 45 min, or at 60°C for 15 min, in the AdvanCE FS96 system and analysed using PROSize software (Advanced Analytical) to identify the best condition for each amplicon digest. Conditions used for *FIGL1* area one and two were 45°C for 30 min, while for *RECQ4* area one and two 45°C for 45 min and 45°C for 30 min, respectively. After identifying plants carrying a potential SNP using PROSize, the target area was re-amplified and Sanger-sequenced (using the respective primer pair) to confirm SNP presence/nature and to identify its exact position. All primers are listed in Supplementary table 2.

3.2.3 Genomic DNA extraction by Phenol-chloroform method

Around 100 mg of barley leaf material was frozen in liquid nitrogen and ground to a fine powder using a homogenizer (Retsch MM400) at 28 Hz for 45 sec. 800 µL of gDNA extraction buffer (1% N-Lauryl-Sarcosine, 100 mM Tris pH 8, 10 mM EDTA pH 8, and 100 mM NaCl) was added followed by phenol-chloroform-isoamyl alcohol (25:24:1). After centrifugation at 12,000 rpm for 2 min, the supernatant was transferred to a new tube containing 70 µL of 3 M sodium acetate and 700 µL of 100% isopropanol. After mixing and centrifugation at 13,000 rpm for 10 min, the supernatant was removed and the pellet was washed in 70% ethanol. After another centrifugation step at 13,000 rpm for 5 min, the pellet was resuspended in ddH_2O. Samples were stored at -20°C or used directly for down-stream applications.

3.2.4 RNA extraction & cDNA synthesis

In barley ~100 mg of young leaf material or 45-55 anthers within a length range of 0.7-1 mm from 1.5-2.5 cm long spikes (containing meiocytes) were frozen in liquid nitrogen. Total RNA

was extracted using GeneJET Plant RNA Purification Mini Kit (Thermo Fisher Scientific). Liquid nitrogen-frozen material was grinded using a homogenizer at 28 Hz for 45 sec. Plant RNA lysis buffer supplemented with ~400 mM Dithiothreitol (DTT; Thermo Fisher Scientific) was added to the powder and incubated at 56°C for 3 min. After centrifugation, the supernatant was transferred to an Eppendorf tube containing 96% ethanol. After mixing, the mixture was transferred to a purification column inserted in a collection tube. After centrifugation and discarding the flow-through, wash buffer I was added. After centrifugation and discarding the flow-through, wash buffer II was added. After centrifugation and discarding the flow-through, RNA was eluted with ddH_2O. Purified RNA was treated with DNase I (RNase-free, NEB) to eliminate contaminating DNA. Two µg of total leaf or 0.5 µg of total anther RNA was mixed with 1X DNase buffer (10 mM Tris-HCl, 2.5 mM MgCl2, and 0.5 mM CaCl2, pH 7.6) and 2 U of DNase I (RNase-free) in a total volume of 20 µL adjusted with ddH_2O. The mix was incubated at 37°C for 10 min and 5 mM of EDTA was added followed by heat inactivation at 75°C for 10 min. DNase-treated RNA was used as a template to synthesize cDNA using the RevertAid H Minus First Strand cDNA Synthesis Kit (Thermo Fisher Scientific). To synthesize the first strand cDNA, 0.5-2 µg of total RNA was added to a mix of 5 µM oligo $(dT)_{18}$ primer, 1X reaction buffer (50 mM Tris-HCl pH 8.3, 50 mM KCl, 4 mM MgCl2, and 10 mM DTT), 20 U riboLock RNase inhibitor, 1 mM dNTPs mix, 200 U RevertAid H Minus M-MuLV reverse transcriptase in a final volume of 20 µL adjusted with ddH_2O. RNA and oligo$(dT)_{18}$ primer mix was incubated at 65°C for 5 min and cooled on ice, in case of presence of a GC-rich RNA template. The total mix was incubated at 45°C for 60 min and at 70°C for 5 min. The synthesized cDNA was stored at -20°C for short-term storage or -80°C for long-term storage.

3.2.5 Enzymatic restriction digest of DNA

Around 100 ng of PCR product or ~400 ng of plasmid DNA were digested by 6 U of a restriction enzyme (NEB) in the respective 1X buffer in a total volume of 15 µL adjusted with ddH_2O. Reactions were incubated at 37°C, except for *Sfi*I at 50°C, for 2-3 hours or overnight.

3.2.6 Barley Plant genotyping

Mutant alleles identified in the TILLING population (*recq4-1*, *figl1-2*, and *figl1-3*) were genotyped based on the Derived Cleaved Amplified Polymorphic Sequences (dCAPS) method (Neff et al., 2002). Primers were designed via dCAPS finder 2.0 (http://helix.wustl.edu/dcaps/). Sequences were amplified using *Taq* DNA polymerase (Thermo Fisher Scientific) with primers MA-225 + MA-227 for *recq4-1*, MA-204 + MA-205 for *figl1-2*, and MA-206 + MA-207 for

figl1-3. The PCR product was digested with *Pvu*I-HF (*recq4-1*), *Xho*I (*figl1-2*), or *Eco*RI-HF (*figl1-3*) and analysed on a 2.5% agarose gel. Primers generated a restriction enzyme site within the WT amplicon; i.e. a complete cut reflects a 'WT' genotype, partial digest reflects a 'het' genotype, and no digest reflects a 'homo' genotype.

CRISPR-Cas9 generated mutants were genotyped using WT or mutant allele-specific primers. To genotype *recq4-2*, primers MA-437 + MA-438 only amplify *RECQ4*, while primers MA-440 + MA-441 only amplify *recq4-2*. To genotype *figl1-4*, primers MA-448 + MA-445 amplify *FIGL1*, while primers MA-448 + MA-447 only amplify *figl1-4*. To genotype *hei10-1*, primers MA-427 + MA-428 did only amplify *HEI10*, while primers MA-426 + MA-428 did only amplify *hei10-1*. To genotype *hei10-2*, primers MA-429 + MA-431 did only amplify *HEI10*, while primers MA-430 + MA-431 did only amplify *hei10-2*. For every PCR cycle number was 28. All primers are listed in the Supplementary table 2.

To assess the hybrid status of plants, two InDel marker between Barke and GP on chromosomes 1H and 3H were employed. A primer pair (SA_1H_F and SA_1H_F) was used in a PCR resulting in an amplicon of 547 bp in Barke (B) or 512 bp in GP, or two (547 + 512 bp) in B/GP hybrid. Another primer pair (SA_3H_F and SA_3H_R) gave a PCR amplicon of 416 bp in B, an amplicon of 564 bp in GP, or the two bands combined (416 + 564 bp) in B/GP hybrid.

3.2.7 PCR & amplicon purification, and qRT-PCR

3.2.7.1 PCR

A typical Phusion DNA polymerase-based PCR set-up consisted of 20-50 ng of template DNA, 0.5 mM each of forward/reverse primer, 0.02 mM of dNTP mix, 1X Phusion polymerase buffer (NEB - 20 mM Tris-HCl, 100 mM KCl, 1 mM DTT, 0.1 mM EDTA, 200 µg/ml BSA, 50% Glycerol, and 1X stabilizers, pH 7.4), and 1 U of Phusion DNA polymerase (NEB) in a final reaction volume of 10 µl adjusted with ddH_2O. A standard PCR program was as follows: 1X cycle of initial denaturation at 98°C for 2 min, 36x cycles of (denaturation at 98°C for 10 sec, annealing at *x*°C for 20 sec, and elongation/extension at 72°C for *y* sec.), 1X cycle of final elongation at 72°C for 5 min, and hold at 4°C. Annealing temperature (*x*°C) is indicated in Supplementary table 2 for each primer pair, while *y* sec. was calculated as 40 sec per 1 kb.

PCR-based genotyping was performed by using *Taq* DNA polymerase (QIAGEN). The setup was similar to the one above-mentioned for Phusion DNA polymerase except 1X CL buffer (QIAGEN) and 0.5 U of *Taq* DNA polymerase were used. The PCR program was as follows:

1X cycle of initial denaturation at 94°C for 2 min, 36x cycles of (denaturation at 94°C for 30 sec, annealing at *x*°C for 30 sec, and elongation/extension at 72°C for *y* sec.), 1X cycle of final elongation at 72°C for 5 min, and hold at 4°C. Annealing temperature (*x*°C) is indicated in Supplementary table 2 for each primer pair, while *y* min was calculated as 1 min per 1 kb.

PCR reactions for screening the TILLING population were composed of 20 ng of gDNA, 0.25 mM of forward primer, 0.25 mM of reverse primer, 1X CL buffer, 200 µM of dNTP mix and 2 U of *Taq* DNA polymerase in a final reaction volume of 30 µl adjusted with ddH_2O.

Liquid culture or colony PCR was performed as follows: 1:50 dilution from 1 µL of overnight liquid culture or part of an overnight-grown colony taken by a sterilized toothpick, 0.5 mM of forward primer, 0.5 mM of reverse primer, 0.02 mM of dNTP mix, 1X CL buffer and 0.5 U of *Taq* DNA polymerase in a final reaction volume of 10 µl adjusted with ddH_2O.

3.2.7.2 Purification of DNA from enzymatic reactions or agarose gels

For DNA purification from enzymatic reactions (DNA digestion, DNA ligation), the QIAquick nucleotide removal kit (QIAGEN) was used according to the manufacturer's instructions. For clean-up of PCR products, the GeneJET PCR Purification Kit (Thermo Fisher Scientific) was used following the manufacturer's instructions. For clean-up of PCR products during screening the TILLING population, the NucleoFast 96 PCR kit (Nacherey-Nagel) was used following the manufacturer's instructions. To purify DNA from agarose gels, the QIAquick Gel Extraction Kit (QIAGEN) was used according to the manufacturer's instructions.

3.2.8 Cloning and bacterial transformation

3.2.8.1 Dephosphorylation of backbone vector cut with restriction enzyme

To prevent self-ligation of a restriction enzyme digested vector, ~0.75 U of rSAP (NEB) were added to the digestion reaction and incubated for 30 min at 37°C followed by 65°C for 5 min.

3.2.8.2 DNA ligation

A typical ligation reaction consisted of 6-100 ng insert DNA (depending on its size – see below), 25 ng of vector DNA, 1X T4 DNA ligase buffer, 2.5 U of T4 DNA ligase and ddH_2O in a final volume of 15 µL. For all ligation reactions, the molar ratio of insert to vector DNA was 3:1 and the quantity of vector DNA was 25 ng.

A blunt-end ligation mix was incubated at RT for 20 min. A sticky-end ligation mix was incubated at 4°C for 2 hours and at 16°C overnight.

3.2.8.3 Bacterial transformation

Transformation of a DNA ligation product (containing ampicillin resistance gene) was performed using the Mix & Go *Escherichia coli* (*E. coli*) transformation kit & buffer set (Zymo research) following the manufacturer's instructions.

For bacterial transformations with large inserts (>3 kb) in DNA ligations, NEB 5-alpha Competent *E. coli* (High Efficiency, C2987H) or 10-beta Competent *E. coli* (High Efficiency, C3019H/C3019I) were used according to the manufacturer's instructions. All antibiotics and concentration used are listed in Supplementary table 4.

3.2.9 Plasmid DNA isolation (Mini-prep)

Isolation of plasmid DNA from *E. coli* cultures was performed using the GeneJET Plasmid Miniprep Kit (Thermo Fisher Scientific) following manufacturer's instructions.

3.2.10 Sanger sequencing and data analysis

Sanger sequencing was performed by Eurofins Genomics. Plasmid DNA samples for Sanger sequencing were prepared as follows: ~1 µg of plasmid DNA, 1.3 µM of primer, and ddH_2O in a total reaction volume of 17 µL. Purified PCR products were sequenced by mixing ~75 ng (up to 1 kb) or ~150 ng (up to 3 kb) of purified DNA, 1.3 µM of primer, and ddH_2O in a total reaction volume of 17 µL. Sequencing data was analysed using SnapGene 4.3.10 software.

3.2.11 Design of CRISPR/Cas9 sgRNAs and construction of T-DNA vector

Three gRNAs targeting exons 5 and 6 within *HvHEI10*, two gRNAs targeting exons 1 and 5 within *HvRECQ4*, and two gRNAs targeting exons 4 in 6 within *HvFIGL1* were selected (Supplementary table 1). To test the activity of selected gRNAs at target sites, initially selected gRNAs targeting *RECQ4* were tested by an *in vitro* Cas9 cleavage-assay. Briefly, sgRNA was assembled by combining 100 µM of crRNA and 100 µM of tracrRNA (IDT) with nuclease-free duplex buffer (IDT - 30 mM HEPES, pH 7.5; 100 mM potassium acetate) by incubating the mix at 95°C for 5 min and at RT for 10-20 min. Ribonucleoprotein (RNP) complexes were generated by mixing 1 µM of the assembled sgRNA, 1 µM of Cas9 (IDT; in 1X PBS with 50% glycerol) and 1X Cas9 buffer (NEB) in a total volume of 14 µL adjusted with ddH_2O. The reaction was incubated at 25°C for 10 min and stored on ice. ~200 ng of *BbvC*I linearized plasmid DNA (pJET1.2-RECQ4 generated by blunt-end ligation of PCR amplicon using primers SH-62 and SH-63 to pJET1.2 vector) were added to the reaction (total volume of 15

µL) and incubated at 37°C for 1 hour, at 70°C for 10 min and stored on ice. *In vitro* cleavage at target sites was confirmed on a 1% agarose gel.

Generation of pGH622:

Annealed oligos for *HvFIGL1* gRNA1-2 were introduced in the pIK7 and pIK8 vectors using *Bsa*I type II restriction enzyme and generating pGH571-2 and pGH576-8, respectively. The vectors contain the TaU6 promoter and a gRNA scaffold. The two gRNA expression units were mobilized using the *Esp*3I enzyme and subcloned in the pIK19 destination vector generating pGH581. After sequencing confirmation using primers IK70 and IK71 in the next step the two gRNA-containing module was assembled with a ZmUBI1P::xCas module (pIK84) and an empty HDR dummy (pIK23) in the vector pIK22 using *Bsa*I restriction enzyme generating pGH594. Finally, all expression units were integrated into the *Sfi*I sites of plasmid p6i-d35S-TE9 (DNA-Cloning-Service, Hamburg, Germany), generating plasmid pGH622.

Generation of pGH616:

Annealed oligos for *HvRECQ4* gRNA1-2 were introduced in the pIK5 and pIK6 vectors using *Bsa*I type II restriction enzyme generating pGH569-2 and pGH570-1. The two gRNA modules were inserted in pIK60 generating pGH579. After sequencing confirmation using primers IK70 and IK71 in the next step the two gRNA-containing module was assembled with a ZmUBI1P::xCas module (pIK84) and an empty HDR dummy (pIK23) in the vector pIK22 using *Bsa*I restriction enzyme generating pGH585. Finally, all expression units were integrated into the *Sfi*I sites of plasmid p6i-d35S-TE9, generating plasmid pGH616.

Generation of pGH619:

Annealed oligos for *HvHEI10* gRNA1-3 were introduced in the pIK5, pIK6 and pIK7 vectors using *Bsa*I type II restriction enzyme generating pGH565-1, pGH567-2 and pGH568-1. All three gRNA expression units were mobilized using the *Esp*3I enzyme and assembled in the pIK19 destination vector generating pGH578. An *Esp*3I-fragment of a pIK11 dummy filled the missing fourth gRNA position. After sequencing confirmation using primers IK70 and IK71 in the next step the four gRNA-containing module was assembled with a ZmUBI1P::xCas module (pIK84) and an empty HDR dummy (pIK23) in the vector pIK22 using *Bsa*I restriction enzyme generating pGH589. Finally, all expression units were integrated into the *Sfi*I sites of plasmid p6i-d35S-TE9, generating plasmid pGH619-2. All vectors are listed in Supplementary table 3.

Presence of transgene within regenerated 21 (pGH616-2, *recq4*), 12 (pGH622-1, *figl1*), and 14 (pGH619-2, *hei10*) T_0 plants was confirmed by PCR on leaf genomic DNA using oligonucleotides Bie475 + GH-zCas9-R1 (Supplementary table 2). Identification of mutations within target sites of T_0 plants and within T_1 offspring family plants from selected T_0 plants was performed by Sanger-Sequencing of PCR products using MA-284 + MA-285 (for *HEI10*), MA-365 + MA-57 (for *RECQ4*), and MA-142 + MA-143 (for *FIGL1*).

3.2.12 Isolation of transgenic barley plants with mutations within *HvHEI10, HvRECQ4 and HvFIGL1*

In collaboration with Jochen Kumlehn's group at the IPK, stable barley cv. GP transformations were performed as described (Hensel et al., 2008) using *Agrobacterium tumefaciens* strain AGL1. Three vectors were designed to target *HvHEI10* (pGH619-2), *HvRECQ4* (pGH616-2), or *HvFIGL1* (pGH622-1).

3.3 Cytology

3.3.1 Barley cytology - male meiotic chromosome analysis

Spikes within size range of 1-3 cm were fixed in 3:1 solution (3 parts ethanol : 1 part glacial acetic acid). Under a Stereomicroscope, spikes were dissected and three anthers were isolated from one spikelet. One anther was placed on a slide with a drop of acetocarmine (Morphisto GmbH), heated for few seconds and squashed under a coverslip using a thumb. The meiotic stage was identified using a light microscope (Zeiss). The remaining two anthers were washed 3x 5 min with 0.01 M citrate buffer and placed in enzyme mix (1% cellulose, 1% pectolyase (Sigma) in 0.01 M citrate buffer, pH 4.5) for ~40 min in a moist chamber at 37°C. Enzymatic digestion was stopped by washing with ice-cold 0.01 M citrate buffer, anthers were placed in a drop of 0.01 M citrate buffer on a Superfrost slide (Thermo Fisher Scientific) and macerated with a brass rod. Ten µl of 60% acetic acid were added on the slide and the material was mixed with a needle (without touching the slide – needle was touching and moving the upper surface of the drop). Two hundred µl of ice-cold 3:1 solution was added quickly and the slide was moved with hands to assure that the 3:1 solution had covered the whole area of the slide where the meiotic cells were fixed on. Slides were then let to dry, dehydrated in an ethanol series (70, 80, 100 % for 2 min each), and let dry again. One µg/mL of DAPI in Vectashield (Vector laboratories) was added and slides were covered with a coverslip.

For scoring rods:rings ratio, only cells with recognizable morphology of all seven bivalents were considered. For scoring extra-terminal:terminal:subterminal:interstitial chiasmata, any recognizable bivalent (not overlapping with another one) were considered, without the necessity that all seven bivalents of a nucleus were distinguishable.

For scoring extra-distal chiasma and calculating their ratio among all chiasmata, only cells with recognizable ratio of rods:rings or scorable MCN were considered to count extra-distal CO.

Immunostaining of pollen mother cells (fresh material) was performed according (Higgins et al., 2012) with minor modifications. Dissected and staged anthers were digested in 20-25 µL of digestion medium (0.4% cytohelicase, 1.5% sucrose, 1% polyvinylpyrrolidone in sterile water) for 8 min in a moist chamber at 37°C on a slide, during which meiocytes were tapped out using a brass rod after 4 min of enzyme incubation. Spreading was done using a needle after adding 17 µL of 1.5% lipsol and 17 µL of ice-cold 4% paraformaldehyde (pH 8). Then slides were dried for around 2 hours. In a moist chamber, specimens were blocked using 1% of BSA and 0.1% of Triton X-100 in phosphate-buffered saline (PBS - 137 mM of NaCl, 2.7 mM of KCl, 10 mM of Na_2HPO_4 and 1.8 mM of KH_2PO_4, pH 7.4) and incubated with primary antibodies overnight at 4°C and with secondary antibodies for 2 h at 37°C. Slides were washed after each antibody incubation in 1 × PBS containing 0.1% Triton X-100. Slides were mounted in Vectashield plus antifade medium with DAPI (1.0 µg/mL - Vector laboratories). Antibodies were diluted in EM solution (1% BSA and 0.1% Triton X-100 in PBS). The following primary antibodies were used at 1:500 dilutions, anti-ZYP1 (rat or rabbit) (Steckenborn et al., 2023), anti-ASY1 (guinea pig or rabbit) (Steckenborn et al., 2023), anti-HEI10 (rabbit) (Desjardins et al., 2020), and anti-REC8 (rabbit) (K. Wang et al., 2009), at 1:200 dilution, anti-HEI10 (guinea pig) (Desjardins et al., 2020), and anti-γH2Ax (Miao et al., 2013). The following secondary antibodies were used at 1:500 dilutions: anti-rat Alexa Fluor 488 (Thermo Fisher), anti-rat Alexa Fluor 594 (Thermo Fisher), anti-rabbit Alexa Fluor 488 (Thermo Fisher), anti-rabbit Alexa Fluor 594 (Thermo Fisher), anti-guinea pig Alexa Fluor 488 (Thermo Fisher), anti-guinea pig Alexa Fluor 594 (Thermo Fisher), anti-guinea pig Alexa Fluor 647 (Thermo Fisher).

To quantify HEI10 foci, immunostaining on 3:1 fixed and spread meiocytes was performed as described above and according (Chelysheva et al., 2010) with following minor modifications: after identifying the meiotic stage of one anther, the two remaining anthers were added on a Superfrost slide (Thermo Fisher Scientific) and stained with acetocarmine. Tipping by the brass rod was performed gently to further spread meiocytes apart. The whole slide was submerged

under liquid nitrogen for around 10 seconds, the cover slip removed using a razor blade, and the slide was transferred immediately into 1x PBS. After five min, the slide was transferred into 10 mM citrate buffer (pH 6), boiled in a microwave at 900 W for exactly 46 seconds, cooled down in 1x PBS and 0.1% triton X-100 (Sigma) for 5 min and another 5 min in 1x PBS.

3.3.2 Microscopy

Male meiotic chromosome spreads were imaged using a Nikon Eclipse Ni-E fluorescence microscope equipped with a Nikon DS-Qi2 camera and NIS-Elements-AR version 4.60 software (Nikon, Tokyo, Japan).

To investigate the ultrastructure and spatial localization of immunosignals at a lateral resolution of ~120 nm (at 488 nm excitation) four-colour spatial structured illumination microscopy (3D-SIM) was employed using a 63×/1.4 Oil Plan-Apochromat objective of an Elyra PS.1 microscope system and its software ZENblack (Carl Zeiss GmbH). Image stacks (step size of 100 nm) were captured separately for each fluorochrome using the 405, 488, 561, and 642 nm laser lines for excitation and proper emission filters (Weisshart et al., 2016). The ZEN software was used to calculate the maximum intensity projections of whole meiocytes.

3.3.3 Image analysis & statistics

Images were processed (SC length, telomere-HEI10 foci distance, inter-HEI10 foci distance) with Fiji/ImageJ. SC length measurements were measured in multiple Z-stacks. 3D-model of late pachytene nuclei was generated using the simple neurite tracer plugin (Longair et al., 2011) in Fiji (Morgan & Wegel, 2020). Foci count was performed manually. Graphs were executed using GraphPad Prism 8. Maximum projection was calculated by ImageJ for images captured by Nikon Eclipse Ni-E fluorescence microscope.

4 Results

4.1 HEI10 is essential for class I CO formation in barley

4.1.1 Identification of HEI10 in barley

In order to identify HEI10 in barley, the barley reference genome (Mayer et al., 2012) was queried using the aa sequences of *A. thaliana* and *O. sativa* HEI10. HORVU6Hr1G040680.2 was identified as the likely barley HEI10 candidate encoding for a 303 aa protein based on eight exons and seven introns. Using cDNA from spikes of cv Golden Promise, Barke and Morex, two isoforms were detected based on alternative splicing at the beginning of exon seven resulting in a CDS of either 885 or 912 bp encoding for a protein of 294 or 303 aa, respectively (Fig 7). Based on intron retention/splicing the last 27 bp of intron six are either included in the CDS or not. A similar alternative splicing event was found in rice HEI10 (K. Wang et al., 2012) (Fig 8). The sequence of *HvHEI10* (isoform encoding 294 aa) shares high identity with *HEI10* sequences from other monocot plants: 98.98% (over 99% of query coverage) with *Triticum aestivum* (MBC2899773.1), 90.85% (over 100% of query coverage) with *Brachypodium distachyon* (KQJ94151.1), 86.78% with *O. sativa* (XP_015623605.1) or 80.68% with *Zea mays* (NP_001152027.1) as well as with *HEI10* in dicot plants such as *A. thaliana* (OAP14004.1) or *Brassica oleracea* (XP_013627001.1) with sequence identities of 67.67% or 67.11%, respectively (all over 100% of query coverage) (Fig 8). Thus, *HEI10* is highly conserved across the plant kingdom. Furthermore, HvHEI10 shares several conserved residues within the RING and coiled-coil domains in its N-terminal region with its orthologous HEI10/Zip3 sequences in budding yeast, fungi, worms, Drosophila and mammals (Fig 8)

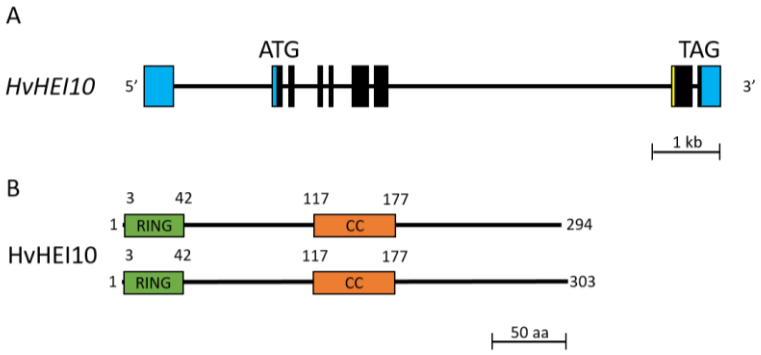

Figure 7 *HvHEI10* gene and protein schematic models.

(A) Exon/intron structure of *HvHEI10*; exons depicted as black boxes, introns as black lines between exons and 5'/3' UTRs as blue boxes. The alternative spliced region highlighted in yellow at the junction between intron 6/exon 7. **(B)** Two protein isoforms based on alternative splicing of *HvHEI10* including conserved RING (aa 3-42) and coiled-coil (CC – aa 117-177) domains.

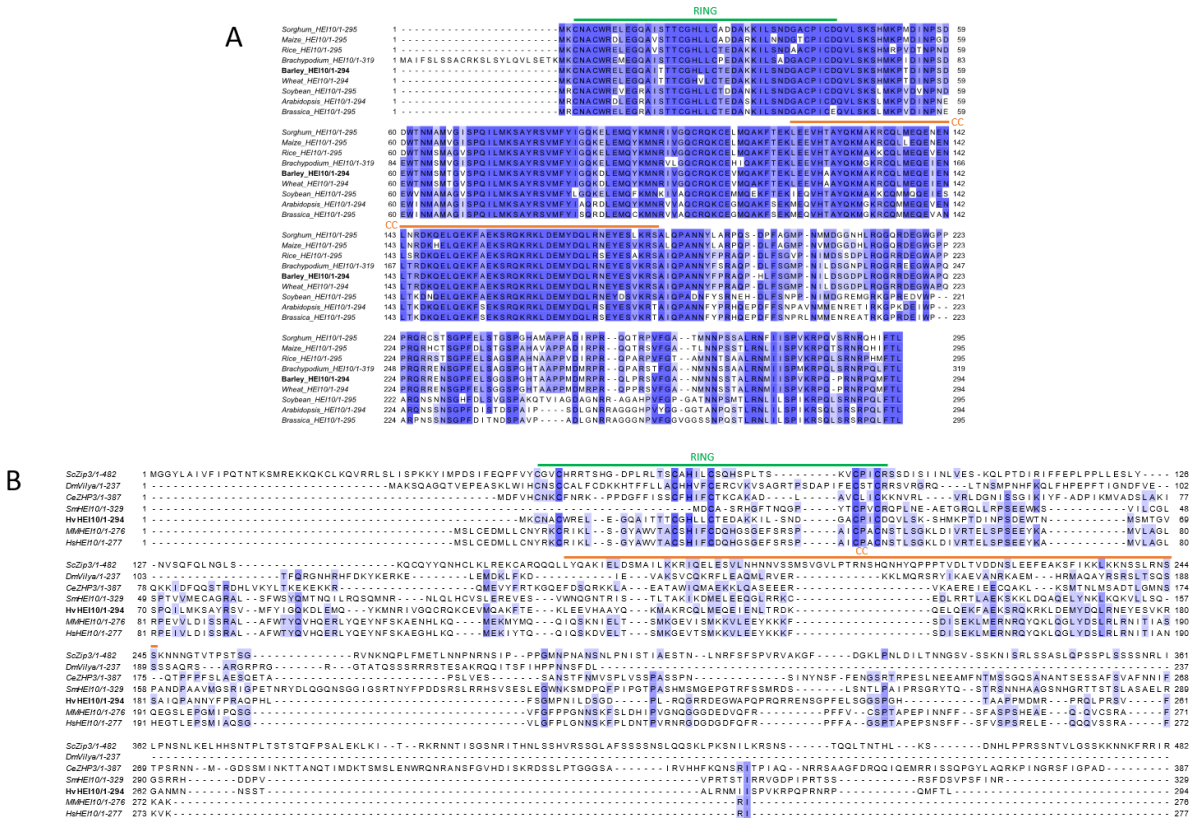

Figure 8 HEI10 sequence conservation among plant and non-plant species.

(A) Multiple plant HEI10 sequence alignment between barley, wheat, rice, maize, sorghum, soybean, brassica and Arabidopsis. **(B)** Multiple sequence alignment between barley HEI10 (HvHEI10), budding yeast (ScZip3), Drosophila (DmVilya), worm (CeZHP-3), Sordaria (SmHei10), mouse (MmHEI10) and human (HsHEI10) showing several conserved residues especially within the RING and CC domains (highlighted with green and orange lines, respectively). Dark blue indicates high homology and light blue indicates low homology among species.

4.1.2 HEI10 localization during prophase I in relation to axis and SC formation

To dissect the spatiotemporal dynamics of HEI10 during prophase I, antibodies raised in rabbit or guinea pig specific against HEI10 (see section 4.1.6; Fig 9) were used together with antibodies against ASY1 (labelling meiotic chromosome axes) and ZYP1 (labelling transverse filaments of the SC) on male meiotic prophase I chromosome spreads. During early prophase I in leptotene, ASY1 appeared as polarized linear signals emerging from one side of the nucleus (likely telomeres) with high signal intensity compared to other nuclear sides with short less-intensity stretches of ASY1 (Fig 9). At this stage, ZYP1 appeared as multiple foci similar to HEI10 with hundreds of foci distributed randomly across nuclei. Bright ZYP1 foci were typically associated with HEI10 foci. ZYP1 foci were always associated with ASY1-positive axis, while most of HEI10 foci colocalized with ASY1 (Fig 9). By early zygotene, axis

formation was complete based on fully linear signals of ASY1 throughout nuclei. Limited bright ZYP1 foci (likely synapsis initiation sites) and short ZYP1 stretches were found emerging from the same pole where highly abundant ASY1 signals were found reflecting a spatiotemporal asymmetry in early prophase I events (Higgins et al., 2012). During mid and late zygotene, (short) ZYP1 stretches were found throughout the nucleus (Fig 9). Most of the bright HEI10 foci colocalized with bright ZYP1 foci and with short ZYP1 stretches (Fig 9). Notably, a focal HEI10 signal was commonly found at one end of short ZYP1 stretches suggesting HEI10 playing a role for either synapsis initiation sites or nascent SC formation (Fig 9). During zygotene and pachytene, synapsis extended starting from multiple initiation sites. Multiple HEI10 foci of different diameter and brightness were found colocalizing with the extended ZYP1 stretches, while ASY1 became weak/faint at synapsed regions (Fig 9, 10).

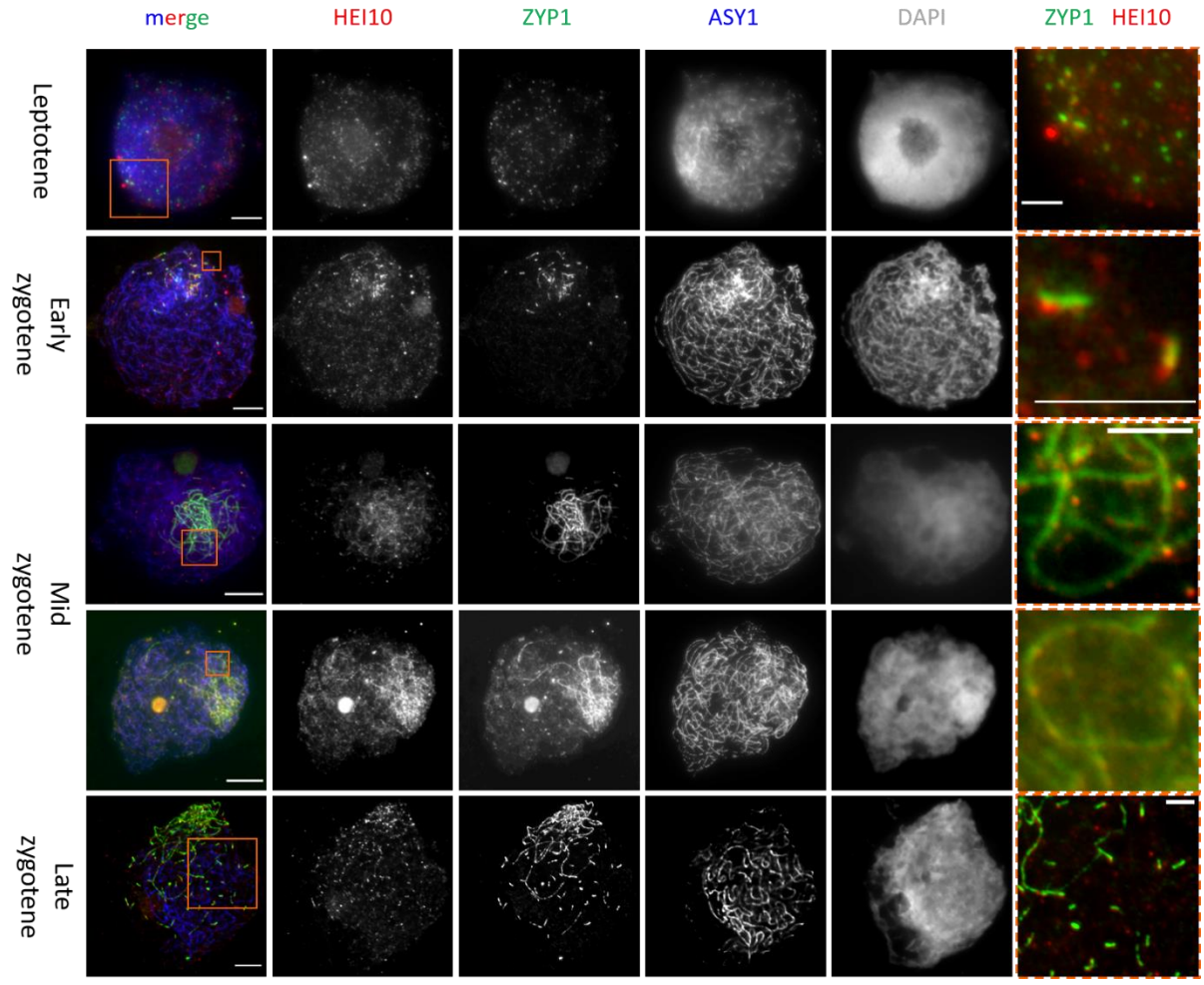

Figure 9 Spatiotemporal dynamics of axes, SC and recombination markers during early prophase I: Leptotene to zygotene.

Leptotene and early, mid and late zygotene nuclei stained with HEI10 (red), ZYP1 (green) and ASY1 (blue) showing their spatiotemporal dynamics during early stages of prophase I of barley cv GP. Insets (right column) depicts colocalization of HEI10 with foci, short stretches and long threads of ZYP1. DNA counterstained with DAPI in grey. In merged and inset images scale bar represents 5 and 2 µm, respectively.

During zygotene, two HEI10 signal patterns existed: (1) on ZYP1 and weak ASY1 signal (synapsed regions) and (2) on bright ASY1 signal (asynapsed regions) and no ZYP1. By late pachytene, the whole nucleus was decorated with long linear ZYP1 signals indicating fully synapsed homologous chromosomes. HEI10 foci numbers were decreased with residual foci being distinct, large and bright foci localizing on long ZYP1 threads. Residual ASY1 colocalized with long ZYP1 threads while ASY1's signal intensity was strongly reduced (Fig 10). At diplotene when desynapsis initiated, the majority of large HEI10 foci were flanked by short "curly" residual stretches of ZYP1. This suggests that the last regions of desynapsis were regions around designated class I CO sites implying a potential stabilizing role of the SC for recombination regions in barley or the other way around with recombination sites temporally stabilizing the surrounding SC regions (Fig 11). However, also HEI10-negative ZYP1 stretches were found.

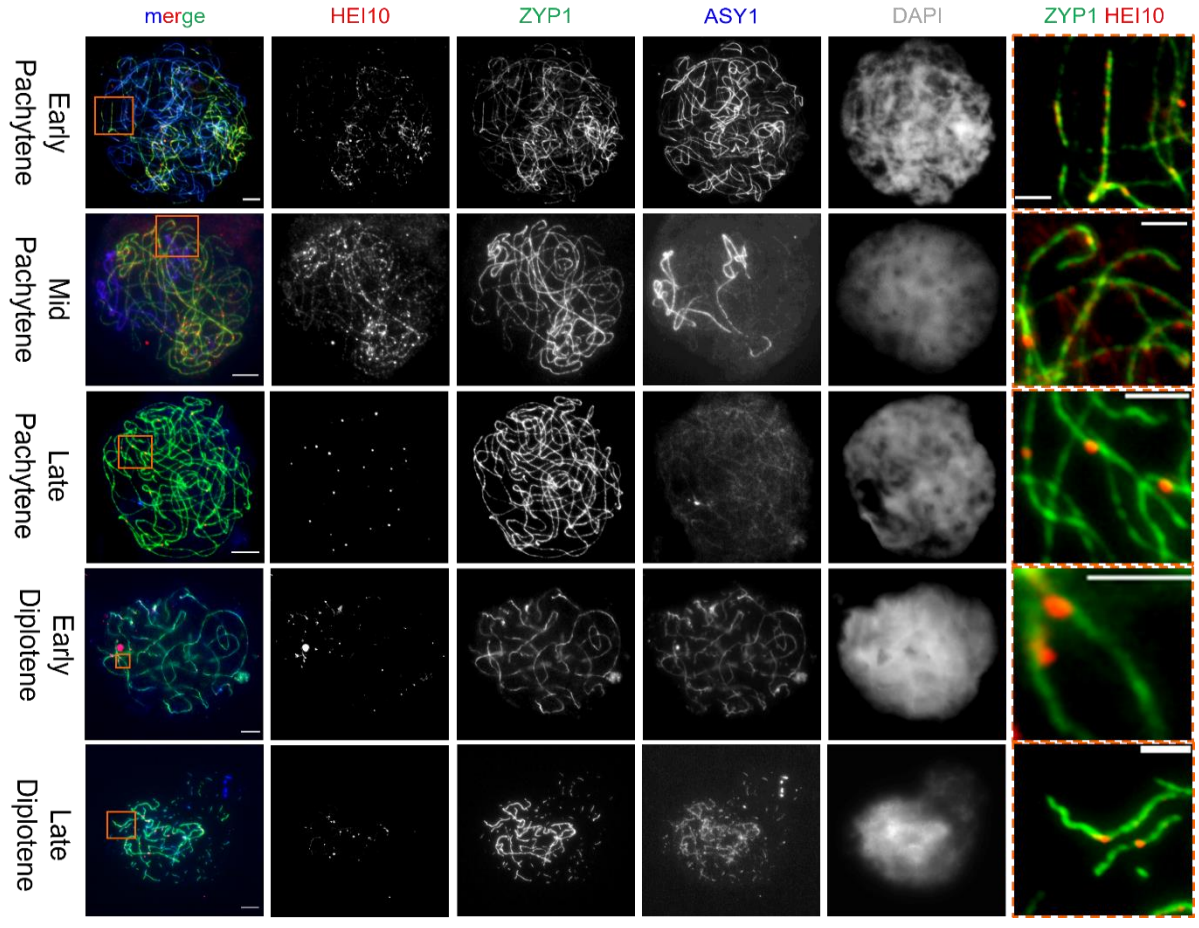

Figure 10 Spatiotemporal dynamics of axes, SC and recombination markers during late prophase I: Pachytene to diakinesis.

Localization dynamics of HEI10 (red), ZYP1 (green) and ASY1 (blue) in late stages of prophase I of barley cv GP. DAPI-stained DNA (grey). Insets (right column) showing the colocalization of different foci types of HEI10 with ZYP1 in early pachytene stages while only large HEI10 foci persist from late pachytene on. In merged and inset images scale bar represents 5 and 2 µm, respectively.

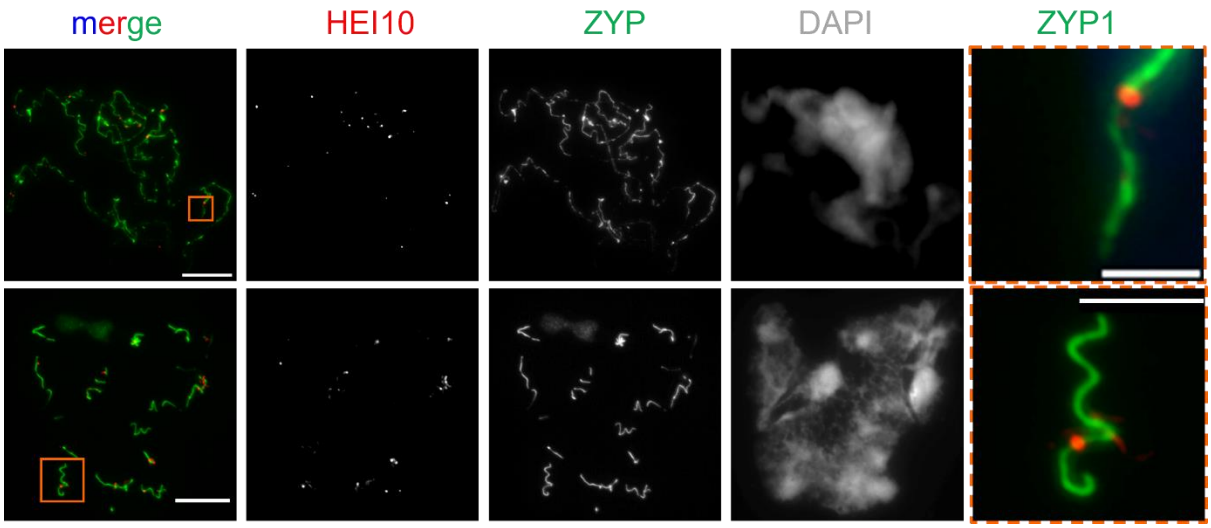

Figure 11 Chromosome regions flanking HEI10-marked recombination sites are typically positive for short ZYP1 stretches.

Diplotene nuclei stained with ZYP1 (green) and HEI10 (red). DNA counterstained with DAPI in grey. In merged and inset images scale bar represents 5 and 2 µm, respectively.

To conclude, spatiotemporal dynamics of axis, SC and class I CO formation were initially polarized at one side of the nucleus with progressive extension initiating from multiple synapsis initiation sites. Throughout prophase I, HEI10 was found highly dynamic.

4.1.3 Negative correlation between HEI10 foci number and progression of meiosis

To quantify HEI10 foci numbers as a potential proxy for class I CO maturation/numbers in barley, 33 meiotic nuclei were staged from early pachytene till late diplotene based on: (1) anther length and (2) SC extension (measured by ZYP1 length). In early pachytene nuclei (SC length range of 900 – 1161 µm) an average HEI10 foci number of 21.1 ± 1.08 (n=11, HEI10 foci range = 19-23) was found, while in late pachytene nuclei (SC length range of 650-900 µm) an average of 17.8 ± 2.2 HEI10 foci (n=22, HEI10 foci range 13-21) was detected (Fig 12). Therefore, class I CO numbers can be estimated to be around 18 based on cytological HEI10 foci counts in late pachytene of male meiocytes in barley.

4.1.4 Cytological evidence for distal crossovers in barley

All seven barley chromosome pairs were completely synapsed in late pachytene nuclei. Using the plugin ‘simple neurite tracer’ (Longair et al., 2011) in Fiji, each single bivalent (based on the SC marker ZYP1) was traced and isolated from 3D image stacks (Fig 13). HEI10 foci on isolated bivalents were manually depicted (Fig 13). The extension of the SC for each isolated

bivalent and per nucleus, the distance of every HEI10 focus to the chromosome end, and HEI10 foci inter-distance was measured. As an example, in a nucleus with 18 HEI10 foci (Fig 13), 14 out of 18 foci were in close vicinity to chromosome ends (i.e. one focus close to every end), while the four remaining foci were located more interstitially (a third focus interstitially on every of the four longest (by SC length) chromosomes). Thus, cytological evidence for terminal CO positions in barley PMCs is shown based on the class I CO marker HEI10.

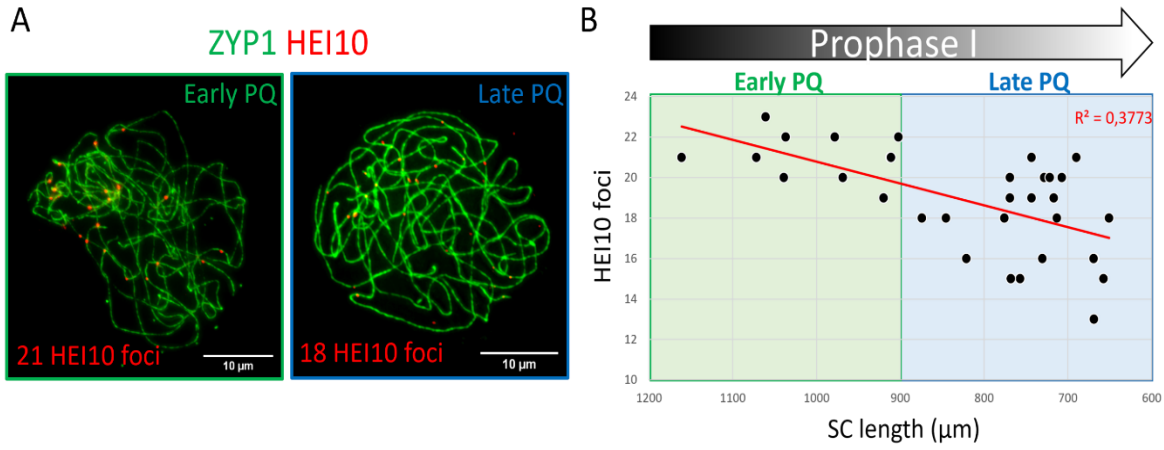

Figure 12 Dynamics of large HEI10 foci during prophase I.

(A) Early and late pachytene nucleus with HEI10 foci number indicated. Nuclei labelled with ZYP1 in green and HEI10 in red. **(B)** Direct relationship between meiotic progression (based on SC/ZYP1 length) and HEI10 foci number through pachytene. Linear regression coefficient (R^2) = 0.3773.

4.1.5 Meiotic dual localization pattern of HEI10 during synapsis

Similar to other species across different kingdoms (Agarwal & Roeder, 2000; Chelysheva et al., 2012; Hesse et al., 2019; A. D. Muyt et al., 2014; Qiao et al., 2014; K. Wang et al., 2012), in barley, HEI10 formed foci on the SC from zygotene to diplotene. Surprisingly, HEI10 also localized at some but not all asynapsed regions (ZYP1-negative) in a "linear-fashion" in 85/210 (38.46%) ($n_{(plants)}$= 12) and in 18/52 (34.62%) ($n_{(plants)}$= 3) zygotene and pachytene nuclei in both cv GP and Barke, respectively, using both HEI10 antibodies raised in Guinea pig and rabbit (Fig 14). During synapsis progression, synapsed regions are marked with ZYP1, HEI10 frequently showed a linear signal emerging from some ends of ZYP1 signals and was further found as bright foci at the branching point together with enriched ZYP1 signal (Fig 14). To depict this localization pattern in more detail, 3D-SIM was employed and confirmed this dual

localization of HEI10 (focal on ZYP1 and linear emerging from some ZYP1 ends) during synapsis in zygotene/pachytene (Fig 14). Thus, the observed linear HEI10 pattern may suggest in addition to its role in class I CO formation/maturation a possible role of HEI10 either in synapsis and/or possibly CO interference.

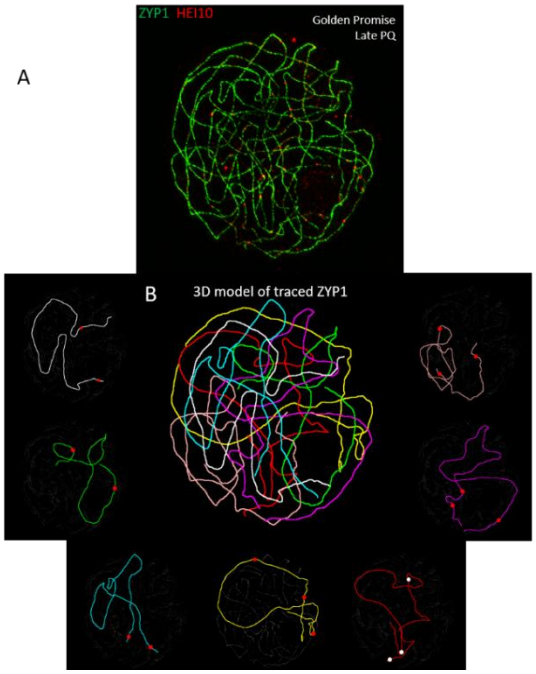

C

chromosome	SC length (µm)	HEI10-telomere distance (µm)		Inter-foci distance (µm)	
magenta	136.0945	7.645	14.7742	101.45	10.94
pink	132.1638	2.2173	4.8852	98.43	24.96
red	125.9274	1.5543	13.0276	72.38	22.93
Yellow	125.3315	17.1849	14.9946	78.04	37.47
cyan	121.7468	1.4986	1.2271	116.7	
green	105.8279	13.9605	9.7402	92.2	
white	105.7351	3.71	11.2374	76.74	

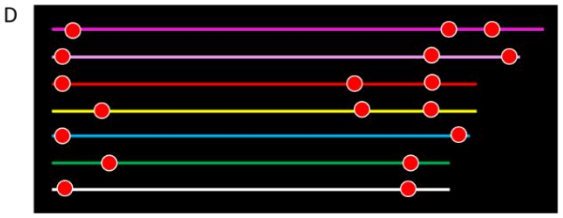

Figure 13 Cytological evidence for distal CO in barley.

(A) Late pachytene nucleus stained with ZYP1 (green) and HEI10 (red) and imaged by 3D-SIM. **(B)** A 3D model of traced homologous chromosomes rendered from the cell in (A). Seven isolated chromosome pairs are shown in separate images in different colours with positions of HEI10 foci (red dots) on each single chromosome. **(C)** Quantifications from (B) including SC length of each chromosome (µm), distances between distal HEI10 foci and telomeres (µm), and inter-foci distance (µm). **(D)** In-scale simulation of the seven chromosomes depicting in-scale HEI10 positions (red dots).

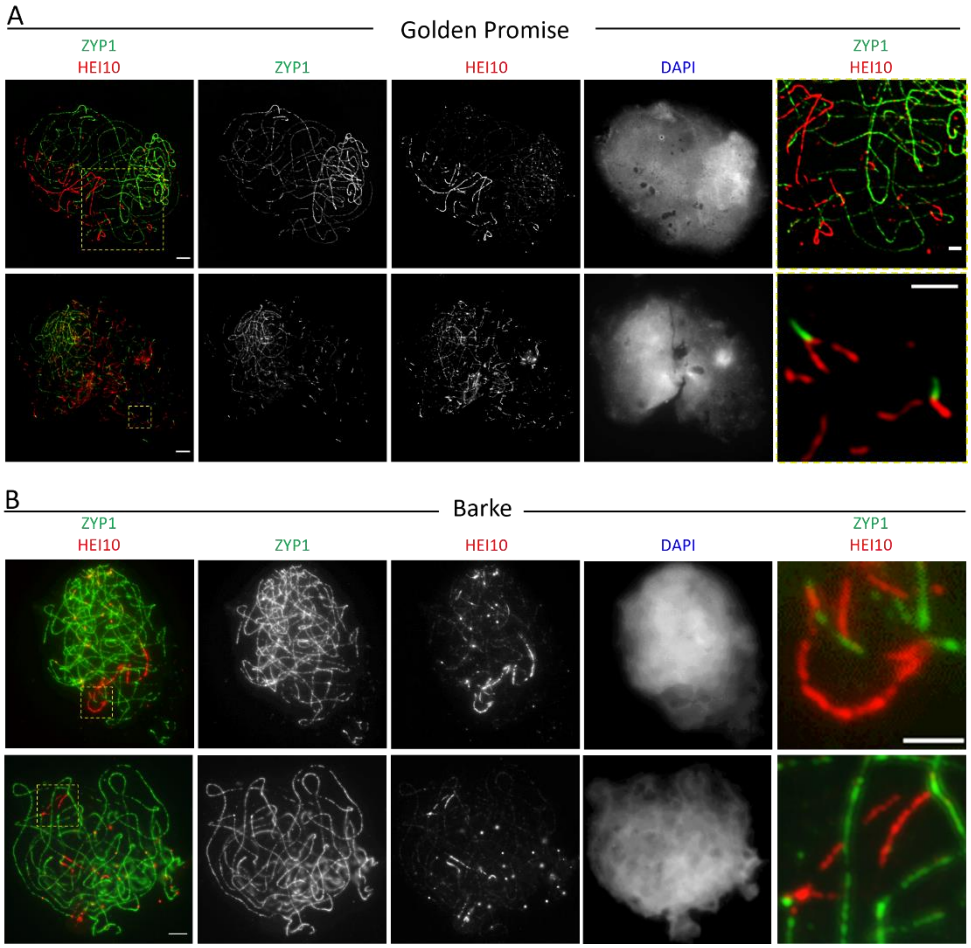

Figure 14 Meiotic dual localization of HEI10 during zygotene in WT.

ZYP1 (green), HEI10 (red) and DAPI-stained DNA (blue) in GP **(A)** and Barke **(B)**. Scale bar represents 5 µm. Insets showing ZYP1 (green) and HEI10 (red), scale bar represents 2 µm.

4.1.6 Isolation of *HEI10*-defective barley plants

To isolate putative mutations within *HvHEI10* enabling to dissect HEI10 function *in planta*, three guide RNA (gRNA) target sites within *HvHEI10* (within exons 5 and 6) were selected for CRISPR/Cas9. In collaboration with Jochen Kumlehn's group at the IPK, barley cv GP was transformed with the vector pGH619-2 expressing the three gRNAs as individual *TaU6* promoter-driven units together with a Ubiquitin-driven monocot codon-optimized *Cas9* designed to target *HvHEI10* (Suppl. table 1). Among 14 independent T_0 plants, 11 plants were PCR-positive for *Cas9*. Two independent mutations within segregating T_1 offspring families (from two T_0 plants) were isolated: *Hvhei10-1* and *Hvhei10-2*. Both mutations are at different positions in exon 6 matching target sites of gRNA two and three. *Hvhei10-1* is an insertion of the base 'A' between 'A' +527 and 'G' +528 (positions based on CDS, relative to ATG). Two bases (GA) are deleted in *Hvhei10-2* (+616 and +617 in CDS, relative to ATG) (Fig 15). Mutations were confirmed by Sanger-sequencing of cDNA/gDNA from *Hvhei10-1* and

Hvhei10-2 plants. *Hvhei10-1* caused a frameshift downstream of E176 and a premature stop codon resulting in a truncated protein of 202 AA. *Hvhei10-2* resulted in a truncated protein of 207 AA based on a frameshift downstream of L205 and a premature stop codon (Fig 15). Based on 3D protein structure prediction using the phyre2 online software (http://www.sbg.bio.ic.ac.uk/~phyre2/html/page.cgi?id=index) visualized by Phyre2/jsmol (Kelley et al., 2015), in both truncated versions of *hei10* 3D structure models (sequence coverage of 94-100% of total residues and confidence of 99%) were largely disrupted, suggesting functional impairment of resulting truncated proteins (Fig 15). To confirm *in silico* predictions, indirect immunolocalization of HEI10 in meiocytes of *hei10-1, -2* and wild-type barley cv GP was performed. In both isolated alleles no HEI10 focal signal on the SC as in the WT was found, suggesting absence of a full-length HEI10 protein in both *hei10-1* and *hei10-2* and specificity of the generated antibodies (Fig 15).

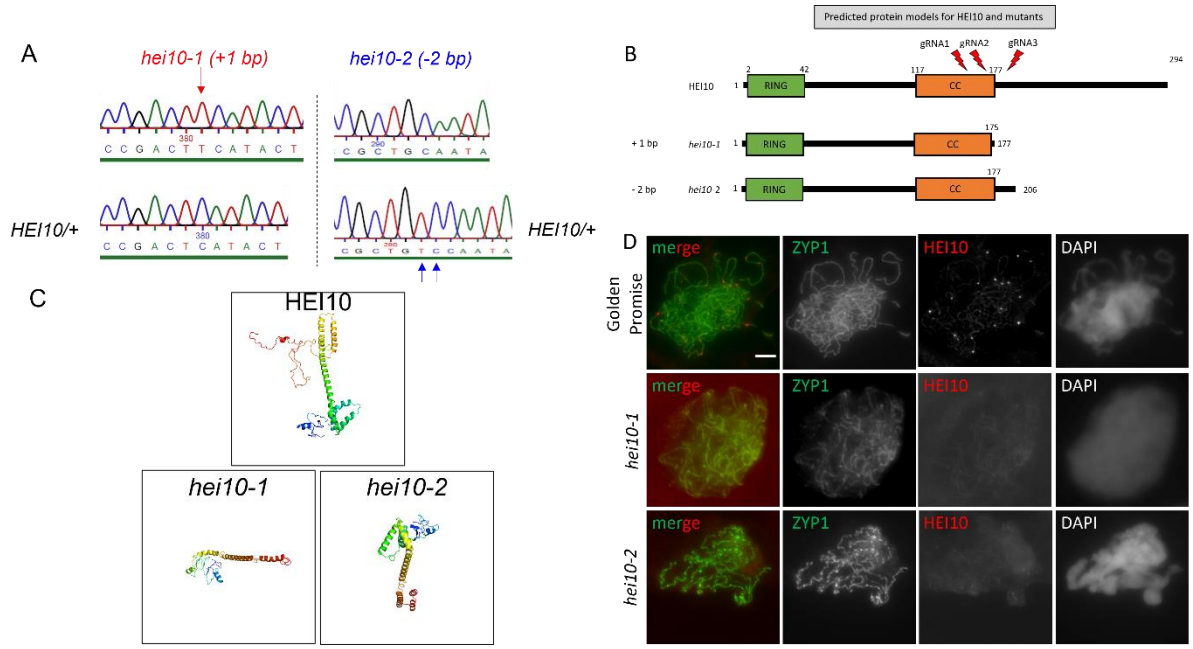

Figure 15 Isolation of *Hvhei10-1* and *Hvhei10-2* in barley.

(A) Sanger-sequencing of *hei10-1* and *hei10-2*: Insertion of 1 bp (red arrow) and deletion of 2 bp (blue arrows) compared to WT, respectively. Predicted protein **(B)** and secondary protein structure **(C)** for HEI10, *hei10-1* and *hei10-2*. **(D)** Zygotene/pachytene nuclei stained with ZYP1 (green), HEI10 (red) and DAPI-stained DNA (grey) in GP, *hei10-1* and *-2*.

4.1.7 Severe fertility reduction in *hei10* plants

All plants (heterozygous/homozygous *hei10-1* and *hei10*-2 as well as WT-segregating siblings) showed normal vegetative growth and development. However, a severe reduction in fertility in homozygous *hei10-1* and *hei10-2* plants was found compared to WT and heterozygous *hei10-*

1 and *hei10-2* plants (Fig 16). In *hei10-2* only three grains and in *hei10-1* only one grain in 35 and 40 spikes collected, respectively, were found (Fig 16). Interestingly, *hei10-1* (n=52) and *hei10-2* (n=49) heterozygous plants showed a reduction in grain number/spike compared to their corresponding segregating WT siblings (n=33) by 17.75% (unpaired t-test between *hei10-1* heterozygous and HEI10-1/HEI10-1, *P*=0.01) and by 12.39% (unpaired t-test between *hei10-2* heterozygous and HEI10-2/HEI10-2, *P*<0.004), respectively (Fig 16).

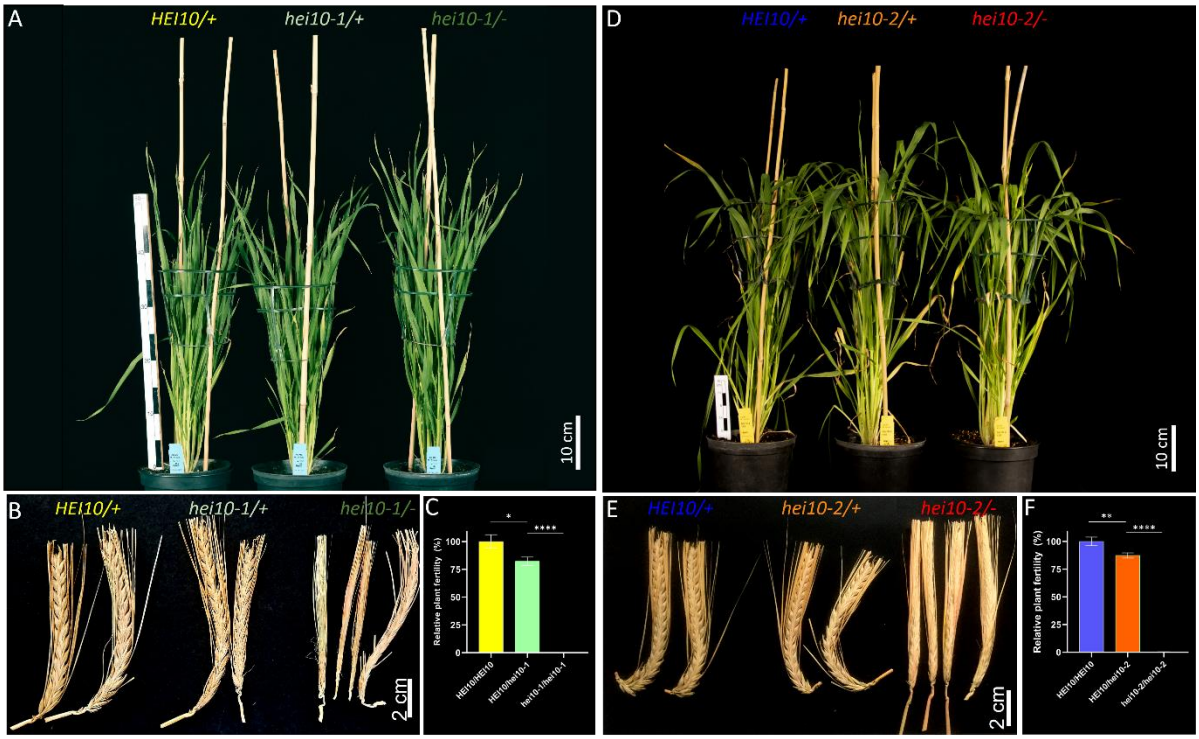

G

Genotype	Viability (%)
HEI10-1/+	98.15
hei10-1/-	2.28
HEI10-2/+	98.075
hei10-2/-	2.425

Figure 16 Phenotype of *hei10* plants.

(A) Six-week-old barley *HEI10/+*, *hei10-1/+* and *hei10-1/-* plants. Spike and grains per spike for **(B, C)** *HEI10/+*, *hei10-1/+*, *hei10-1/-* and for **(E, F)** *HEI10/+*, *hei10-2/+*, *hei10-2/-*. **(D)** Ten-week-old barley *HEI10/+*, *hei10-2/+* and *hei10-2/-* plants. **(G)** Pollen viability assessed by I_2-KI staining in plants homozygous for *hei10-1* and *-2* and their WT segregating siblings. At least five independent plants per genotype used to score grain setting. A minimum of 4000 pollen grains were counted from a least three independent plants from each genotype.

4.1.8 Meiotic abnormalities in *hei10* plants

Whether meiosis was affected causing the reduced fertility in *Hvhei10-1* and *-2*, male meiotic chromosome spread analysis was performed. In WT, homologs align and synapse during zygotene and pachytene. During diplotene, desynapsis occurs and chromosomes condense until diakinesis resulting in homologous chromosome pairs being visible as bivalents connected by chiasmata, either as rod- (at least one CO) or ring-shaped (at least two CO) bivalent. At

metaphase I, all seven bivalents are aligned on the metaphase I plate. Homologous chromosomes are segregated into two opposing poles at anaphase I resulting into seven chromosomes at each side. At metaphase II, chromosomes are aligned at two metaphase plates inside the pollen mother cell. Sister chromatids are segregated during anaphase II forming four sets each with seven chromatids. Tetrads are formed at the end of meiosis II and four pollen grains develop (Fig 17).

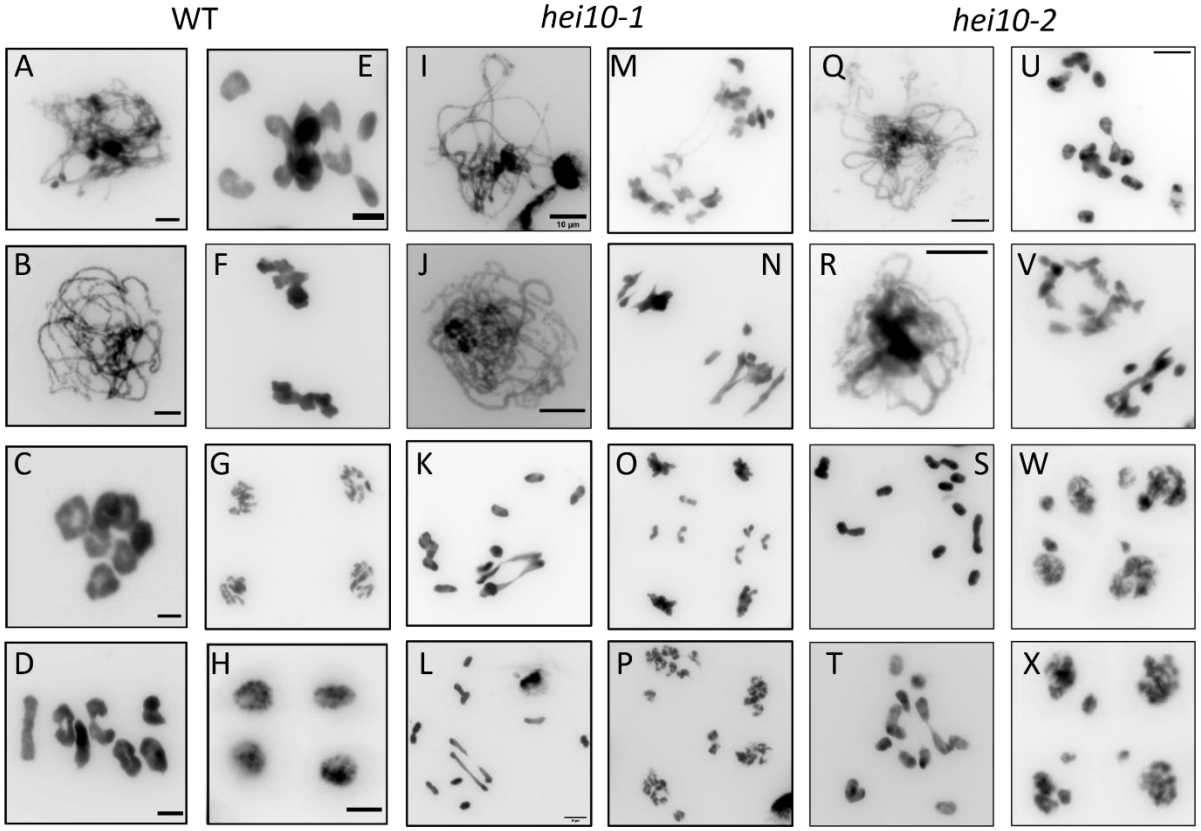

Figure 17 Meiotic atlas in the WT GP (A-H) as well as in *hei10-1* (I-P) and hei10-2 (Q-X).

(A&I&Q) zygotene, (B&J&R) pachytene, (C&K&S) (D&L&T) metaphase I, (E&M&U) anaphase I, (F&N&V) metaphase II, (G&O&W) anaphase II, (H&P&X) tetrad. DAPI-stained DNA in grey. Scale bar represents 10 µm.

In *Hvhei10-1* and *-2*, early prophase I nuclei until diplotene/diakinesis were similar to WT. At diakinesis, while in WT invariably seven bivalents were found, a high rate of univalents was found in *hei10-1* and *-2* reflecting a low number of CO. A minimum chiasma number (MCN) of 1.55 ± 1 (range 0-5) in *hei10-1* (n=93) and of 2.28 ± 1.3 (range 0-6) in *hei10-2* (n=58) was found compared with 14.34 ± 1.5 (n=68) in WT (Fig 18). Residual chiasmata numbers were significantly different between both *hei10* alleles (unpaired t-test, *P*=0.0002) (Fig 18), with slightly more chiasmata in *hei10-2* suggesting possibly residual activity of an aberrant HEI10 protein in *hei10-2*. In both mutant alleles, univalents migrated randomly to the opposite poles during anaphase I and II leading finally to unbalanced tetrads and micronuclei. Notably, in

anaphase I of *hei10-1* lagging chromosomes were rarely found, but no signs of chromosome fragmentation. Moreover, precociously separated sister chromatids at anaphase I were found in *hei10-1* similar to rice *hei10* (K. Wang et al., 2012).

While chiasma formation was reduced in *hei10*, it was not abolished with 84% and 95% of analyzed *hei10-1* and *hei10-2* cells, respectively, forming at least one bivalent. Among those, in *hei10-1*, 95.6% of bivalents were rods and only 4.4% were rings, and in *hei10-2*, 93.5% formed rods and 6.5% formed rings. In contrast, in WT most bivalents were found as rings (92.9%) and only 7.1% were rods (Fig 18).

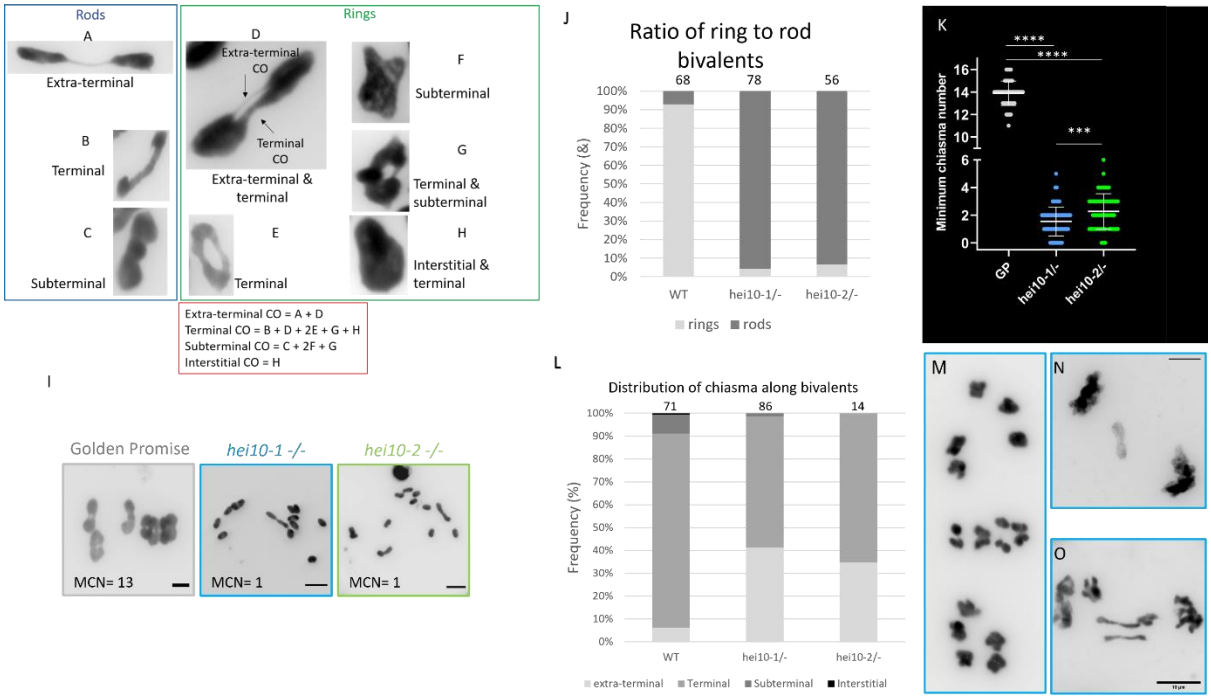

Figure 18 Residual chiasmata are proportionally enriched at chromosome ends in *hei10*.

Different positions of chiasma along bivalents during diakinesis/metaphase I scored as extra-terminal, terminal, subterminal and interstitial. Rod bivalents (blue square): **(A)** extra-terminal, **(B)** terminal, **(C)** and subterminal chiasmata. Ring bivalents (green square): **(D)** extra-terminal/terminal, **(E)** terminal/terminal, **(F)** subterminal/subterminal, **(G)** terminal/subterminal and **(H)** interstitial/terminal chiasmata. **(I, K)** Diakinesis/metaphase I bivalents in WT (GP), *hei10-1* and *hei10-2*; indicated the scored MCN per example. Scale bar represents 10 µm. **(J)** Bar plot showing ratio of ring to rod (light and dark grey, respectively) bivalents in GP, *hei10-1* and *hei10-2*. **(L)** Bar plot showing frequencies of extra-terminal (light grey), terminal (grey), subterminal (dark grey) and interstitial (black) chiasmata along bivalents in WT (GP), *hei10-1* and *hei10-2*. **(M)** Precocious sister chromatid separation (middle) in *hei10-1*. **(N, O)** Lagging chromosomes at anaphase I in *hei10-1*. Scale bar represents 10 µm.

In WT, most chiasmata were found at chromosome ends (93.9% of 893 chiasmata scored from 68 nuclei). In *hei10-1* and *-2*, residual chiasmata were proportionally enriched at chromosome ends with 98.7% (n=150; scored from 86 nuclei) and 100% (n=130; scored from 56 nuclei) analyzed chiasmata being terminal, respectively. While in WT, limited chiasmata (59 out of

893) were also found in subterminal (6.6%) and interstitial (0.6%) chromosome regions, in *hei10-1* (1.3% subterminal, no interstitial) and *hei10-2* (neither subterminal nor interstitial) they were reduced or abolished, respectively. Hence, in *hei10* among residual chiasmata a proportional enrichment of terminal chiasmata was found. Notably, a considerable fraction of terminal chiasma in *hei10-1* and *hei10-2* was found very distally named 'extra-terminal chiasma'. These chiasmata represented 6.1% of total scored chiasmata in WT, while 41.3% and 43.9% among residual chiasmata in *hei10-1* and *hei10-2*, respectively. These data imply that in *hei10* residual chiasmata are proportionally enriched towards chromosome ends particularly in form of extra-terminal chiasmata.

To evaluate the distribution of residual HEI10-independent chiasmata, the chiasma frequency distribution per cell was analyzed. In WT, the majority of chiasmata are sensitive to interference which leads to a non-random numerical distribution between cells and the mean chiasma frequency significantly deviating from a Poisson distribution $\chi 2(GP) = 66.53$, $P < 0.0001$) (Fig 19). In *hei10-1* and *-2* the chiasma frequency per cell follows a Poisson distribution $\chi 2(hei10\text{-}1) = 8.19$, $P = 0.08$), $\chi 2(hei10\text{-}2) = 4.1$, $P = 0.39$), suggesting that residual HEI10-independent chiasmata were randomly distributed between cells reminiscent of class II chiasmata that are not sensitive to interference.

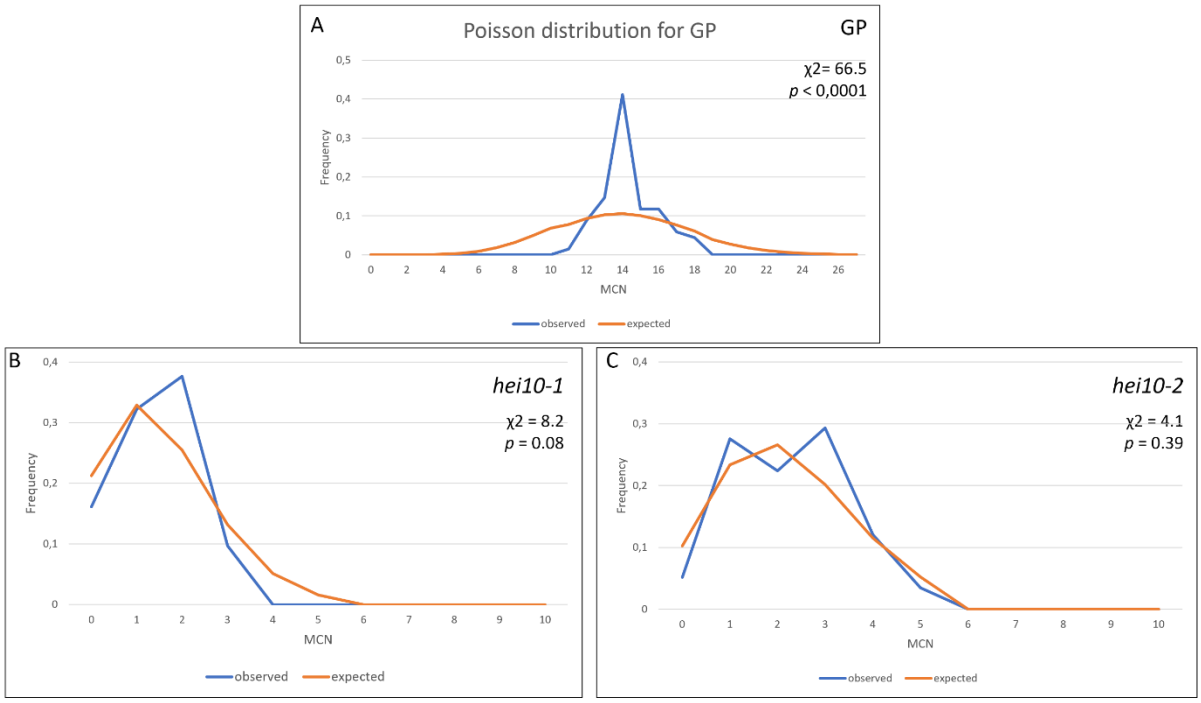

Figure 19 Residual chiasmata in *hei10* are randomly distributed among cells.

Chiasma distribution in **(A)** WT (GP), **(B)** *hei10-1* and **(C)** *hei10-2*. Observed values are represented as blue lines, while expected values according to the Poisson distribution are represented as orange lines. χ^2 and *p*-values are indicated for each genotype.

4.1.9 *hei10* is haploinsufficient

Slightly reduced fertility in plants heterozygous for *hei10-1* or *-2* compared to WT, suggested that in barley *hei10* may be haploinsufficient similar to *Arabidopsis* and mouse (Reynolds et al., 2013; Ziolkowski et al., 2017). To explore chiasma numbers in *Hvhei10-1/+* and *-2/+*, male meiotic chromosome spread analysis was performed. MCN was slightly, but statistically significant (P<0.0001), reduced in plants heterozygous for *hei10-1* and *hei10-2* to an average of 12.75 ± 1 (n=83) and 12.80 ± 1.1 (n=112), respectively, compared with 14.34 ± 1.5 (n=68) in WT (Fig 20). In terms of chiasma distribution along bivalents, a slight reduction in subterminal chiasmata rates was seen in *hei10-1/+* and *-2/+* compared to WT (Fig 20).

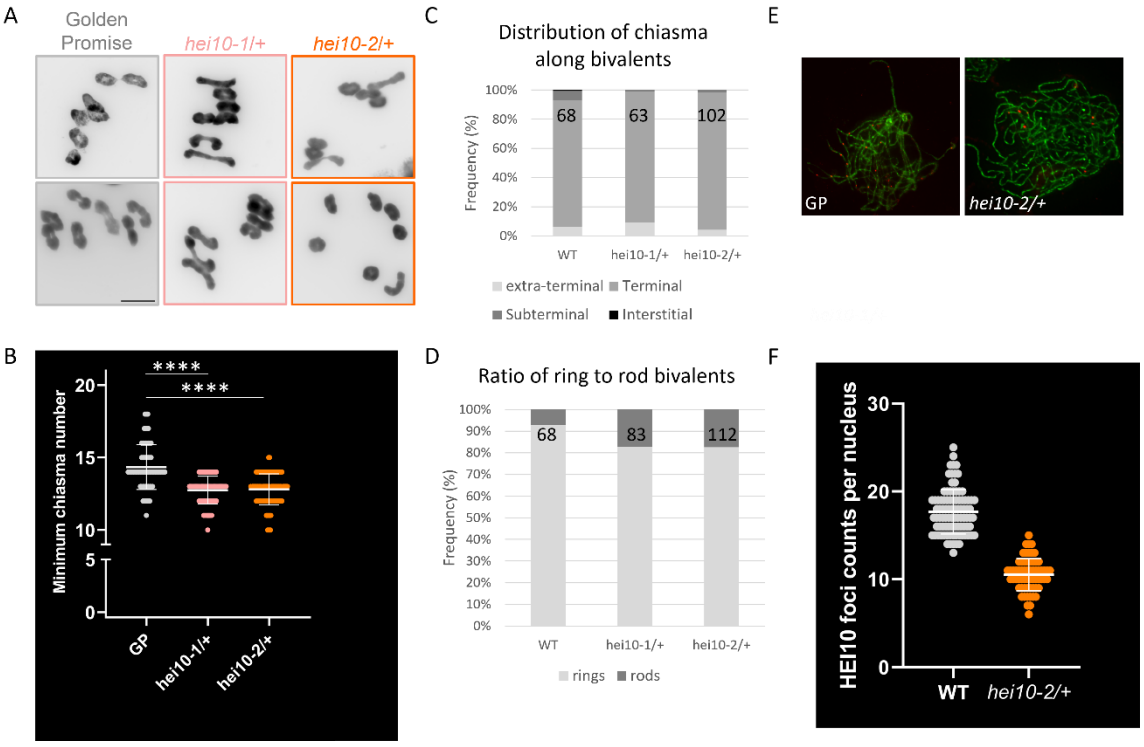

Figure 20 HEI10 shows haploinsufficiency.

(A) Diakinesis/metaphase I nuclei in GP, *hei10-1/+* and *-2/+* with their MCN quantified **(B)** shown in a dot-plot. Scale bar represents 10 µm. Frequency of chiasmata positions (extra-terminal, terminal, subterminal or interstitial) **(C)** and ratio of ring to rod bivalents **(D)** in GP, *hei10-1/+* and *-2/+*. **(E)** Male meiocytes stained with ZYP1 (green) and HEI10 (red) during pachytene in GP (left) and *hei10-2/+* (right). Scale bar represents 5 µm. **(F)** HEI10 foci quantified in *hei10-2/+* and GP.

To test *hei10* haploinsufficiency, in *hei10-2* heterozygotes as well as WT HEI10 foci numbers were scored. In WT, on average 17.69 ± 2.51 foci were scored during pachytene (n=92). In a pilot experiment using two plants for GP, a single plant for *hei10-2/+*, HEI10 foci numbers were reduced to an average of 10.53 ± 1.83 in *hei10-2/+* (Fig 20). However, the rate of reduction (~40%) of HEI10 foci in *hei10-2/+* compared to WT, was not reflected by the mild

reduction of chiasma numbers. Further experiments are needed to explain the discrepancy between chiasma counts and HEI10 foci numbers in *hei10-2/+*. These data imply that reduction of *HEI10* expression in *hei10/+* leads to (1) significant decrease in class I CO numbers and (2) a slight reduction of chiasmata rates in male meiosis.

4.1.10 DSB formation and synapsis are normal in *hei10*

For all further analysis *hei10-1* was used, given its slightly stronger phenotype in terms of residual chiasmata formation compared with *hei10-2* and absence of HEI10 focus formation. In most organisms, HEI10 loss does not impact DSB induction and synapsis (Agarwal & Roeder, 2000; Chelysheva et al., 2012; Hesse et al., 2019; A. D. Muyt et al., 2014; Qiao et al., 2014; K. Wang et al., 2012). Based on male meiotic chromosome spreads no cytological difference between WT and *hei10* was found during prophase I until diplotene/diakinesis (Fig 21). To decipher whether subtle differences between WT and *hei10* occur, DSB formation as well as axis and SC morphogenesis were dissected based on immunolocalization of γH2Ax (phosphorylated form of histone H2AX, a marker for DSBs) (Rogakou et al., 1998), ASY1 and ZYP1. In leptotene, no obvious difference in the abundance of γH2Ax was found in *hei10* compared with the WT. The dynamics and localization of ASY1 and ZYP1 were similar to WT during zygotene. By late pachytene, all chromosomes were fully synapsed labelled with ZYP1 with no asynapsed regions in *hei10* (Fig 21). Thus, in *hei10* DSB formation as well as axis and SC dynamics are cytologically similar to WT, while ZMM-dependent CO are absent with residual CO being non-interfering class II CO representing ~10% of the total CO number in barley.

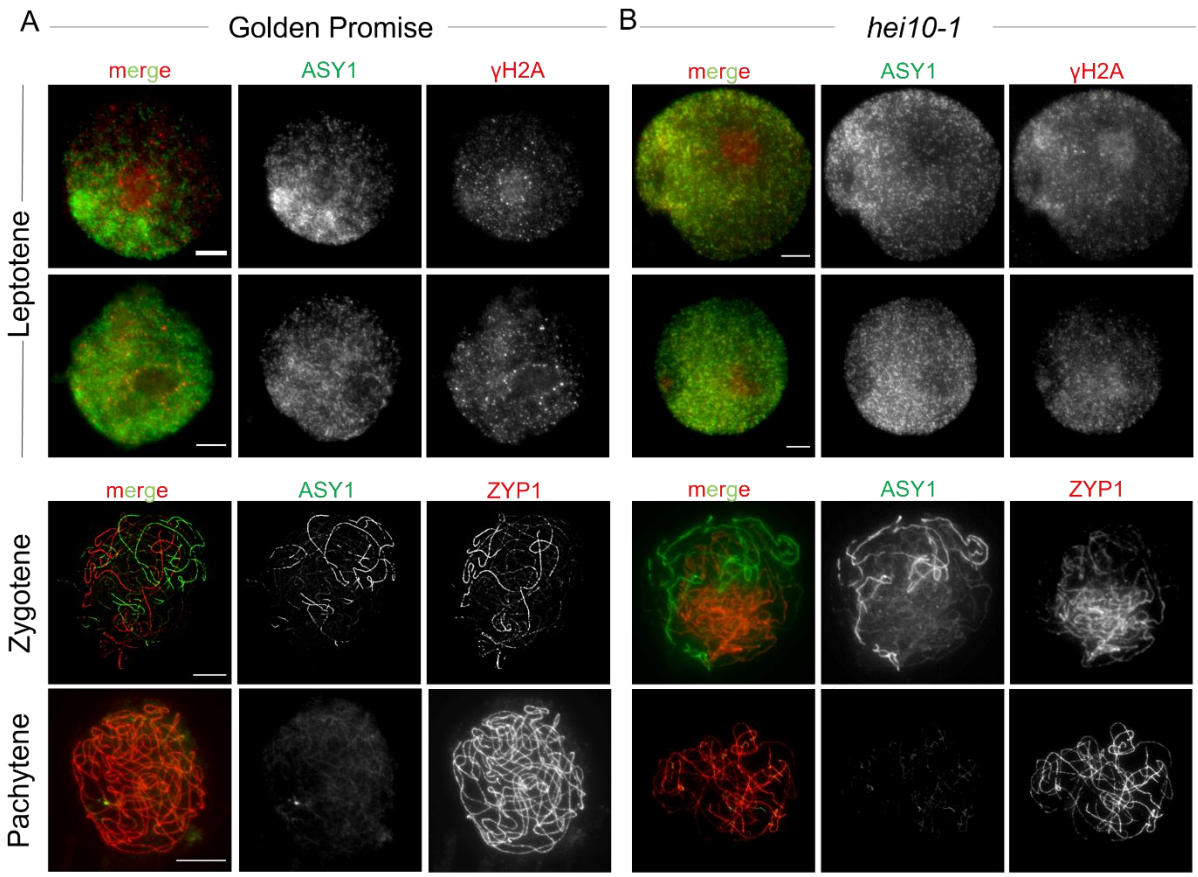

Figure 21 HEI10 is not required for DSB induction and synapsis completion.

Male WT **(A)** and *hei10-1* **(B)** meiocytes immunostained for ASY1 (green) and γH2Ax (red) during leptotene (upper images) or for ASY1 (green) and ZYP1 (red) during zygotene and pachytene (lower images). Scale bar represents 10 µm.

4.2 Anti-CO factors in barley

4.2.1 RECQ4

4.2.1.1 Identification of RECQ4 in barley

To identify RECQ4 in barley, the barley reference genome (Mayer et al., 2012) was queried using the RECQ4 aa sequence of *A. thaliana*. Two predicted models for barley *RECQ4* encoding for a 1035 (MLOC_4523.2) or 551 (HORVU2Hr1G075870.37) aa protein were identified using two different databases released in 2012 and 2016. Both versions share the downstream sequence and vary in the position of their start codon. Sequencing *RECQ4* from cDNA of spikes of cv GP and Barke, confirmed that the predicted long RECQ4 version to be the actual barley homolog. *HvRECQ4* (MLOC_4523.2) consists of 22 exons and 21 introns encoding for 3105 bp of CDS which are translated into a 1035 aa protein (Fig 22). Five synonymous SNPs were found in GP compared to the Morex CDS: 'A' at +1317 in Morex is 'T' in GP, 'G' at +1440 in Morex is 'A' in GP, 'T' at +1791 in Morex is 'C' in GP, 'C' at +1965 in Morex is 'T' in GP and 'A' at +2286 in Morex is 'T' in GP.

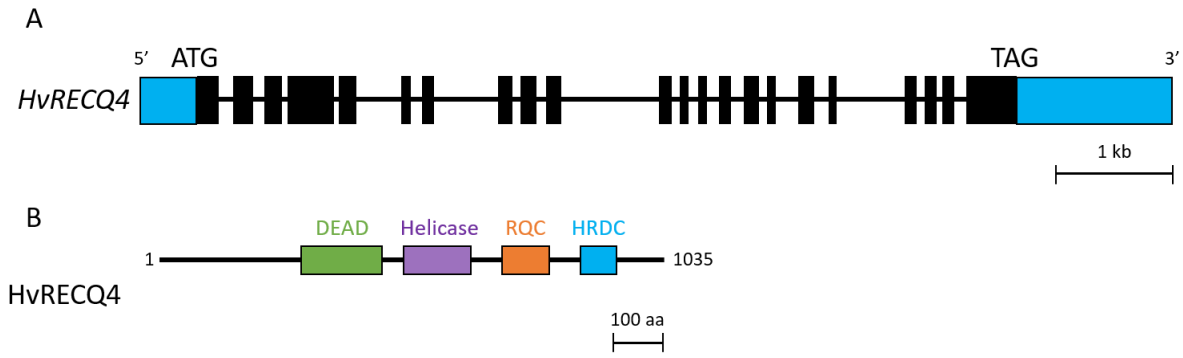

Figure 22 *HvRECQ4* gene and protein schematic models.

(A) Exon/intron structure model of *HvRECQ4*, exons in black boxes, introns are represented in black lines between exons, 5' and 3' UTRs are in blue boxes. **(B)** Protein model of HvRECQ4 highlighting the main domains; DEAD, Helicase, RQC and HRDC.

4.2.1.2 Isolation of *Hvrecq4* by CRISPR-Cas9

To isolate putative mutations within *HvRECQ4* enabling to dissect RECQ4 function *in planta*, three guide RNA (gRNA) target sites within *HvRECQ4* (within exons 1 and 5) were selected for CRISPR/Cas9. Before transformation, activity at target sites of the three gRNAs was initially confirmed *in vitro* (Fig 23). Two of the gRNAs were selected based on their secondary structure prediction and used for stable genetic transformation of barley cv GP with the vector (pGH616-2) expressing the selected two gRNAs as individual units each driven by a *TaU6* promoter together with a Ubiquitin-driven monocot codon-optimized *Cas9* designed to target

HvRECQ4 (Supplementary table 1). Among 21 T_0 plants transformed with vector (pGH616-2) to target *HvRECQ4*, 20 plants (BG857E01-21 except BG857E06) were positive for *Cas9*. Four plants showed mutations in *RECQ4* (BG857E09, BG857E11, BG857E14 and BG857E19). BG857E11 showed severe developmental defects leading to sterility and hence was not considered further. The remaining three plants showed the following mutations (positions relative to *RECQ4*'s ATG) in *RECQ4*: BG857E19 had a deletion of 'TG' at positions +146 and +147 in exon one and deletion of 'TGG' at positions +927 till +929 in exon five (named *recq4-2*), BG857E14 had a deletion of 3 bp 'TGG' at positions +146 till +148 in exon one (named *recq4-3*) and BG857E09 had a deletion of 21 bp in exon five at positions +909 till +929 (named *recq4-4*) (Fig 28). Because the open reading frame was not affected in *recq4-3* and *recq4-4*, *recq4-2* was selected for further studies.

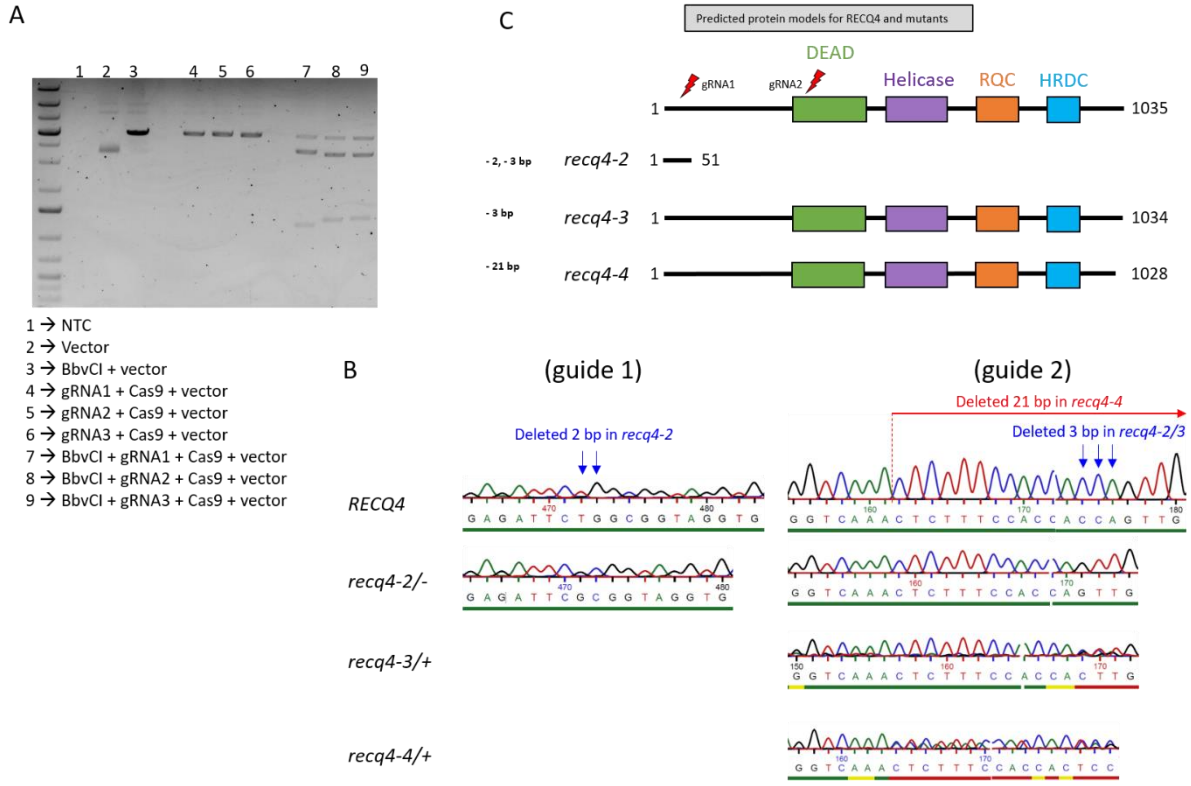

Figure 23 Isolation of *recq4* using CRISPR-Cas9 in barley.

(A) An *in-vitro* Cas9 cleavage assay confirms activity of all three gRNAs at target sites within *RECQ4*. **(B)** Sanger-sequencing chromatogram of *Hvrecq4-2*, *Hvrecq4-3* and *Hvrecq4-4* showing the position of a deletion of 2 bp 'CA' in guide RNA 1 position marked by blue arrows in *recq4-2*, deletion of 3 bp 'TGG' in *recq4-2* and *recq4-3* in guide RNA 2 position marked by three blue arrows and deletion of 21 bp in *recq4-4* in guide RNA 2 position marked by the red arrow. **(C)** Predicted primary protein models for RECQ4 in *recq4-2, recq4-3 and recq4-4* including functional domains of RECQ4 (DEAD, helicase, RQC and HRDC) and their predicted total length.

4.2.1.3 Isolation of *Hvrecq4* from a barley TILLING population

Using the barley cv Barke TILLING population (Gottwald et al., 2009), two regions within *RECQ4* were selected to search for mutations. Area one was close to the RECQ4's ATG, while area two was within helicase and RQC domains. The two areas were selected in order to possibly isolate null mutants or mutations in RECQ4's functional domains. Among ~10,000 plants, ten mutations were isolated and named: *recq4-1, -5, -6, -7, -8, -9, -10, -11, -12* and *-13* (Fig 24). A nonsense mutation (*recq4-1*) causing a pre-mature stop codon, six missense mutations including two mutations (*recq4-8* and *-9*) in the helicase domain and two silent mutations (*recq4-6* and *-7*) were isolated (Fig 24). The impact of mutations on RECQ4 was predicted using PROVEAN (http://provean.jcvi.org/seq_submit.php). Three mutations (*recq4 1, -8* and *-9*) were predicted to be deleterious, while all other mutations were predicted being neutral (Fig 24). Based on the *in-silico* prediction, *recq4-1, -8* and *-9* were selected for further experiments. In addition, *recq4-5* was considered for further studies. Plants heterozygous for *recq4-1* were backcrossed to lower secondary mutations load.

4.2.1.4 Plant fertility

To assess whether mutations in *RECQ4* cause any defects in terms of plant development or fertility in barley, plant growth and grain formation were studied for different *recq4* alleles. *recq4-1* and *-2* plants showed delayed growth and mature plants never reached the same height of either GP, Barke, segregating WT or heterozygous sibling plants (Fig 25). Two SNP *recq4* mutants (*recq4-5* and *-8*) showed a slight and severe reduction in grain setting, respectively (Fig 26). *recq4-8* and *-5* plants showed a clear delayed growth similar to *recq4-1* and *-2*, while *recq4-9* did not show any sign of defects in grain setting rates or plant growth (Fig 26). To sum up, the majority of *recq4* mutants (including *recq4-1* and *-2*) showed a slowed rate of growth and significant reduced grain numbers.

A

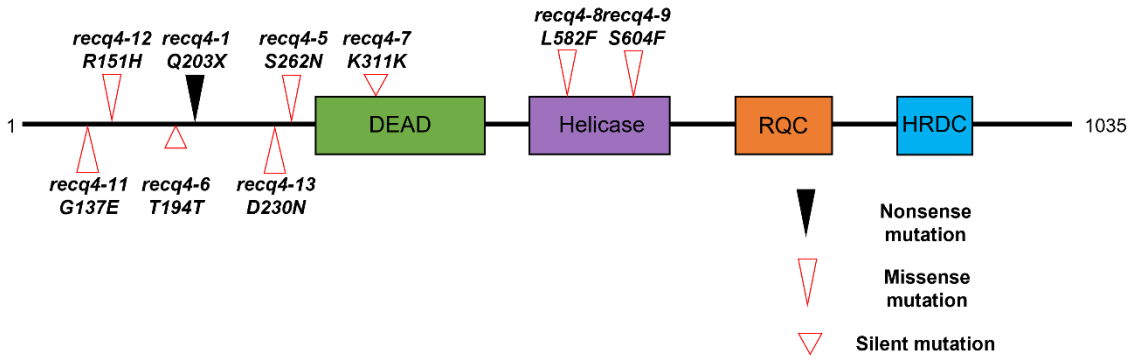

B

Mutant	Plant no.	Original AA	New AA	AA position	Mutation type	PROVEAN Prediction	PROVEAN Score (cutoff = -2.5)
recq4-1	13948	Gln	STOP	308	Nonsense	Deleterious	
recq4-5	4012	Ser	Asn	297	Missense	Neutral	-0.8
recq4-6	4142	Thr	Thr	194	Silent	Neutral	0
recq4-7	12713	Lys	Lys	311	Silent	Neutral	0
recq4-8	3112	Leu	Phe	582	Missense	Deleterious	-2.9
recq4-9	3138	Ser	Phe	604	Missense	Deleterious	-2.9
recq4-11	12937	Gly	Glu	137	Missense	Neutral	0.5
recq4-12	14283	Arg	His	151	Missense	Neutral	-2.0
recq4-13	8402	Asp	Asn	230	Missense	Neutral	-0.07

Figure 24 Mutations in *RECQ4* identified in the cv Barke TILLING population.

(A) Positions of the nine identified mutations within RECQ4 are depicted. Any change in the amino acid sequence caused by a SNP is shown. Nonsense mutation is shown by the black triangle, missense mutations are shown by long red triangle, and silent mutations are shown by short red triangle. **(B)** Isolated *recq4* mutants from the TILLING barley population. For each mutant, plant no, original AA, new AA, mutation type, prediction by PROVEAN software are indicated.

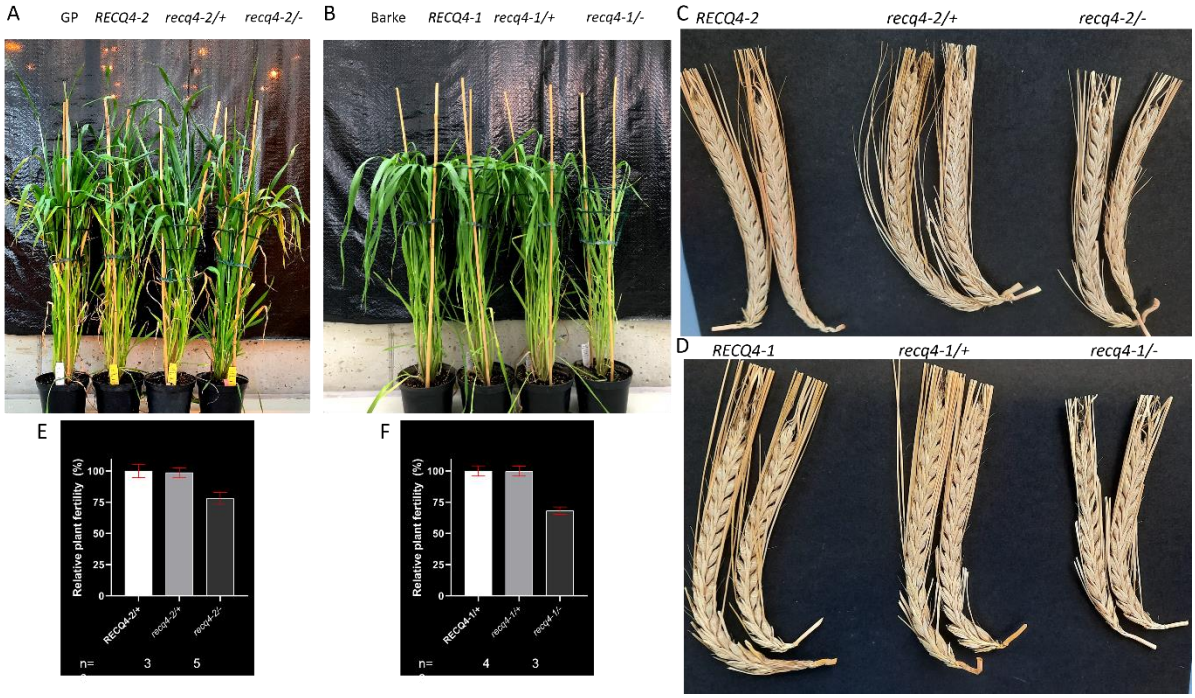

Figure 25 Phenotype of *recq4-1* and *recq4-2* plants.

(A) 10-week-old plants of GP (GP), RECQ4-2/+, *recq4-2/+*, and *recq4-2/-* as well as **(B)** Barke, RECQ4-1/+, *recq4-1/+* and *recq4-1/-*. Representative spikes of plants wild-type, hetero- and homozygous for *recq4-2* **(C)** or for *recq4-1* **(D)**. **(E)** Relative fertility of plants hetero- and homozygous for *recq4-2* or for **(F)** *recq4-1* compared to their corresponding WT siblings. Numbers of used plants are indicated below.

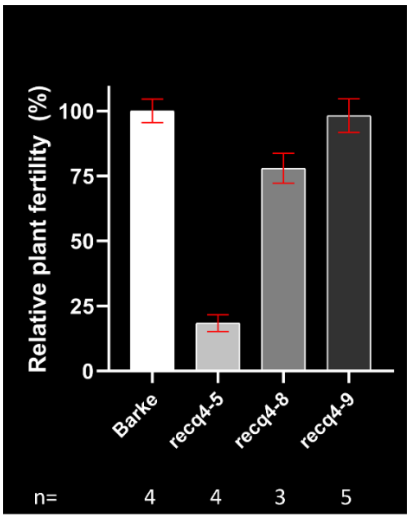

Figure 26 Fertility of *recq4-5*, *recq4-8* and *recq4-9* plants.

Plant fertility of *recq4-5*, *-8* and *-9* relative to Barke. Numbers of studied plants are indicated below.

4.2.1.5 Meiotic and mitotic behavior of *recq4*: higher chiasma numbers, change in CO distribution and meiotic and mitotic aberrations

To analyse meiotic chromosome behavior in *recq4*, male meiotic chromosome spread analysis was performed in *recq4-1*, *-2*, *-5*, *-8* and *-9*. In all mutants, the seven bivalents were always found indicating that obligatory CO is unaffected in *recq4* (Fig 27, 28). Chiasma numbers were counted at late diakinesis/metaphase I spreads. For *recq4-2*, scored average MCN was 15.55 ± 1.4 ($n_{(meiocytes)}$=75, $n_{(plants)}$=4) that was higher than those scored in GP with an average scored MCN of 14.34 ± 1.5 ($n_{(meiocytes)}$=68, $n_{(plants)}$=4) (unpaired t-test, P<0.0001) (Fig 29).

In SNP mutants, the average of MCN was 14.08 ± 0.5 ($n_{(meiocytes)}$=13, $n_{(plants)}$=1), 13.89 ± 0.3 ($n_{(meiocytes)}$=9, $n_{(plants)}$=1) and 14 ± 0.6 ($n_{(meiocytes)}$=20, $n_{(plants)}$=2) for *recq4-5*, *recq4-8* and *recq4-9*, respectively (Fig 29). These numbers were not significantly different compared to MCN in Barke which scored average MCN of 14 ± 0.8 ($n_{(meiocytes)}$=138, $n_{(plants)}$=5) (unpaired t-test, $P_{(recq4\text{-}5 \text{ and Barke})}$=0.76, $P_{(recq4\text{-}8 \text{ and Barke})}$=0.67, $P_{(recq4\text{-}9 \text{ and Barke})}$=0.97) (Fig 29). However, the null *recq4-1* showed a slight, but statistically significant, increase in the average of MCN 16.69 ± 2 ($n_{(meiocytes)}$ =35, $n_{(plants)}$=4) (unpaired t-test, P<0.0001). Moreover, more frequent interstitial and subtelomeric chiasmata were scored cytologically in *recq4-1* and *-2* compared to Barke and GP, respectively (Fig 29). Whether these increased chiasmata rates are dependent on the class I CO pathway, HEI10 foci counts were performed in diplotene nuclei of *recq4-2* and GP. No clear variation was found in numbers of HEI10 foci (on average 15.36 ± 2.52 in GP (n=28), and average of 15.27 ± 2.77 in *recq4-2* (n=22)) (Fig 30). Whether also in *recq4-1* with a similar cytological increase in chiasmata as *recq4-2* class I CO numbers (HEI10 foci numbers) are unchanged compared with the WT needs to be addressed.

The reduced number of grains and growth defects in *recq4* plants suggested possibly both meiotic and mitotic defects, respectively. To address these points, DAPI-stained chromosome spreads were performed to check the integrity of meiotic and mitotic divisions. In *recq4-2*, several chromosomal aberrations were found. DNA fragments were found after the first and second meiotic chromosome segregation leading to the formation of micronuclei and unbalanced gametes as well as after mitotic chromosome segregation (Fig 27). Moreover, chromosomal bridges were also found at anaphase I. Around 30% of total scored nuclei in meiosis I and in meiosis II/tetrads showed chromosomal abnormalities in *recq4-2*. Similar defects were found in *recq4-1* with around 20% of total meiosis I and 13% of total meiosis II nuclei exhibiting chromosomal aberrations.

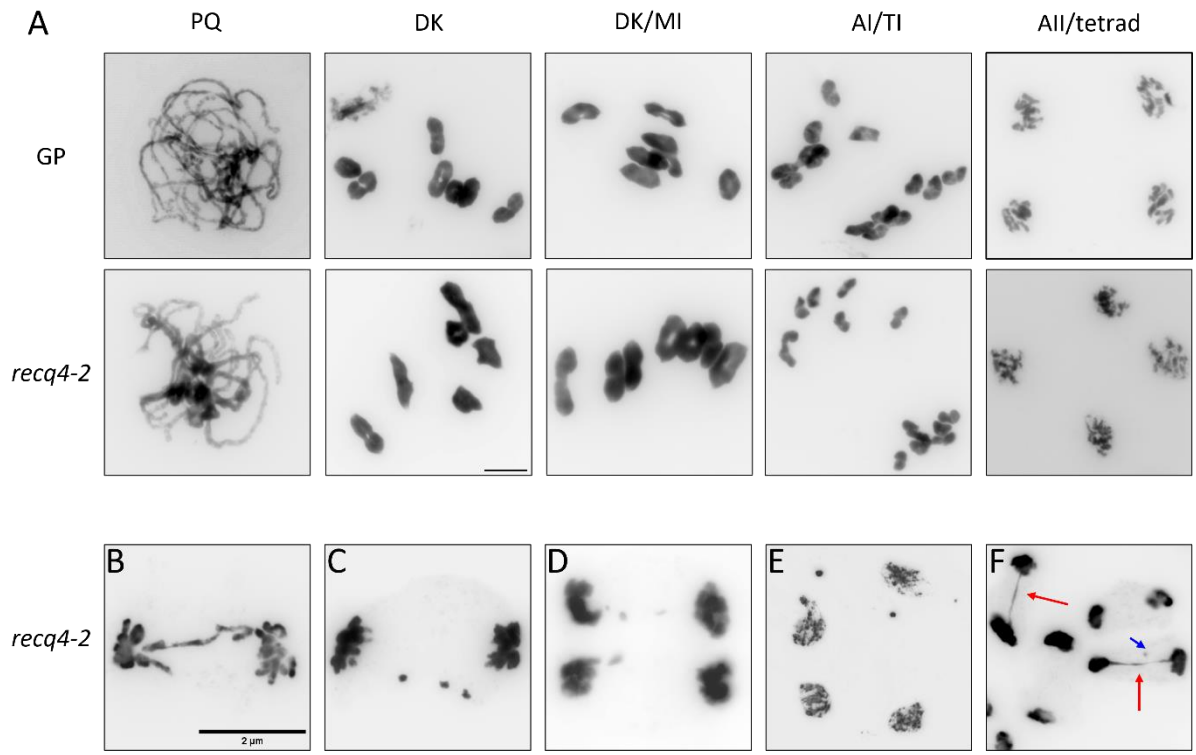

Figure 27 Chromosome spreads in *recq4-2*.

(A) Meiotic stages of pachytene, diakinesis, metaphase I, anaphase I/interkinesis and anaphase II/tetrad in *recq4-2* and GP. Scale bar represents 10 µm. **(B-F)** Defects in *recq4-2*. Scale bar represents 2 µm. **(B)** Chromosome bridge at anaphase I, chromosomal fragments at telophase I **(C)**, at telophase II **(D)**, and at tetrad stage **(E)** as well as mitotic chromosomal anaphase bridges with or without DNA fragments (red arrows point at bridges, blue arrow points at a fragment) **(F)**.

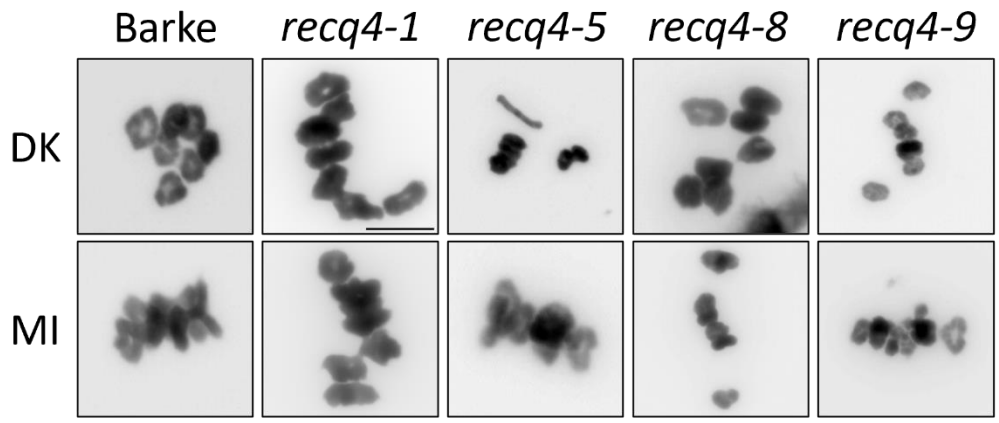

Figure 28 Diakinesis and metaphase I spreads of Barke, *recq4-1, -5, -8* and *-9*.

Scale bar represents 10 µm.

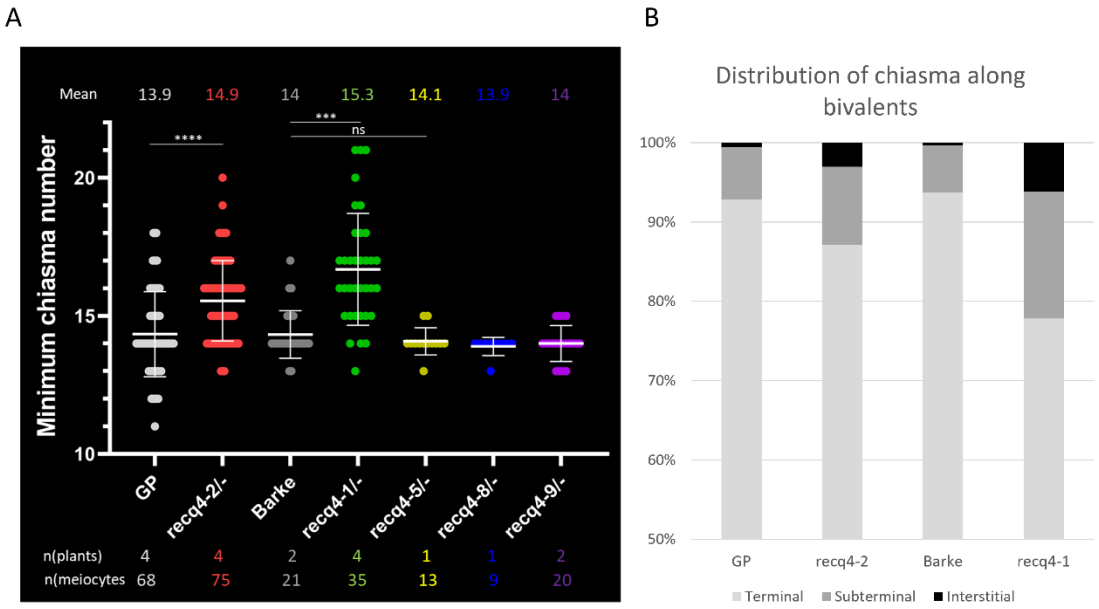

Figure 29 Null *recq4* alleles show a slight increase in chiasma numbers and more interstitial chiasmata.

(A) Quantification of MCN for all *recq4* mutant alleles and their corresponding WT. **(B)** Bar plot showing frequencies of terminal (light grey), subterminal (dark grey) and interstitial (black) chiasmata along bivalents in GP, *recq4-2*, Barke and *recq4-1*.

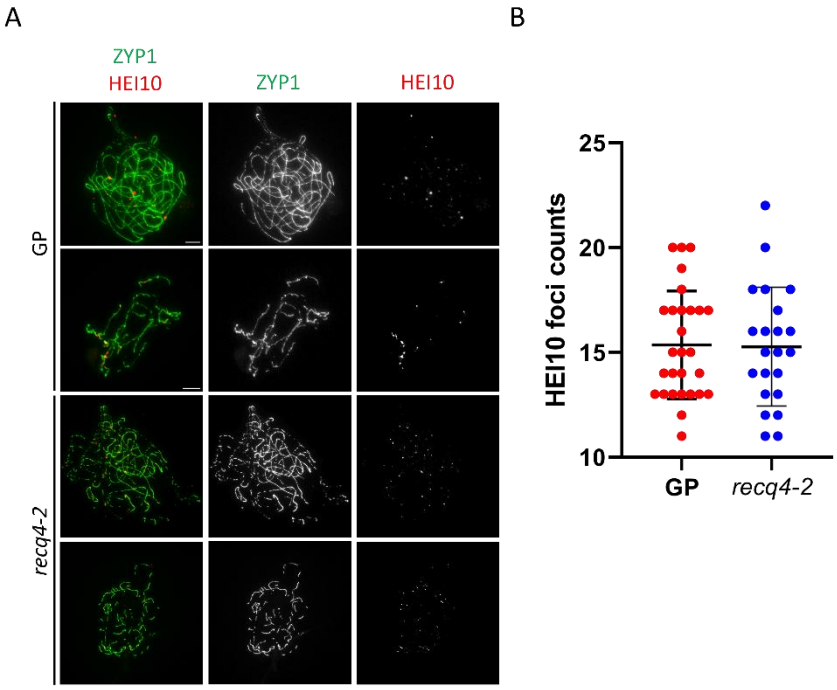

Figure 30 Cytological analysis of HEI10-dependent class I CO formation in *recq4-2*.

(A) Male meiocytes immunostained for ZYP1 (green), HEI10 (red) and DAPI-stained DNA (blue) in diplotene of *recq4-2* and GP. Scale bar represents 5 µm. Quantification **(B)** of HEI10 foci number localized on the SC (ZYP1) in diplotene nuclei in *recq4-2* and GP.

Altogether, the two *recq4* null alleles showed a slight, but statistically significant, increase in chiasmata numbers compared to their WT, while that was not observed in SNP mutant alleles. CO patterning is changed in the two null *recq4* where interstitial chiasmata were observed more frequently than in their corresponding WT. Retarded plant growth and reduced grain numbers are likely caused by genomic instability found in mitosis and meiosis in *recq4*.

4.2.1.6 Does RECQ4 have a role in mitotic DNA repair?

In Arabidopsis, RECQ4 plays a role in somatic DNA repair as the TDNA insertion mutant *Atrecq4A* showed hypersensitivity against the DNA damaging agents MMS and cis-platin (Hartung, Suer, et al., 2007). No reports showed any somatic function of *RECQ4* in crop species. Given the reduced plant height in *recq4* plants suggesting possibly genome instability, mitotic chromosome behavior was analyzed in *recq4-1* and *recq4-2* in comparison to their corresponding WT siblings. In both alleles increased frequencies of mitotic aberrations including anaphase bridges or lagging chromosomes were found compared to each WT (Fig 27). To further corroborate these findings and to decipher whether *Hvrecq4* is sensitive to DNA damaging agents zeocin (induces both single- and double-stranded DNA breaks) and MMC (induces mostly inter-strand DNA crosslinks), *recq4* and WT were challenged with 100 µg/ml zeocin or 3 µg/ml MMC and measurements of root growth were taken. Both likely null alleles of *recq4* along with their corresponding WT were tested. Both *recq4-1* and *recq4-2* plants showed hypersensitivity to zeocin compared to their corresponding WT (Barke and GP, respectively) plants as root growth was impaired in both mutant alleles compared with their respective WT plants upon zeocin treatment (Fig 31). In contrast, both *recq4* alleles did not show any obvious difference in root length compared to their WT plants when treated with MMC. In *recq4-1* and *-2* plants rates of root growth inhibition were similar as in Barke and GP plants when challenged with MMC (Fig 31). Whether under higher concentrations of MMC *recq4* plants show hypersensitivity (reduced root growth) was not tested. However, under the applied MMC concentration WT plants were impaired in root growth and *figl1* plants showed hypersensitivity (see Fig 31, 38), demonstrating that the chosen concentration was sufficient to trigger DNA damage and plant sensitivity. To sum up, increased rates of reduction in root lengths was scored in *recq4* compared to the corresponding WT when germinated grains are challenged with the single and double-stranded breaks inducer zeocin but not when challenged with MMC. The data above suggest that RECQ4 is vital for normal somatic development in barley via repairing DSBs but not repairing inter-strand DNA crosslinks.

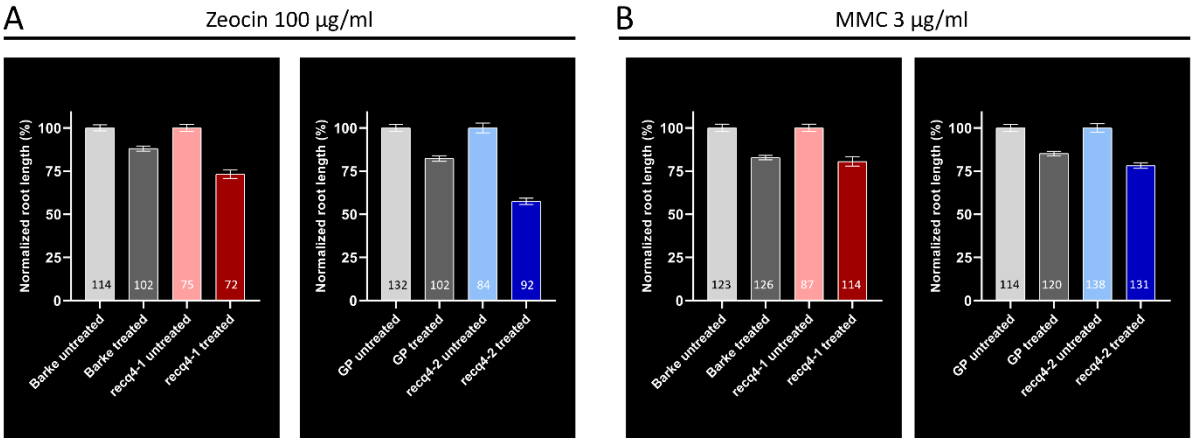

Figure 31 *recq4* is hypersensitive against Zeocin but not against MMC.

Normalized root length of 'untreated' and 'Zeocin-treated' (A) or 'untreated' and 'MMC-treated' (B) plants of *recq4-1*, *recq4-2* and their corresponding WT. Sample size of measured roots are indicated above the X-axis.

4.2.2 FIGL1

4.2.2.1 Identification of FIGL1 in barley

To identify FIGL1 in barley, the barley reference genome (Mayer et al., 2012) was queried using the aa sequence of *A. thaliana* (KM055500). As likely barley FIGL1 candidate(s), two predicted models (MLOC_6021 and HORVU5Hr1G029910.8) were identified encoding for a 681 and 519 aa protein, respectively. Both versions share ~central 430 aa and differ at N- and C- termini and vary in the position of their start codon. By sequencing *FIGL1* from cDNA from spikes of cv GP and Barke, the longer FIGL1 model (MLOC_6021) was confirmed suggesting being the actual barley homolog.

Based on the barley reference genome (Mayer et al., 2012), MLOC_6021 represents *HvFIGL1* containing 13 exons and 12 introns (Fig 32). *HvFIGL1* encodes for 2046 bp of coding sequence translated into a 682 aa protein. To establish the sequence of *FIGL1* in GP in order to design specific gRNAs, young spike cDNA was used for Sanger-sequencing. A synonymous SNP was found between GP and Morex CDS, i.e. relative to ATG 'A' at +1745 in Morex is 'G' in GP. *FIGL1* was found to be alternatively spliced in the first half of *FIGL1* transcript. Nevertheless, a central region (downstream of alternatively spliced region) including the sequence coding for the functional domain was found conserved in all sequenced *FIGL1* CDNA clones allowing to design gRNAs targeting this conserved region (Fig 32).

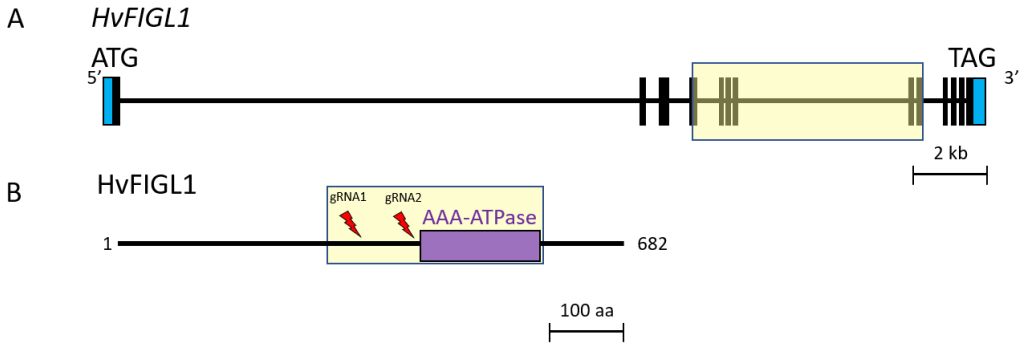

Figure 32 *HvFIGL1* gene and protein schematic models.

(A) Exon/intron structure of *HvFIGL1*; exons depicted as black boxes, introns as black lines between exons and 5'/3' UTRs as blue boxes. **(B)** The predicted protein including positions of two selected gRNAs upstream of the AAA-ATPase domain. The yellow box in (A) and (B) highlight the conserved region in all alternative splicing forms of *HvFIGL1* transcript.

4.2.2.2 Isolation of *Hvfigl1* by CRISPR-Cas9

Two guide RNA (gRNA) target sites within *HvFIGL1* (within exons four and six) were selected for CRISPR/*Cas9* to isolate mutant(s) of *figl1*. The vector (pGH622) expressing the selected two gRNA target sites of *FIGL1* as individual units each driven by a *TaU6* promoter together with a Ubiquitin-driven monocot codon-optimized *Cas9* was used to transform Barley cv GP (Suppl. table 1). Eleven plants were PCR-positive for *Cas9* among 12 independent T_0 plants. Using Sanger sequencing, a deletion of two nucleotides 'GC' that is located +1279 and +1280 and a deletion of one nucleotide 'A' located +955 in CDS, relative to ATG were found in two plants named *figl1-4* and *figl1-5*, respectively.

4.2.2.3 Isolation of *Hvfigl1* in a barley TILLING population

Two areas of interest were selected to search for mutations in *FIGL1*, using the available barley population of EMS-induced mutations. Both areas were selected based on a similar approach as for *RECQ4*. Among ~10,000 barley plants, three mutations were isolated and named: *figl1-1*, *-2* and *-3* (Fig 33). These missense SNP mutations lie within the AAA-ATPase domain. Using PROVEAN protein software (http://provean.jcvi.org/seq_submit.php), the impact of *figl1-2* and *-3* mutations was predicted, which showed both mutants are likely to have a deleterious effect (Fig 33). For *figl1-1*, a single seed was obtained that did not germinate. To reduce the secondary mutations load, *figl1-2* and *-3* were backcrossed.

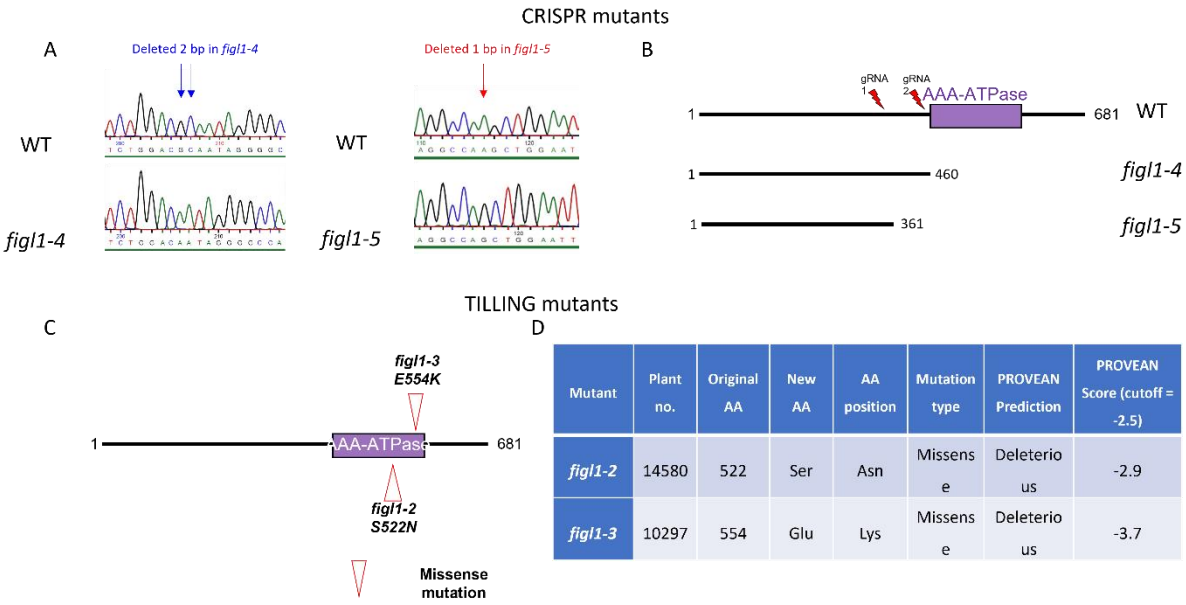

Mutant	Plant no.	Original AA	New AA	AA position	Mutation type	PROVEAN Prediction	PROVEAN Score (cutoff = -2.5)
figl1-2	14580	522	Ser	Asn	Missense	Deleterious	-2.9
figl1-3	10297	554	Glu	Lys	Missense	Deleterious	-3.7

Figure 33 Isolation of *figl1* in barley.

(A) Sanger-sequencing chromatogram of *figl1-4* and *figl1-5* (mutants generated by CRISPR): Deletion of 2 bp (blue arrows) in *figl1-4* and deletion of 1 bp (red arrow) in *figl1-5* both compared to WT. **(B)** Predicted protein of *figl1-4* and *figl1-5* with absence of AAA-ATPase domain compared to WT. **(C)** Two mutations identified in the TILLING population within *FIGL1* and their positions indicated. Missense mutations are shown by long red triangle. **(D)** For each mutant of two *figl1* mutants from the TILLING population, plant no, original AA, new AA, mutation type, prediction by PROVEAN software are indicated.

4.2.2.4 Plant fertility

Grain numbers/spike and plant growth were measured for different *figl1* mutants to evaluate whether *figl1* mutants have any influence. Grain numbers were reduced in *figl1-4* and *-5* compared to their segregating WT sibling plants suggesting that *figl1-4* and *-5* might have defects during meiosis/reproduction and/or post-fertilization events (Fig 34 and 35). Notably, a slight delay in plant growth was observed in *figl1-4* compared to GP, their WT or heterozygous segregating sibling plants (Fig 34). On the other hand, *figl1-2* and *-3* showed no difference in grain numbers or plant growth compared to their WT or heterozygous segregating sibling plants (Fig 36). Together, the null *figl1-4* showed a modest delay in plant growth and lower grain numbers, while *figl1-2* and *-3* showed no obvious difference compared with WT.

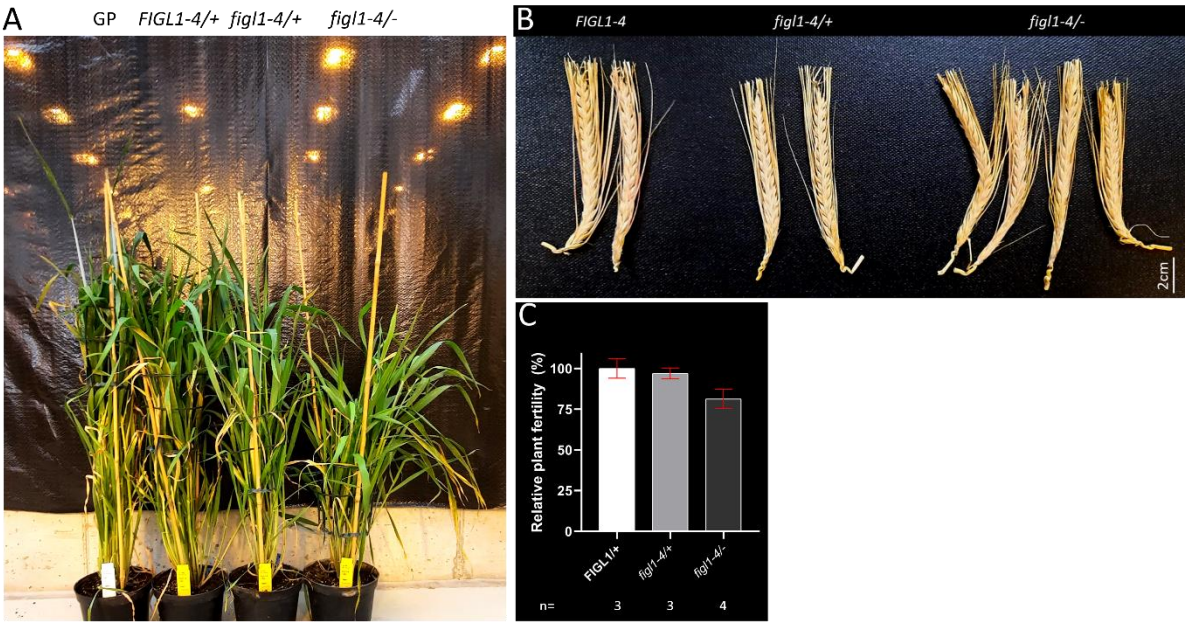

Figure 34 Fertility data of *figl1-4*.

(A) 10-week-old plants of GP, FIGL1-4/+, *figl1-4/+*, and *figl1-4/-*. **(B)** Representative spikes of each wild-type, hetero- and homozygous of *figl1-4*. **(C)** Quantification of relative plant fertility for hetero- and homozygous of *figl1-4* relative to their corresponding WT sibling of FIGL1-4/+.

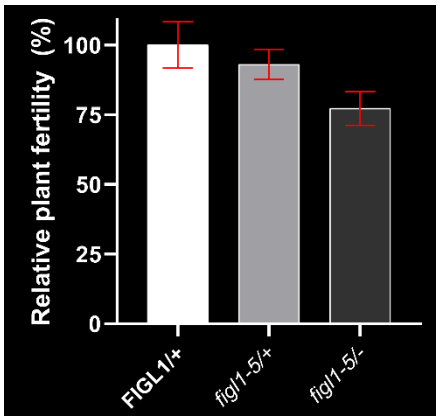

Figure 35 Fertility data of *figl1-5*.

Quantification of relative plant fertility for plants homozygous and heterozygous for *figl1-5* relative to their corresponding WT siblings of FIGL1-5/+.

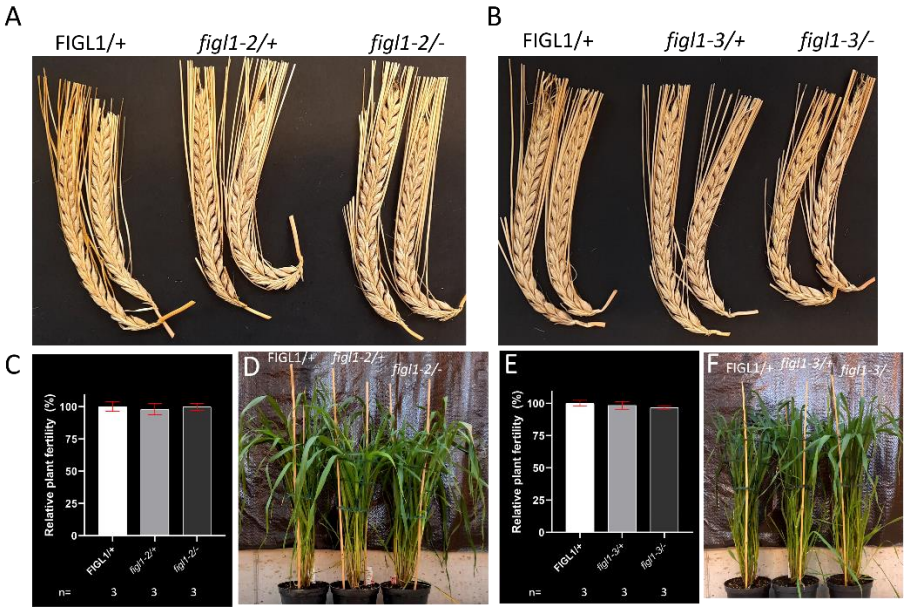

Figure 36 Fertility data of *figl1-2* and *-3*.

(A) 10-week-old plants of GP, FIGL1-4/+, *figl1-4/+*, and *figl1-4/-*. (B) Representative spikes of each wild-type, hetero- and homozygous of *figl1-4*. (C) Quantification of relative plant fertility for heterozygous of *figl1-4* relative to their corresponding WT sibling of FIGL1-4/+.

4.2.2.5 Meiotic behavior of *figl1*: less chiasma numbers and loss of obligatory CO

The reduction in fertility in the likely null mutants (*figl1-4* and *figl1-5*) suggested potentially chromosomal aberrations during meiosis. To investigate this, chromosome behavior was evaluated cytologically in male meiosis in different alleles of *figl1*. Using late diakinesis/metaphase I spreads, chiasma numbers were scored in *figl1-4*, *-5*, *-2* and *-3* parallel to GP and Barke. Surprisingly, the average MCN in *figl1-4* was 12 ± 1.61 ($n_{(meiocytes)}$=63, $n_{(plants)}$=3) and 12.4 ± 1.2 in *figl1-5* (n(meiocytes)=139, n(plants)=2) which are lower than the average of GP 14.34 ± 1.5 ($n_{(meiocytes)}$=68, $n_{(plants)}$=4) (unpaired t-test, P<0.0001) (Fig 37). In SNP mutants, the average MCN of *figl1-3* was 13.52 ± 0.85 ($n_{(meiocytes)}$=21, $n_{(plants)}$=2), a slightly reduced level compared to Barke (14 ± 0.8, $n_{(meiocytes)}$=138, $n_{(plants)}$=5) (unpaired t-test, P=0.01). However, there was no significant change in *figl1-2* (13.82 ± 0.55, $n_{(meiocytes)}$=24, $n_{(plants)}$=2)) compared to Barke (unpaired t-test, P=0.33) (Fig 37). Also, no obvious change in CO patterning was observed in any of the four *figl1* mutants.

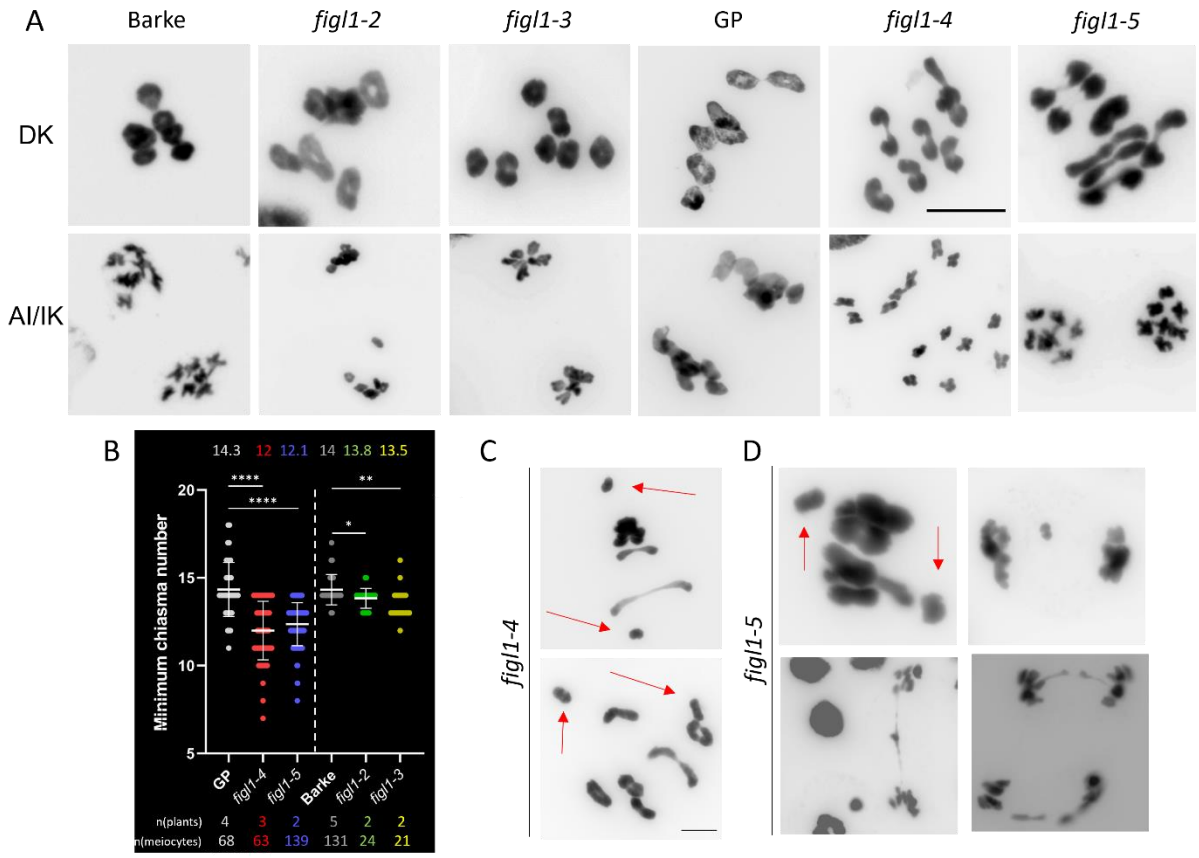

Figure 37 Null *figl1-4* and *figl1-5* show decreased chiasma numbers.

(A) Diakinesis and anaphase I/interkinesis spreads of *figl1-2*, *-3*, *-4* and *-5* along with Barke and GP. Scale bar represents 10 µm. **(B)** Quantification of MCN for all *figl1* mutant alleles and their corresponding WT. **(C)** Rare univalents (marked with red arrows) found in DK/MI spreads of *figl1-4*. **(D)** In *figl1-5*, from top left to bottom right: presence of univalents (marked with red arrows), a lagging chromosome at anaphase I, chromosome bridges during anaphase I as well as lagging chromosome and chromosomal bridges during anaphase II. Scale bar represents 5 µm.

The formation of the obligatory CO (ensuring the formation of at least one CO per chromosome pair) is one of the hallmarks of CO regulation. Interestingly, loss of the obligatory CO was found in both *figl1-4* and *figl1-5* (9/62 and 13/139 metaphase I cells showed one pair of univalents, respectively) (Fig 37) while it was neither observed in any of the SNP alleles *figl1-2* (n=24) or *figl1-3* (n=21) nor in WT (n = 64). However, 85.5% and 90.6% of metaphase I cells in *figl1-4* and *figl1-5*, respectively, did not show any sign of univalent presence. Additional meiotic defects were found in both mutants including lagging chromosomes and/or DNA fragments at both anaphase I/II and hence formation of micronuclei during the second meiotic division/tetrads. Notably, the defects were more pronounced at the second meiotic division compared to the first, suggesting majorly inter-sister DNA repair defects in *figl1*.

To summarise, *figl1-4* and *-5* showed (1) reduced chiasma rates compared to the WT, (2) the occurrence of univalents, (3) the presence of DNA fragments and/or lagging chromosome

during anaphase I/II, (4) the presence of chromosome bridges during anaphase I/II and (5) the formation of micronuclei at tetrad stage. In *figl1-3*, but not in *figl1-2*, only a modest decrease in cytological chiasma numbers was seen compared to the WT Barke.

4.2.2.6 Does FIGL1 have a role in mitotic DNA repair?

FIGL1 plays a role in somatic DNA repair in *A. thaliana*, as the *Atfigl1* mutant showed hypersensitivity against the DNA damaging agents MMC (Kumar et al., 2019). Given the reduced plant growth in *figl1* plants suggesting genome instability and the observed meiotic aberrations suggesting majorly defective inter-sister repair, it was explored whether *Hvfigl1* is also (hyper)sensitive to DNA damage. To do so, WT and *figl1* plants (the likely null allele *figl1-4* and the corresponding WT as well as *figl1-2* and *-3* and their corresponding WT Barke) were challenged with either 3 µg/ml of MMC or 100 µg/ml of zeocin and measurements of root growth were taken. In case of MMC treatment, while *figl1-4* plants were hypersensitive neither were *figl1-2* nor *figl1-3*. Root growth was reduced by almost 3-fold in *figl1-4* plants compared to GP plants, while there was no difference in root growth between *figl1-2* or *figl1-3* and Barke plants (Fig 37,38). In case of zeocin treatment, a similar situation was found as in the case of the MMC treatment. *figl1-2* and *figl1-3* plants did not show any hypersensitivity to zeocin, while *figl1-4* plants were hypersensitive to zeocin. *figl1-4* root growth was reduced to almost 75% of the root growth scored in GP plants, and no variation in root growth rates was noted when comparing *figl1-2* or *-3* with Barke plants challenged with zeocin (Fig 38 and 39). Altogether, SNP mutant alleles (*figl1-2* and *-3*) do not behave as the likely null *figl1-4* as they do not show any hypersensitivity against MMC or zeocin indicating no impact of these SNP mutations on DNA damage response at least in somatic cells.

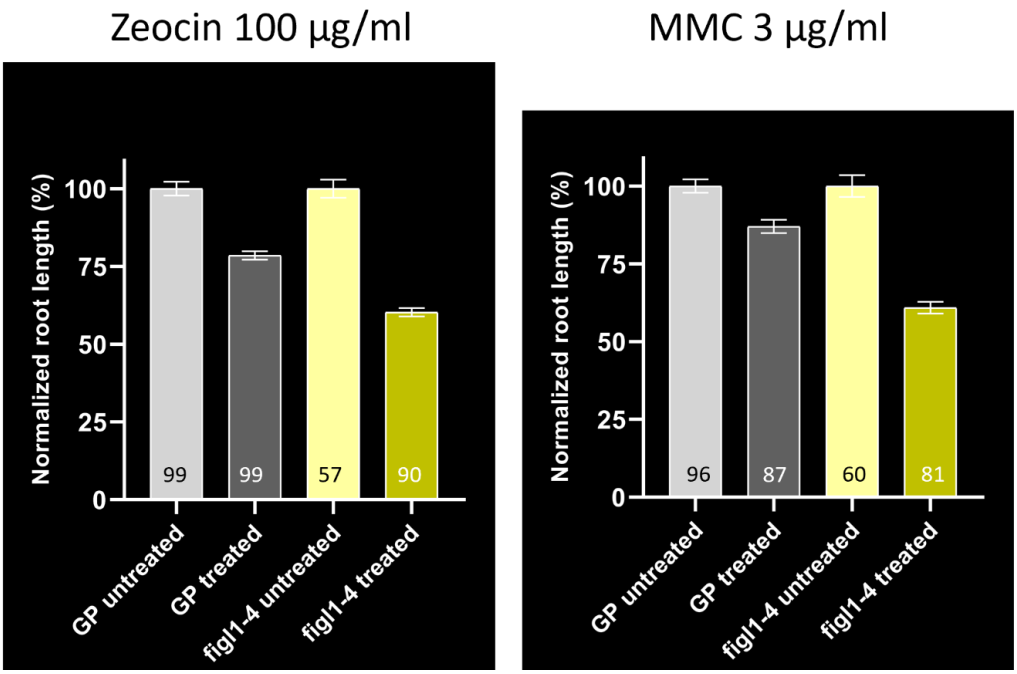

Figure 38 *figl1-4* is hypersensitive against Zeocin and MMC.

Normalized root length of 'untreated' and 'Zeocin-treated' **(A)** or 'untreated' and 'MMC-treated' **(B)** of *figl1-4* and their corresponding WT. Sample size of measured roots are indicated above the X-axis.

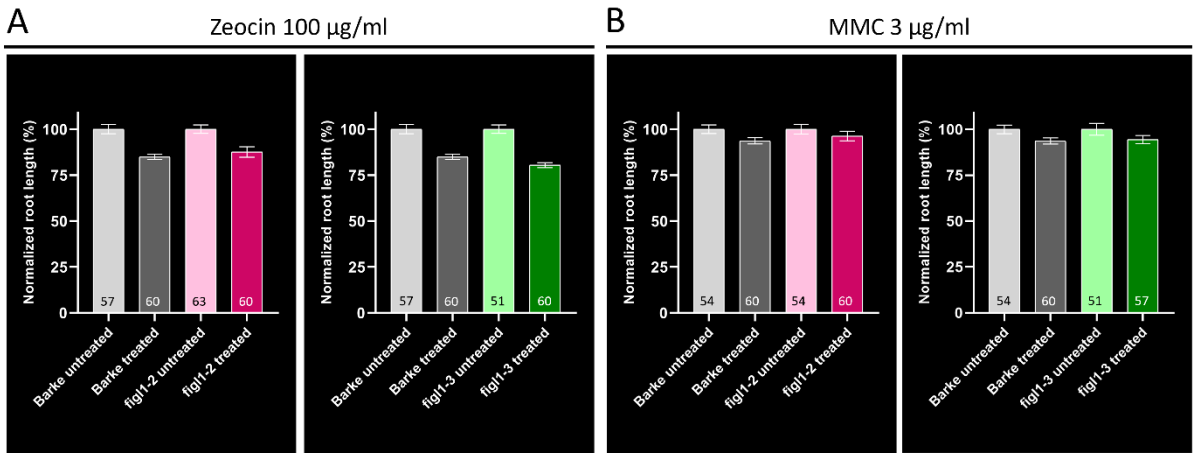

Figure 39 *figl1-2* and *-3* are not sensitive against Zeocin or MMC.

Normalized root length of 'untreated' or 'Zeocin-treated' (A) or 'untreated' and 'MMC-treated' (B) of *figl1-2* or *figl1-3* and their corresponding WT. Sample size of measured roots are indicated above the X-axis.

5 Discussion

5.1 Spatiotemporal patterning of HEI10 in barley male prophase I

During early leptotene, HEI10 appeared as hundreds of foci, with the majority being found colocalized with ZYP1 foci (usually bright foci). This suggests that HEI10 plays a role in synapsis initiation in barley similar to wheat (Osman et al., 2021). Another possibility is that pre-synaptic ZYP1 foci derive from non-homologous chromosome interactions preceding DSB-induced homology search. These interactions are stabilized by transient associations with SC proteins including Zip1, that are later detached by the 26S proteasome in yeast (Ahuja et al., 2017). Whether this is linked to the ubiquitin E3 ligase HEI10 function is to be investigated. At early zygotene, HEI10 foci localized typically at one end of short ZYP1 stretches indicating that HEI10 is either required at synapsis initiation sites or for nascent SC formation. High-resolution meiotic live cell imaging would be a helpful tool to clarify HEI10's localization/role at this stage. Interestingly, HEI10 follows the spatiotemporal localization pattern of ASY1 and ZYP1 that first start to appear at one side of the nucleus where telomeres are aggregating (Higgins et al., 2012). Therefore, axis formation, synapsis and recombination events start at telomeric positions first and then progressively extend into proximal regions, probably due to those telomeric regions being replicated first (Higgins et al., 2012). At mid/late zygotene, barley HEI10 showed a similar pattern as HEI10 in fungi, Arabidopsis and wheat, with multiple evenly-spaced small foci along the extending SC threads (beads on strings) likely marking early recombination events (Chelysheva et al., 2012; A. D. Muyt et al., 2014; Osman et al., 2021).

By late pachytene, a small fraction of the HEI10 foci acquire more molecules as they appear brighter likely marking late recombination events (i.e. more specifically class I CO). A cytological evidence for distally located bright HEI10 foci (class I CO sites) is provided after computationally isolating individual seven bivalents in late pachytene. Interestingly, most of the large HEI10 foci are flanked by the residual desynapsing ZYP1 stretches during diplotene. This is possibly due to a temporal stabilization of the SC by these HEI10-positive recombination events or inversely a transient stabilization of class I CO by the SC. A crosstalk between the SC and meiotic recombination was described in various species (Martinez-Perez et al., 2008; Rog et al., 2017; Storlazzi et al., 2008), hence a possible crosstalk also between class I CO and the SC at diplotene seems likely. However, HEI10 is not absolutely required for synapsis initiation or completion.

Interestingly, a dual localization pattern was observed for HEI10 during synapsis progression in zygotene and pachytene. Around 35% of meiotic nuclei in GP and Barke displayed a linear signal of HEI10 at asynapsed regions emerging from some ends of progressing SCs (marked by ZYP1) in addition to the typical focal HEI10 signal on synapsed regions. Given that not all zygotene/pachytene nuclei with asynapsed chromosome regions and also not all asynapsed regions in a given nucleus show this linear HEI10 signal, possibly this linear HEI10 signal might appear at quite short time windows playing a role in synapsis progression and/or CO interference. Given that HEI10 is typically used as class I CO marker at late pachytene and beyond, possibly a transient linear signal early during prophase I has been neglected. Hence, whether a linear HEI10 signal early on might also be found in other (plant) species is unclear. In wheat, MSH4 and MSH5 (also ZMM members) also showed some linear signals during zygotene and pachytene (Desjardins et al., 2020). ZMM members might have roles beyond their canonical function in meiotic recombination. At least in Sordaria data suggest that HEI10 also plays a ZMM-independent role in spindle pole bodies (SPB)/centrosomes dynamics (A. D. Muyt et al., 2014).

In a nutshell, HEI10 as a major regulator ZMM protein appears dynamic during early and late prophase I with different patterns across prophase I stages. Identifying the substrate(s) for the E3 ligase HEI10 would allow to better understand the functions of HEI10 during meiosis.

5.2 HEI10 is a ZMM member in barley's meiosis

ZMM proteins have been studied in various species including yeasts, worms, flies, plants and mammals (Bhalla et al., 2008; Jantsch et al., 2004; Qiao et al., 2014; Reynolds et al., 2013; Ward et al., 2007). In plants, multiple ZMMs were characterized in Arabidopsis and rice (Chelysheva et al., 2012; K. Wang et al., 2012). However, in large-genome crops such as barley, wheat or rye only limited reports are found on ZMMs like ZYP1 in barley (Barakate et al., 2014), ZYP4 (Martín et al., 2021) and MSH4/MSH5 (Desjardins et al., 2020) in wheat. To identify key genes important for CO regulation, it is critical to investigate the role of ZMMs in barley. HEI10 was selected as ZMM candidate due to two reasons. In Arabidopsis, HEI10 (1) is a dosage-dependent regulator of CO formation as its overexpression leads to higher CO rates and its heterozygous mutants show less CO numbers compared with WT as well as HEI10 (2) has no significant role in SC formation.

Two pre-mature stop codon *hei10* mutants were isolated using a CRISPR/Cas9 approach. Both *hei10-1* and *-2* barley plants showed almost sterility, i.e. basically no grain formation and pollen

grains were shrunk and dead. Despite zygotene and pachytene proceeding similar to the WT with WT levels of DSB formation and synapsis, meiotic defects became apparent by diakinesis. Occurrence of several pairs of univalents (reflecting the loss of the obligate CO) resulted in unbalanced meiotic chromosome segregation in anaphase I and II leading to the formation of unbalanced tetrads and micronuclei. The residual chiasmata were ~11% and ~16% of total chiasma counts in *hei10-1* and *-2* compared to the WT. This is a typical range of residual chiasma levels in *zmms* in Arabidopsis as *hei10* (Chelysheva et al., 2012), *msh4* (Higgins et al., 2004), *msh5* (Higgins et al., 2008), *shoc1*/*zip2* (Macaisne et al., 2008), and *zip4* (Chelysheva et al., 2007). However, the effect of absence of functional HEI10 in rice is less stringent as around 30% of remaining chiasma are found in *Oshei10* compared to WT (K. Wang et al., 2012). This means in rice either class I CO or at least HEI10-dependent class I CO represent around 70% of total CO numbers which are less compared to Arabidopsis and barley. *hei10-1* showed stronger phenotypes (less residual CO numbers and no produced grains) compared to *hei10-2* that showed slightly higher residual CO numbers and very limited number of produced grains. That is likely since the mutation in *hei10-1* is further upstream when compared to the position of the mutation in *hei10-2*. Additionally, the coiled-coil domain is entirely intact in *hei10-2* which is not the case in *hei10-1* as the last two aa (of the coiled-coil domain) do not exist. Notably, precocious separation of sister chromatids and lagging chromosome events were observed in both mutants indicating that loss of HEI10 led to promiscuous bipolar orientation of sister kinetochores in meiosis I similar to the phenotype of *hei10* in rice (K. Wang et al., 2012). However, no signs of chromosome fragmentation were found in *hei10*. The reduction in CO numbers was not due to any defect in earlier meiotic events. DSB formation and synapsis took place in *hei10-1* similar to the WT with no obvious defects.

In Arabidopsis, *hei10* shows to some extent haploinsufficiency by showing reduced levels of meiotic recombination. In this study, plants heterozygous for *hei10-2/+* showed significantly lower values of HEI10 foci during pachytene suggesting a reduced expression of HEI10 in the heterozygous mutant, but also referring to less class I CO. However, chiasma counts did not reflect the major reduction in HEI10 foci by showing only ~1.5 chiasma less than WT average. Further experiments are required to explain the inconsistency between chiasma numbers and HEI10 foci numbers in *hei10-2/+*. Whether also in plants heterozygous for *hei10-1*, that show slightly reduced levels of chiasmata, lower numbers of HEI10 foci are found, needs to be addressed. In Arabidopsis, reports showed that not all HEI10 foci are colocalizing with all detected MLH1/3 foci (Lloyd et al., 2018). The unavailability of a working MLH1 antibody

prevented to test this hypothesis. For certain breeding practices, it is beneficial to employ crop plants with reduced recombination rates (ideally being fertile and genetically stable) in order to fix 'desirable' linked traits. However, the reduction of recombination was not that dramatic in heterozygous *hei10* lines as well as these lines are not fully fertile. Therefore, *hei10* heterozygous lines could be good starting material to be combined with other genetic mutant(s) or environmental stress(es) to further lower meiotic recombination in barley and ideally having normal fertility rates.

To sum up, the isolation and the functional characterization of *Hvhei10* represents the first in-depth dissection of a ZMM in barley based on a null *zmm* allele. HEI10 is evolutionary highly conserved with *Hvhei10* mimicking what has been reported across kingdoms (Chelysheva et al., 2012; Reynolds et al., 2013; K. Wang et al., 2012). Loss of HEI10 led to the loss of approximately 89% of total chiasma counts, similar to the known range of residual chiasma levels in other *zmms* in Arabidopsis. In the rather large genome of barley, with seven bivalents each requiring at least one CO to assure faithful meiotic chromosome segregation, only ~1.5 chiasmata per PMC are obviously not enough to assure meiotic fidelity and hence plant fertility. No defects in early meiotic events were detected in *hei10*. Notably, *hei10-2* shows haploinsufficiency leading to decreased recombination rates in plants heterozygous for *hei10* compared to WT. On the other hand, to increase CO rates which is what breeders are primarily seeking, *HEI10* overexpression barley lines (by transforming additional copies of *HEI10*) were isolated. These lines are being cytologically characterized and analyzed for potentially elevated recombination rates. Other strategies could be in future explored in barley as reported recently in rice (Wei et al., 2023). Genome editing at transcriptional regulatory regions (5' UTRs) in *OsHEI10* resulted in rice lines with elevated *HEI10* expression and elevated recombination rates while seed setting was not greatly reduced (Wei et al., 2023).

5.3 What are the CO numbers in barley?

Estimating CO numbers in large-genome crops is not a trivial task. Different methods applied to different cultivars result in different scored numbers. A classic report showed a cytological estimation of chiasma numbers in diverse barley cultivars that differ in row number but do not drastically differ in chiasma numbers: two-rowed Bowman (13.72) or Sultan (14.05) and six-rowed Morex (13.65) or H350-1554 (13.81) (Bennett et al., 1973). The genetic map length of barley is 1136 cM (H. Li et al., 2010) that is equivalent to 22.7 CO per pollen mother cell (PMC), which is far from any of the cytological chiasmata estimations. This difference can be

explained by the difficulty to properly estimate CO numbers by counting chiasmata cytologically. Given that microscopy does not offer magnification power to resolve two (or more) adjacent CO in highly compact bivalents during diakinesis/metaphase I, it is likely that multiple adjacent CO occur at a single chiasma position. Therefore, typically chiasma counts are an underestimation of the true CO numbers in a PMC. Therefore, cytological counts are commonly called minimum chiasma numbers (MCNs). In this study, the minimum chiasma numbers were estimated (cytologically) at 14.34 ± 1.5 ($n_{(meiocytes)}$=68, $n_{(plants)}$=4) in GP and 14 ± 0.8, $n_{(meiocytes)}$=138, $n_{(plants)}$=5) in Barke. There seems to be no significant difference between both studied cultivars. Barke and GP are both two-rowed cultivars and the scored MCN for both are in a similar range as reported for other two- (and six-rowed) cultivars.

Another method used to estimate CO numbers is counting foci of class I CO markers (e.g. HEI10, MLH1 or MLH3). This method has the advantage of higher resolution compared to chiasma counts, but it neglects the minor class II CO pathway. In plants, class II CO typically represent 15% of the total CO numbers found. Hence, considering CO numbers based on genetic maps and class I CO numbers, a general estimation for the total number of CO is possible. For example, the average number of MLH3 foci in Morex is 19.2 per PMC (Phillips et al., 2013). In case this number represents 85% of total CO numbers, then the expected total CO numbers would be 22.6 which is very close to the estimated CO numbers by genetic mapping (22.7). In this study, the average HEI10 foci number during late pachytene in GP was 17.8. Given that class I CO represent around 90% of total CO numbers in GP, then the estimated numbers of CO in GP would be 20 CO per PMC. This is also in the range of the estimated total CO numbers calculated using genetic mapping.

In sum, the estimated total CO numbers in GP is 20 CO per PMC. Developing a reliable and novel method to measure directly class II CO rates would allow to strengthen this estimation.

5.4 RECQ4 is an anti-CO factor in barley

RECQ4 is the strongest identified anti-CO factor in plants so far. Hence, *RECQ4* represents a promising target gene to boost meiotic recombination in crop breeding. In pea, tomato and rice hybrids knocking out *RECQ4* resulted in a 3.2-, 2.7- and 4.7-fold CO increase compared with each corresponding WT (Mieulet et al., 2018). In a recent study in barley (Arrieta et al., 2021), a single amino acid substitution mutation (G700D) within the helicase domain of RECQ4 restored fertility in the semi-sterile *des10* (*Hvmlh3* – 53 aa deletion mutation). This mutation was shown to cause an increase in recombination rates by 2-fold compared to WT (cv Bowman)

or by 4-fold in *mlh3 recq4*$_{G700D}$ compared to *mlh3*. Also, this single mutant showed only an increase in recombination in distal chromosome regions while no effect has been found in interstitial chromosome regions using genetic mapping (Arrieta et al., 2021). So far, no report showed the effect of a null mutation of *recq4* in barley.

Here, in two barley cultivars a series of mutations in *RECQ4* was isolated using either CRISPR/Cas9 in GP or the available TILLING population in Barke. Two null mutants (*recq4-1* and *-2* in cultivars Barke and GP, respectively) showed retarded growth and reduced grain setting rates. Notably, unlike Arabidopsis, rice and tomato, *recq4* caused a major drop in plant fertility in pea (Mieulet et al., 2018). Hence, RECQ4 has a vital role in plant fertility in barley and pea. This notion was supported by observing different chromosomal abnormalities during both meiotic divisions like chromosome bridges and fragments leading to the formation of micronuclei and ultimately unbalanced gametes. In *recq4-2*, around 30% of total nuclei in meiosis I and meiosis II/tetrads showed signs of genomic instability. Similarly, about 30% of meiosis I nuclei and 18% of meiosis II /tetrads in *recq4-1* showed similar signs of genomic instability. Notably, the reduced rates of abnormalities found after the first meiotic chromosomal division compared to the second meiotic chromosomal division in *recq4-1* might be due to the difficulty to identify unbalanced tetrads (i.e. counting seven chromatids per gamete in tetrad stage). Quantification of abnormalities (at meiosis II/tetrads) were only based on the appearance of micronuclei. Thus, RECQ4 is important for male genomic stability during meiosis and consequently for plant fertility.

By checking bivalent morphology, chiasma counts were scored in *recq4-1*, *-2*, Barke and GP. Both *recq4* alleles displayed higher frequencies of recombination compared to their corresponding WT. The increase in chiasma counts was subtle being 8.5% and 16.5% in *recq4-2* and *-1* compared to their corresponding WT, but these are likely underestimates due to the low resolution of microscopy hampering to distinguish multiple adjacent CO occurring on a single chiasma. Those increased recombination events are likely linked with the class II CO pathway since HEI10 foci numbers in *recq4-2* were equivalent to those in GP. This is in agreement with class II-dependent extra recombination events found in *recq4* in Arabidopsis (Séguéla-Arnaud et al., 2017). The absence of a reliable antibody marking class II CO events hampered to decipher whether indeed the extra recombination events in *recq4* are class II CO.

Surprisingly, CO positioning was changed in both *recq4* alleles, too. Normally, interstitial chromosome regions display a low frequency of recombination events as CO are generally

skewed towards telomeric/distal regions. In *recq4-1*, 29 interstitial chiasmata were scored in *recq4-1* out of total scored 469 chiasmata (n=33), while in Barke only one interstitial chiasma was scored out of total scored 287 chiasmata (n=26). Similarly, 29 interstitial chiasmata out of total scored 965 chiasmata in *recq4-2* (n=69) which is higher than interstitial rates in Golden Promise: 5 interstitial chiasmata out of total 893 chiasmata (n=68). The change in CO distribution was not found in the SNP mutant allele $recq4_{G700D}$ that might be explained by potential residual function of RECQ4 in this mutant allele. However, another tool (a high-throughput recombination measurement e.g. single barley pollen genotyping based on crystal Digital PCR (Y. J. Ahn et al., 2021), see outlook) might be needed to confirm the cytological observation seen in *recq4-1* and *-2*. Additionally, to see the extent of CO increase and whether it also works in a hybrid background, meiotic recombination should be assessed in *recq4-1 x recq4-2* hybrids.

The human homolog of RECQ4 is BLM. Mutations in BLM cause bloom syndrome characterized by the tendency to form cancer and developmental defects (Chu & Hickson, 2009). Barley RECQ4 has also a somatic role as null alleles caused retarded plant growth. Using root sensitivity assay to chemical drugs inducing DNA damage, *recq4-1* and *-2* were hypersensitive to ss- and ds-DNA breaks induced by Zeocin but not sensitive to interstrand DNA crosslinks created by MMC. This is surprising since *recq4a/b* Arabidopsis plants were hypersensitive to crosslinking agents (MMS and cis-platin) (Hartung, Suer, et al., 2007). An evolutionary divergence in the mitotic role for RECQ4 could have taken place between Arabidopsis and barley. In addition, chromosomal aberrations like chromosome fragments or bridges were found during mitotic division. This provides a cytological evidence for the genomic instability found in *recq4*. However, RECQ4 could be still considered for breeders. *recq4* plants show increased recombination rates and more importantly changed CO positioning as interstitial CO were found. Because of the genomic instability and slightly reduced grain numbers, *recq4* plants can be used for a few rounds of meiosis to achieve a novel shuffling of barley genes before *recq4* mutations can be crossed out. Moreover, obtaining barley plants with higher grain numbers are not the only aim for breeders, plants with e.g. strong defence mechanisms against biotic and abiotic stresses, that could be obtained by a new combination of alleles, are also advantageous.

In a nutshell, RECQ4 has significant roles in DNA repair during meiosis and mitosis. Loss of barley RECQ4 led to (1) reduced grain numbers likely due to genomic instability during

meiosis, (2) higher rates of cytological chiasmata, (3) increased rates of interstitial chiasmata and (4) retarded plant growth & hypersensitivity to Zeocin due to mitotic genomic instability.

5.5 Is FIGL1 an anti-CO factor in barley?

Although FIGL1 in pea, tomato and rice is essential for fertility, barley *figl1-4* and -*5* showed only 20% and 25% reduction in grain numbers compared to their corresponding WT segregating sibling plants. This resembles the reduction in produced seeds/fruits in Col-0 of *A. thaliana* (Fernandes, Séguéla-Arnaud, et al., 2018). Strikingly, *figl1-4* and -*5* showed instead of higher rates of chiasmata as found in Arabidopsis, the frequent occurrence of univalents (loss of obligatory CO phenomenon) and a lower number of scored chiasmata compared to GP. The loss of the obligatory CO indicates that FIGL1 could even play a role in promoting class I CO in barley similar to FANCM's role in wheat (Desjardins et al., 2022). In future, counting HEI10 foci in *figl1* as proxy for class I formation/numbers will be critical to test this hypothesis. Whether FIGL1 also has an anti-CO factor function in barley, determining class II CO rates by crossing *figl1* with a *zmm* e.g. *hei10* would be essential. Genome instability was also noted in *figl1-4* and -*5* plants. Multiple chromosomal defects were found during both meiotic divisions, but defects during the second meiotic division were more frequent suggesting a role for FIGL1 in inter-sister DNA repair in barley. Defects like fragmentation, lagging chromosomes, chromosome bridges and micronuclei were found. *Hvfigl1-4* plants showed retarded and slow growth, similar to those harboring *Hvrecq4-1* and -*2*. This indicates that FIGL1 might also have a somatic role. That was confirmed by showing *figl1-4* being hypersensitive to DNA damage created by Zeocin and MMC. The variation in function of FIGL1 in fertility and recombination pathways in Arabidopsis, pea, tomato, rice and barley indicates for an evolutionary divergence.

To sum up, FIGL1 shows a lack of functional conservation across plant species as mutations in *HvFIGL1* caused only a reduction in grain numbers, unlike other crops like pea, rice and tomato where mutations in *FIGL1* led to plant sterility. More surprisingly, *figl1* showed less scored chiasmata and the loss of the obligatory CO, indicating that FIGL1 in barley is likely required for the class I CO pathway. In addition, meiotic defects (DNA fragments, lagging chromosomes, chromosome bridges and micronuclei) were noted in *figl1* that are likely causing the reduced grain numbers. The applicability for usage of *FIGL1* in breeding is still to be explored. If the meiotic recombination map using a high-throughput method e.g. single pollen nucleus genotyping in hybrids showed no significant change in CO landscape in *figl1* then it might not be considered a suitable candidate gene for plant breeding. Further experiments are

required to reveal FIGL1 function in the class II CO pathway. Finally, FIGL1 is required for DNA repair in somatic and meiotic cells.

5.6 How CO distribution can be modified?

In various mutagenesis studies performed to modify/boost meiotic recombination, extra recombination events occurred within distal regions of chromosomes. For example, in Arabidopsis mutants of *recq4a/b*, *figl1*, *zyp1*, *hcr1* and *sni1* all showed increased recombination rates but mainly at distal chromosomal regions (Capilla-Pérez et al., 2021; Fernandes, Séguéla-Arnaud, et al., 2018; France et al., 2021; Girard et al., 2015; Nageswaran et al., 2021b; Séguéla-Arnaud et al., 2017; Zhu et al., 2021). That is beneficial for application in crop breeding, but to get the full potential of mixing parental alleles, especially in large-genome crops where the vast majority of chromosomes are composed of heterochromatin, it would be more beneficial to also allow meiotic recombination events in (naturally) rarely recombining (peri-)centromeric regions. Is meiotic recombination in (peri)centromeric regions lethal? Recombination around centromeres was associated with chromosome segregation defects and aneuploidy (Rockmill et al., 2006). However, the genetic polymorphisms in Arabidopsis centromeric repeats caused by various mechanisms including gene conversions (Ma & Bennetzen, 2006) suggests the existence of centromere-proximal recombination events.

A few studies have shown the potential to modify CO distribution leading to increased CO rates in interstitial/(peri)centromeric regions. In Arabidopsis, in mutants causing disruption of non-CG DNA methylation and H3K9me2, higher rates of pericentromeric recombination were found (Underwood et al., 2018). Overexpression of HEI10 in Arabidopsis leads to an increase in recombination rates majorly in distal chromosomal regions, but a slight increase was observed at interstitial regions, too (Ziolkowski et al., 2017). It will be exciting to either find new ways to manipulate recombination events close to (peri)centromeric region or to apply these Arabidopsis approaches testing the influence of disrupted H3K9me2 and non-CG DNA methylation or overexpression of HEI10 in barley and other crops.

6 Outlook

In future, the following points should be addressed:

1- Whether increased HEI10 dosage results in elevated levels of meiotic recombination in barley, isolated plants with additional copies of *HEI10* and higher HEI10 dosage should be analyzed both cytological (meiotic chromosome behavior, chiasmata and HEI10 foci counts) and molecular (recombination rates in segregating offspring populations and/or in hybrid pollen nuclei) for altered recombination rates.

2- Assessing whether *recq4* also leads to increased meiotic recombination rates in hybrid plants. To do so, meiotic recombination rates should be dissected in *recq4-1* x *recq4-2* plants based on molecular markers in segregating offspring populations and/or via high-throughput crystal digital PCR-based single pollen nucleus genotyping in F_1 hybrids.

3- Deciphering which CO pathway is affected in *figl1* by i) counting HEI10 foci in *figl1* and by ii) introgression of *figl1* in *hei10* plants being defective for class I CO formation to analyze their fertility (grain counts) and meiotic behavior (chiasmata counts, immunolocalization of key meiotic proteins).

4- Addressing whether despite presence of univalents in *figl1*, absence of *figl1* leads to increased CO rates and/or to an altered meiotic recombination landscape based on recombination rate measurements in segregating offspring populations and/or single pollen nucleus genotyping in hybrids.

5- Isolation of *recq4 figl1* double mutant barley plants, to study their combined effect on meiosis/fertility (plant growth, grain setting, meiotic chromosome behavior, chiasma counts, immunolocalization of key meiotic proteins) and on the recombination landscape (recombination frequencies in offspring plants and/or pollen nuclei).

7 Summary

Here, strategies to alter the meiotic recombination landscape in barley haven been both explored and developed.

i) Various mutant alleles of the anti-CO factors *RECQ4* and *FIGL1* were isolated in two different barley cultivars through CRISPR/Cas9 or screening of a TILLING population and cytologically characterized.

ii) Mutations in *RECQ4* (*recq4-1* and -*2*) caused increased numbers of chiasma and a change in CO distribution as more interstitial and subtelomeric chiasma were cytologically scored in barley. Hence, *recq4* could be valuable for barley breeders to explore the potential of increased shuffling of typically low-recombining genomic regions. However, *HvRECQ4* is also required for both meiotic and mitotic DNA repair leading to reduced plant growth and reduced grain numbers.

iii) Absence of *FIGL1* affected plant fertility but it did not result in lethality as in other crop plants. However, different to Arabidopsis where *figl1* results in a *hyperrecombination* phenotype, in barley *figl1* showed the loss of the obligate CO (limited frequency of univalents) and cytologically a decreased number of chiasmata. Moreover, HvFIGL1 is required for both faithful meiotic and mitotic DNA repair and hence absence of *figl1* results in genome instability characterized by reduced fertility and plant growth.

iv) To characterize in-depth the first ZMM member in barley, HEI10 spatiotemporal dynamics were studied cytological and two CRISPR/Cas9-isolated mutant alleles of *HEI10* were characterized.

v) HEI10 followed the spatiotemporal asymmetric localization pattern of ASY1 (axes) and ZYP1 (SC) that starts from telomeres and gradually extends towards centromeric regions likely linked to the skewed CO distribution in barley.

vi) HEI10 showed a dual localization pattern relative to ZYP1; focal at synapsed and linear at selected asynapsed regions. This may suggest a role of HEI10 apart from localizing at recombination sites, possibly related to CO interference or synapsis.

vii) In barley, HEI10-dependent class I CO account for ~90% of total CO numbers.

viii) *Hvhei10* showed haploinsufficiency as fertility and chiasma numbers were reduced. *HEI10* dosage is involved in class I CO numbers and hence *HEI10* could be a good candidate for breeders that seek to alter the meiotic recombination landscape.

8 Zusammenfassung

Im Rahmen dieser Arbeit wurden Strategien zur Veränderung der meiotischen Rekombinationslandschaft in der Gerste sowohl erforscht als auch entwickelt.

i) Verschiedene Mutantenallele der Anti-CO-Faktoren *RECQ4* und *FIGL1* wurden in zwei verschiedenen Gerstensorten mittels CRISPR/Cas9 oder in einer TILLING-Population isoliert und zytologisch charakterisiert.

ii) Mutationen in *RECQ4* (*recq4-1* und *-2*) führten zu einer erhöhten Anzahl von Chiasmata und einer Veränderung der CO-Verteilung, da zytologisch mehr interstitielle und subtelomerische Chiasmata in der Gerste gefunden wurden. Somit könnte *recq4* für Gerstenzüchter von praktischem Nutzen sein, um das Potenzial einer verstärkten genetischen Durchmischung von typischerweise wenig rekombinanten genomischen Regionen zu ergründen. Jedoch ist *HvRECQ4* auch für eine fehlerfreie meiotische und mitotische DNA-Reparatur erforderlich, was sich in einem geringeren Pflanzenwachstum und einer geringeren Kornanzahl in *recq4* manifestiert.

iii) Das Fehlen von *FIGL1* beeinträchtigte die pflanzliche Fertilität, führte aber nicht wie bei anderen Kulturpflanzen zur Letalität. Anders als in Arabidopsis, wo *figl1* zu einem Hyperrekombinationsphänotyp führt, kam es bei *figl1* in der Gerste zum Verlust des obligaten CO (begrenztes Vorliegen von Univalenten) und zytologisch zu einer verringerten Anzahl von Chiasmata. Darüber hinaus ist *HvFIGL1* sowohl für die fehlerfreie meiotische als auch für die mitotische DNA-Reparatur essentiell. Das Fehlen von *FIGL1* führt zu genomischer Instabilität, welches sich in einer verminderten Fertilität und einem geringeren Pflanzenwachstum zeigt.

iv) Um das erste ZMM-Mitglied in der Gerste eingehend zu charakterisieren, wurden die räumlich-zeitliche Dynamik von HEI10 zytologisch sowie zwei CRISPR/Cas9-isolierte Mutantenallele von HEI10 funktionell analysiert.

v) HEI10 folgte dem räumlich-zeitlichen asymmetrischen Lokalisierungsmuster von ASY1 (Chromosomenachse) und ZYP1 (Synaptonemaler Komplex), ausgehend von den Telomeren und sich allmählich in Richtung zentromerischer Regionen ausdehnend. Dieses hängt sehr wahrscheinlich mit der ungleichen CO-Verteilung in der Gerste zusammen.

vi) HEI10 zeigte ein duales Lokalisationsmuster im Verhältnis zu ZYP1: fokal in synaptischen und linear in ausgewählten asynaptischen Regionen. Dies könnte darauf

hindeuten, dass HEI10 neben der Lokalisierung an Rekombinationsstellen noch eine andere Rolle spielt, möglicherweise im Zusammenhang mit der CO-Interferenz oder Synapsis.

vii) In der Gerste machen HEI10-abhängige Klasse I CO ~90% der gesamten CO aus. *Hvhei10* zeigte Haploinsuffizienz, da sowohl die Fruchtbarkeit als auch die Anzahl der Chiasmata reduziert waren. Die HEI10-Dosis ist somit an der Regulation der Anzahl der Klasse I CO beteiligt. Demzufolge könnte HEI10 ein interessanter Kandidat für die Züchtung sein basierend auf einer HE110-dosisabhängigen Veränderung der meiotischen Rekombinationslandschaft.

9 References

Agarwal, S., & Roeder, G. S. (2000). Zip3 provides a link between recombination enzymes and synaptonemal complex proteins. *Cell*, *102*(2), 245–255. https://doi.org/10.1016/S0092-8674(00)00029-5

Ahn, Y. J., Fuchs, J., Houben, A., & Heckmann, S. (2021). High-throughput measuring of meiotic recombination rates in barley pollen nuclei using Crystal Digital PCRTM. *Plant Journal*, *107*(2), 649–661. https://doi.org/10.1111/tpj.15305

Ahn, Y.-J., Cuacos, M., Ayoub, M. A., Kappermann, J., Houben, A., & Heckmann, S. (2020). In Planta Delivery of Chemical Compounds into Barley Meiocytes: EdU as Compound Example. In *Methods in Molecular Biology* (Vol. 2061). https://doi.org/10.1007/978-1-4939-9818-0_27

Ahuja, J. S., Sandhu, R., Mainpal, R., Lawson, C., Henley, H., Hunt, P. A., Yanowitz, J. L., & Börner, G. V. (2017). Control of meiotic pairing and recombination by chromosomally tethered 26S proteasome. *Science*, *355*(6323), 408–411. https://doi.org/10.1126/science.aaf4778

Alexander, M. P. (1969). Differential Staining of Aborted and Nonaborted Pollen. *Stain Technology*, *44*(3), 117–122. https://doi.org/10.3109/10520296909063335

Anderson, L. K., Lohmiller, L. D., Tang, X., Hammond, D. B., Javernick, L., Shearer, L., Basu-Roy, S., Martin, O. C., & Falque, M. (2014). Combined fluorescent and electron microscopic imaging unveils the specific properties of two classes of meiotic crossovers. *Proceedings of the National Academy of Sciences of the United States of America*, *111*(37), 13415–13420. https://doi.org/10.1073/pnas.1406846111

Andronic, L. (2012). Viruses as triggers of DNA rearrangements in host plants. *Canadian Journal of Plant Science*, *92*(6), 1083–1091. https://doi.org/10.4141/CJPS2011-197

Armstrong, S. J., Caryl, A. P., Jones, G. H., & Franklin, F. C. H. (2002). Asy1, a protein required for meiotic chromosome synapsis, localizes to axis-associated chromatin in Arabidopsis and Brassica. *Journal of Cell Science*, *115*(18), 3645–3655. https://doi.org/10.1242/jcs.00048

Arrieta, M., Macaulay, M., Colas, I., Schreiber, M., Shaw, P. D., Waugh, R., & Ramsay, L. (2021). An Induced Mutation in HvRECQL4 Increases the Overall Recombination and Restores Fertility in a Barley HvMLH3 Mutant Background. *Frontiers in Plant Science*, *12*. https://doi.org/10.3389/fpls.2021.706560

Barakate, A., Higgins, J. D., Vivera, S., Stephens, J., Perry, R. M., Ramsay, L., Colas, I., Oakey, H., Waugh, R., Franklin, F. C. H., Armstrong, S. J., & Halpin, C. (2014). The synaptonemal complex protein ZYP1 is required for imposition of meiotic crossovers in barley. *Plant Cell*, *26*(2), 729–740. https://doi.org/10.1105/tpc.113.121269

Bennett, M. D., Finch, R. A., Smith, J. B., & Rao, M. K. (1973). The time and duration of female meiosis in wheat, rye and barley. *Proceedings Biological Sciences*, *183*(1072), 301–319. https://doi.org/10.1098/rspb.1973.0019

Bennett, M. D., & Rees, H. (1970). Induced variation in chiasma frequency in Rye in response to phosphate treatments. *Genetical Research*, *16*(3), 325–331. https://doi.org/10.1017/S0016672300002585

Berchowitz, L. E., Francis, K. E., Bey, A. L., & Copenhaver, G. P. (2007). The Role of AtMUS81 in Interference-Insensitive Crossovers in A. thaliana. *PLOS Genetics*, *3*(8), e132. https://doi.org/10.1371/journal.pgen.0030132

Bhalla, N., Wynne, D. J., Jantsch, V., & Dernburg, A. F. (2008). ZHP-3 acts at crossovers to couple meiotic recombination with synaptonemal complex disassembly and bivalent formation in C. elegans. *PLoS Genetics*, *4*(10). https://doi.org/10.1371/journal.pgen.1000235

Bishop, D. K., Park, D., Xu, L., & Kleckner, N. (1992). *DMCI : A Meiosis-Specific Yeast Homolog of E. coli recA Required for Recombination , Synaptonemal Complex Formation , and Cell Cycle Progression*. *69*, 439–456.

Blary, A., & Jenczewski, E. (2019). Manipulation of crossover frequency and distribution for plant breeding. *Theoretical and Applied Genetics*, *132*(3), 575–592. https://doi.org/10.1007/s00122-018-3240-1

Bomblies, K., Higgins, J. D., & Yant, L. (2015). Meiosis evolves: Adaptation to external and internal environments. *New Phytologist*, *208*(2), 306–323. https://doi.org/10.1111/nph.13499

Börner, G. V., Kleckner, N., & Hunter, N. (2004). Crossover/noncrossover differentiation, synaptonemal complex formation, and regulatory surveillance at the leptotene/zygotene transition of meiosis. *Cell*, *117*(1), 29–45. https://doi.org/10.1016/S0092-8674(04)00292-2

Cahoon, C. K., & Hawley, R. S. (2016). Regulating the construction and demolition of the synaptonemal complex. *Nature Structural & Molecular Biology*, *23*(5), Article 5. https://doi.org/10.1038/nsmb.3208

Capilla-Pérez, L., Durand, S., Hurel, A., Lian, Q., Chambon, A., Taochy, C., Solier, V., Grelon, M., Mercier, R., Institut, B., & Bourgin, J.-P. (2021). The synaptonemal complex imposes crossover interference and heterochiasmy in Arabidopsis. *Pnas*, *118*(12). https://doi.org/10.1073/pnas.2023613118/-/DCSupplemental

Chambon, A., West, A., Vezon, D., Horlow, C., Muyt, A. D., Chelysheva, L., Ronceret, A., Darbyshire, A., Osman, K., Heckmann, S., Franklin, F. C. H., & Grelon, M. (2018). Identification of ASYNAPTIC4, a

component of the meiotic chromosome axis. *Plant Physiology*, *178*(1), 233–246. https://doi.org/10.1104/pp.17.01725

Chelysheva, L., Gendrot, G., Vezon, D., Doutriaux, M. P., Mercier, R., & Grelon, M. (2007). Zip4/Spo22 is required for class I CO formation but not for synapsis completion in Arabidopsis thaliana. *PLoS Genetics*, *3*(5), 802–813. https://doi.org/10.1371/journal.pgen.0030083

Chelysheva, L., Grandont, L., Vrielynck, N., Guin, S. L., Mercier, R., & Grelon, M. (2010). An easy protocol for studying chromatin and recombination protein dynamics during Arabidopsisthaliana meiosis: Immunodetection of cohesins, histones and MLH1. *Cytogenetic and Genome Research*, *129*(1–3), 143–153. https://doi.org/10.1159/000314096

Chelysheva, L., Vezon, D., Chambon, A., Gendrot, G., Pereira, L., Lemhemdi, A., Vrielynck, N., Guin, S. L., Novatchkova, M., & Grelon, M. (2012). The Arabidopsis HEI10 is a new ZMM protein related to Zip3. *PLoS Genetics*, *8*(7). https://doi.org/10.1371/journal.pgen.1002799

Choi, K., & Henderson, I. R. (2015). Meiotic recombination hotspots—A comparative view. *Plant Journal*, *83*(1), 52–61. https://doi.org/10.1111/tpj.12870

Choulet, F., Alberti, A., & Feuillet, C. (2014). Structural and functional partitioning of bread wheat chromosome 3B. *Science (New York, N.Y.)*, *345*(6194), 288–295. https://doi.org/10.1126/science.1251788

Chu, W. K., & Hickson, I. D. (2009). RecQ helicases: Multifunctional genome caretakers. *Nature Reviews Cancer*, *9*(9), 644–654. https://doi.org/10.1038/nrc2682

Colas, I., Macaulay, M., Higgins, J. D., Phillips, D., Barakate, A., Posch, M., Armstrong, S. J., Franklin, F. C. H., Halpin, C., Waugh, R., & Ramsay, L. (2016). A spontaneous mutation in MutL-Homolog 3 (HvMLH3) affects synapsis and crossover resolution in the barley desynaptic mutant des10. *New Phytologist*, *212*(3), 693–707. https://doi.org/10.1111/nph.14061

Cole, F., Kauppi, L., Lange, J., Roig, I., Wang, R., Keeney, S., & Jasin, M. (2012). Homeostatic control of recombination is implemented progressively in mouse meiosis. *Nature Cell Biology*, *14*(4), 424–430. https://doi.org/10.1038/ncb2451

Crismani, W., Girard, C., Froger, N., Pradillo, M., Santos, J. L., Chelysheva, L., Copenhaver, G. P., Horlow, C., & Mercier, R. (2012). FANCM Limits Meiotic Crossovers. *Science*, *336*(6088), 1588–1590. https://doi.org/10.1126/science.1220381

de Muyt, A., Pereira, L., Vezon, D., Chelysheva, L., Gendrot, G., Chambon, A., Lainé-Choinard, S., Pelletier, G., Mercier, R., Nogué, F., & Grelon, M. (2009). A High Throughput Genetic Screen Identifies New Early

Meiotic Recombination Functions in Arabidopsis thaliana. *PLOS Genetics*, *5*(9), e1000654. https://doi.org/10.1371/journal.pgen.1000654

de Muyt, A., Vezon, D., Gendrot, G., Gallois, J.-L., Stevens, R., & Grelon, M. (2007). AtPRD1 is required for meiotic double strand break formation in Arabidopsis thaliana. *The EMBO Journal*, *26*(18), 4126–4137. https://doi.org/10.1038/sj.emboj.7601815

Demirci, S., Dijk, A. D. J. van, Perez, G. S., Aflitos, S. A., Ridder, D. de, & Peters, S. A. (2017). Distribution, position and genomic characteristics of crossovers in tomato recombinant inbred lines derived from an interspecific cross between Solanum lycopersicum and Solanum pimpinellifolium. *Plant Journal*, *89*(3), 554–564. https://doi.org/10.1111/tpj.13406

Desjardins, S. D., Ogle, D. E., Ayoub, M. A., Heckmann, S., Henderson, I. R., Edwards, K. J., & Higgins, J. D. (2020). MutS homologue 4 and MutS homologue 5 maintain the obligate crossover in wheat despite stepwise gene loss following polyploidization1[CC-BY]. *Plant Physiology*, *183*(4), 1545–1558. https://doi.org/10.1104/pp.20.00534

Desjardins, S. D., Simmonds, J., Guterman, I., Kanyuka, K., Burridge, A. J., Tock, A. J., Sanchez-Moran, E., Franklin, F. C. H., Henderson, I. R., Edwards, K. J., Uauy, C., & Higgins, J. D. (2022). FANCM promotes class I interfering crossovers and suppresses class II non-interfering crossovers in wheat meiosis. *Nature Communications*, *13*(1), 3644. https://doi.org/10.1038/s41467-022-31438-6

Dion, É., Li, L., Jean, M., & Belzile, F. (2007). An Arabidopsis MLH1 mutant exhibits reproductive defects and reveals a dual role for this gene in mitotic recombination. *Plant Journal*, *51*(3), 431–440. https://doi.org/10.1111/j.1365-313X.2007.03145.x

Durand, S., Lian, Q., Jing, J., Ernst, M., Grelon, M., Zwicker, D., & Mercier, R. (2022). *Dual control of meiotic crossover patterning* (p. 2022.05.11.491364). bioRxiv. https://doi.org/10.1101/2022.05.11.491364

Emmanuel, E., Yehuda, E., Melamed-Bessudo, C., Avivi-Ragolsky, N., & Levy, A. A. (2006). The role of AtMSH2 in homologous recombination in Arabidopsis thaliana. *EMBO Reports*, *7*(1), 100–105. https://doi.org/10.1038/sj.embor.7400577

Fedak, G. (1973). Increased chiasma frequency in desynaptic barley in response to phosphate treatments. *Canadian Journal of Genetics and Cytology. Journal Canadien de Genetique et de Cytologie*, *15*(3), 647–649. https://doi.org/10.1139/g73-076

Ferdous, M., Higgins, J. D., Osman, K., Lambing, C., Roitinger, E., Mechtler, K., Armstrong, S. J., Perry, R., Pradillo, M., Cuñado, N., & Franklin, F. C. H. (2012). Inter-homolog crossing-over and synapsis in

arabidopsis meiosis are dependent on the chromosome axis protein atasy3. *PLoS Genetics*, *8*(2). https://doi.org/10.1371/journal.pgen.1002507

Fernandes, J. B., Duhamel, M., Seguéla-Arnaud, M., Froger, N., Girard, C., Choinard, S., Solier, V., Winne, N. D., Jaeger, G. D., Gevaert, K., Andrey, P., Grelon, M., Guerois, R., Kumar, R., & Mercier, R. (2018). FIGL1 and its novel partner FLIP form a conserved complex that regulates homologous recombination. *PLoS Genetics*, *14*(4). https://doi.org/10.1371/journal.pgen.1007317

Fernandes, J. B., Séguéla-Arnaud, M., Larchevêque, C., Lloyd, A. H., & Mercier, R. (2018). Unleashing meiotic crossovers in hybrid plants. *Proceedings of the National Academy of Sciences of the United States of America*, *115*(10), 2431–2436. https://doi.org/10.1073/pnas.1713078114

Foss, E., Lande, R., Stahl, F. W., & Steinberg, C. M. (1993). Chiasma interference as a function of genetic distance. *Genetics*, *133*(3), 681–691.

France, M. G., Enderle, J., Röhrig, S., Puchta, H., Franklin, C. H., & Higgins, J. D. (2021). ZYP1 is required for obligate cross-over formation and cross-over interference in Arabidopsis. *Pnas*, *118*(14). https://doi.org/10.1073/pnas.2021671118/-/DCSupplemental

Fujitani, Y., Mori, S., & Kobayashi, I. (2002). A reaction-diffusion model for interference in meiotic crossing over. *Genetics*, *161*(1), 365–372.

Gardiner, L. J., Wingen, L. U., Bailey, P., Joynson, R., Brabbs, T., Wright, J., Higgins, J. D., Hall, N., Griffiths, S., Clavijo, B. J., & Hall, A. (2019). Analysis of the recombination landscape of hexaploid bread wheat reveals genes controlling recombination and gene conversion frequency. *Genome Biology*, *20*(1), 1–16. https://doi.org/10.1186/s13059-019-1675-6

Girard, C., Chelysheva, L., Choinard, S., Froger, N., Macaisne, N., Lehmemdi, A., Mazel, J., Crismani, W., & Mercier, R. (2015). AAA-ATPase FIDGETIN-LIKE 1 and Helicase FANCM Antagonize Meiotic Crossovers by Distinct Mechanisms. *PLoS Genetics*, *11*(7), 1–22. https://doi.org/10.1371/journal.pgen.1005369

Girard, C., Crismani, W., Froger, N., Mazel, J., Lemhemdi, A., Horlow, C., & Mercier, R. (2014). FANCM-associated proteins MHF1 and MHF2, but not the other Fanconi anemia factors, limit meiotic crossovers. *Nucleic Acids Research*, *42*(14), 9087–9095. https://doi.org/10.1093/nar/gku614

Gottwald, S., Bauer, P., Komatsuda, T., Lundqvist, U., & Stein, N. (2009). TILLING in the two-rowed barley cultivar “Barke” reveals preferred sites of functional diversity in the gene HvHox1. *BMC Research Notes*, *2*. https://doi.org/10.1186/1756-0500-2-258

Gray, S., & Cohen, P. E. (2016). Control of Meiotic Crossovers: From Double-Strand Break Formation to Designation. *Annual Review of Genetics*, *50*, 175–210.

Grelon, M., Vezon, D., Gendrot, G., & Pelletier, G. (2001). AtSPO11-1 is necessary for efficient meiotic recombination in plants. *EMBO Journal*, *20*(3), 589–600. https://doi.org/10.1093/emboj/20.3.589

Hartung, F., & Puchta, H. (2006). The RecQ gene family in plants. *Journal of Plant Physiology*, *163*(3), 287–296. https://doi.org/10.1016/j.jplph.2005.10.013

Hartung, F., Suer, S., Knoll, A., Wurz-Wildersinn, R., & Puchta, H. (2008). Topoisomerase 3α and RMI1 suppress somatic crossovers and are essential for resolution of meiotic recombination intermediates in Arabidopsis thaliana. *PLoS Genetics*, *4*(12). https://doi.org/10.1371/journal.pgen.1000285

Hartung, F., Suer, S., & Puchta, H. (2007). Two closely related RecQ helicases have antagonistic roles in homologous recombination and DNA repair in Arabidopsis thaliana. *Proceedings of the National Academy of Sciences*, *104*(47), 18836–18841. https://doi.org/10.1073/pnas.0705998104

Hartung, F., Wurz-Wildersinn, R., Fuchs, J., Schubert, I., Suer, S., & Puchta, H. (2007). The catalytically active tyrosine residues of both SPO11-1 and SPO11-2 are required for meiotic double-strand break induction in Arabidopsis. *Plant Cell*, *19*(10), 3090–3099. https://doi.org/10.1105/tpc.107.054817

He, Y., Wang, M., Dukowic-Schulze, S., Zhou, A., Tiang, C. L., Shilo, S., Sidhu, G. K., Eichten, S., Bradbury, P., Springer, N. M., Buckler, E. S., Levy, A. A., Sun, Q., Pillardy, J., Kianian, P. M. A., Kianian, S. F., Chen, C., & Pawlowski, W. P. (2017). Genomic features shaping the landscape of meiotic double-strand-break hotspots in maize. *Proceedings of the National Academy of Sciences of the United States of America*, *114*(46), 12231–12236. https://doi.org/10.1073/pnas.1713225114

Hensel, G., Valkov, V., Middlefell-Williams, J., & Kumlehn, J. (2008). Efficient generation of transgenic barley: The way forward to modulate plant-microbe interactions. *Journal of Plant Physiology*, *165*(1), 71–82. https://doi.org/10.1016/j.jplph.2007.06.015

Hesse, S., Zelkowski, M., Mikhailova, E., Keijzer, C., Houben, A., & Schubert, V. (2019). Ultrastructure and dynamics of synaptonemal complex components during meiotic pairing of rye A and B chromosomes. *Front. Plant Sci.*, *10*(773). www.frontiersin.org

Higgins, J. D., Armstrong, S. J., Franklin, F. C. H., & Jones, G. H. (2004). The Arabidopsis MutS homolog AtMSH4 functions at an early step in recombination: Evidence for two classes of recombination in Arabidopsis. *Genes and Development*, *18*(20), 2557–2570. https://doi.org/10.1101/gad.317504

Higgins, J. D., Ferdous, M., Osman, K., & Franklin, F. C. H. (2011). The RecQ helicase AtRECQ4A is required to remove inter-chromosomal telomeric connections that arise during meiotic recombination in Arabidopsis. *Plant Journal*, *65*(3), 492–502. https://doi.org/10.1111/j.1365-313X.2010.04438.x

Higgins, J. D., Perry, R. M., Barakate, A., Ramsay, L., Waugh, R., Halpin, C., Armstrong, S. J., & Franklin, F. C. H. (2012). Spatiotemporal asymmetry of the meiotic program underlies the predominantly distal distribution of meiotic crossovers in barley. *Plant Cell*, *24*(10), 4096–4109. https://doi.org/10.1105/tpc.112.102483

Higgins, J. D., Vignard, J., Mercier, R., Pugh, A. G., Jones, G. H., & Ge, S. D. (2008). *AtMSH5 partners AtMSH4 in the class I meiotic crossover pathway in Arabidopsis thaliana , but is not required for synapsis*. 28–39. https://doi.org/10.1111/j.1365-313X.2008.03470.x

Jackson, N., Sanchez-Moran, E., Buckling, E., Armstrong, S. J., Jones, G. H., & Franklin, F. C. H. (2006). Reduced meiotic crossovers and delayed prophase I progression in AtMLH3-deficient Arabidopsis. *EMBO Journal*, *25*(6), 1315–1323. https://doi.org/10.1038/sj.emboj.7600992

Jantsch, V., Pasierbek, P., Mueller, M. M., Schweizer, D., Jantsch, M., & Loidl, J. (2004). Targeted Gene Knockout Reveals a Role in Meiotic Recombination for ZHP-3, a Zip3-Related Protein in Caenorhabditis elegans. *Molecular and Cellular Biology*, *24*(18), 7998–8006. https://doi.org/10.1128/mcb.24.18.7998-8006.2004

Kelley, L. A., Mezulis, S., Yates, C. M., Wass, M. N., & Sternberg, M. J. E. (2015). The Phyre2 web portal for protein modeling, prediction and analysis. *Nature Protocols*, *10*(6), 845–858. https://doi.org/10.1038/nprot.2015.053

Kim, J., Park, J., Kim, H., Son, N., Kim, E.-J., Kim, J., Byun, D., Lee, Y., Park, Y. M., Nageswaran, D. C., Kuo, P. C., Rose, T., Dang, T., Hwang, I., Lambing, C., Henderson, I. R., & Choi, K. (2022). Arabidopsis HEAT SHOCK FACTOR BINDING PROTEIN is required to limit meiotic crossovers and HEI10 transcription. *The EMBO Journal*, *41*(14), e109958. https://doi.org/10.15252/embj.2021109958

King, J. S., & Mortimer, R. K. (1990). A polymerization model of chiasma interference and corresponding computer simulation. *Genetics*, *126*(4), 1127–1138.

Kleckner, N., Zickler, D., Jones, G. H., Dekker, J., Padmore, R., Henle, J., & Hutchinson, J. (2004). A mechanical basis for chromosome function. *Proceedings of the National Academy of Sciences of the United States of America*, *101*(34), 12592–12597. https://doi.org/10.1073/pnas.0402724101

Kovalchuk, I., Kovalchuk, O., Kalck, V., Boyko, V., Filkowski, J., Heinlein, M., & Hohn, B. (2003). Pathogen-induced systemic plant signal triggers DNA rearrangements. *Nature*, *423*(6941), 760–762. https://doi.org/10.1038/nature01683

Kumar, R., Duhamel, M., Coutant, E., Ben-Nahia, E., & Mercier, R. (2019). Antagonism between BRCA2 and FIGL1 regulates homologous recombination. *Nucleic Acids Research*, *47*(10), 5170–5180. https://doi.org/10.1093/nar/gkz225

Kurzbauer, M. T., Pradillo, M., Kerzendorfer, C., Sims, J., Ladurner, R., Oliver, C., Janisiw, M. P., Mosiolek, M., Schweizer, D., Copenhaver, G. P., & Schlögelhofer, P. (2018). Arabidopsis thaliana FANCD2 promotes meiotic crossover formation. *Plant Cell*, *30*(2), 415–428. https://doi.org/10.1105/tpc.17.00745

Lambing, C., Franklin, F. C. H., & Wang, C. J. R. (2017). Understanding and manipulating meiotic recombination in plants. *Plant Physiology*, *173*(3), 1530–1542. https://doi.org/10.1104/pp.16.01530

Lambing, C., & Heckmann, S. (2018). Tackling Plant Meiosis: From Model Research to Crop Improvement. *Frontiers in Plant Science*, *9*. https://www.frontiersin.org/article/10.3389/fpls.2018.00829

Lambing, C., Osman, K., Nuntasoontorn, K., West, A., Higgins, J. D., Copenhaver, G. P., Yang, J., Armstrong, S. J., Mechtler, K., Roitinger, E., & Franklin, F. C. H. (2015). Arabidopsis PCH2 Mediates Meiotic Chromosome Remodeling and Maturation of Crossovers. *PLoS Genetics*, *11*(7). https://doi.org/10.1371/journal.pgen.1005372

Law, C. N. (1963). *An effect of potassium on chiasma frequency and recombination*. 313–329.

Lawrence, C. W. (1961). The effect of the irradiation of different stages in microsporogenesis on chiasma frequency. *Heredity*, *16*, 83–89.

Li, F., Storme, N. D., & Geelen, D. (2017). Dynamics of male meiotic recombination frequency during plant development using Fluorescent Tagged Lines in Arabidopsis thaliana. *Scientific Reports*, *7*. https://doi.org/10.1038/srep42535

Li, H., Kilian, A., Zhou, M., Wenzl, P., Huttner, E., Mendham, N., McIntyre, L., & Vaillancourt, R. E. (2010). Construction of a high-density composite map and comparative mapping of segregation distortion regions in barley. *Molecular Genetics and Genomics*, *284*(5), 319–331. https://doi.org/10.1007/s00438-010-0570-3

Li, X., Li, L., & Yan, J. (2015). Dissecting meiotic recombination based on tetrad analysis by single-microspore sequencing in maize. *Nature Communications*, *6*, 1–9. https://doi.org/10.1038/ncomms7648

Li, X., Yu, M., Bolaños-Villegas, P., Zhang, J., Ni, D., Ma, H., & Wang, Y. (2021). Fanconi anemia ortholog FANCM regulates meiotic crossover distribution in plants. *Plant Physiology*, *186*(1), 344–360. https://doi.org/10.1093/plphys/kiab061

Lipkin, S. M., Moens, P. B., Wang, V., Lenzi, M., Shanmugarajah, D., Gilgeous, A., Thomas, J., Cheng, J., Touchman, J. W., Green, E. D., Schwartzberg, P., Collins, F. S., & Cohen, P. E. (2002). Meiotic arrest and aneuploidy in MLH3-deficient mice. *Nature Genetics*, *31*(4), 385–390. https://doi.org/10.1038/ng931

Lloyd, A., Morgan, C., Franklin, F. C. H., & Bomblies, K. (2018). Plasticity of meiotic recombination rates in response to temperature in arabidopsis. *Genetics*, *208*(4), 1409–1420. https://doi.org/10.1534/genetics.117.300588

Longair, M. H., Baker, D. A., & Armstrong, J. D. (2011). Simple neurite tracer: Open source software for reconstruction, visualization and analysis of neuronal processes. *Bioinformatics*, *27*(17), 2453–2454. https://doi.org/10.1093/bioinformatics/btr390

Ma, J., & Bennetzen, J. L. (2006). Recombination, rearrangement, reshuffling, and divergence in a centromeric region of rice. *Proceedings of the National Academy of Sciences*, *103*(2), 383–388. https://doi.org/10.1073/pnas.0509810102

Maagd, R. A. de, Loonen, A., Chouaref, J., Pelé, A., Meijer-Dekens, F., Fransz, P., & Bai, Y. (2020). CRISPR/Cas inactivation of RECQ4 increases homeologous crossovers in an interspecific tomato hybrid. *Plant Biotechnology Journal*, *18*(3), 805–813. https://doi.org/10.1111/pbi.13248

Macaisne, N., Novatchkova, M., Peirera, L., Vezon, D., Jolivet, S., Froger, N., Chelysheva, L., Grelon, M., & Mercier, R. (2008). SHOC1, an XPF Endonuclease-Related Protein, Is Essential for the Formation of Class I Meiotic Crossovers. *Current Biology*, *18*(18), 1432–1437. https://doi.org/10.1016/j.cub.2008.08.041

Macaisne, N., Vignard, J., & Mercier, R. (2011). SHOC1 and PTD form an XPF-ERCC1-like complex that is required for formation of class I crossovers. *Journal of Cell Science*, *124*(16), 2687–2691. https://doi.org/10.1242/jcs.088229

Mao, B., Zheng, W., Huang, Z., Peng, Y., Shao, Y., Liu, C., Tang, L., Hu, Y., Li, Y., Hu, L., Zhang, D., Yuan, Z., Luo, W., Yuan, L., Liu, Y., & Zhao, B. (2021). Rice MutLγ, the MLH1–MLH3 heterodimer, participates in the formation of type I crossovers and regulation of embryo sac fertility. *Plant Biotechnology Journal*, *19*(7), 1443–1455. https://doi.org/10.1111/pbi.13563

Marston, A. L., & Amon, A. (2004). Meiosis: Cell-cycle controls shuffle and deal. *Nature Reviews Molecular Cell Biology*, *5*(12), Article 12. https://doi.org/10.1038/nrm1526

Martín, A. C., Alabdullah, A. K., & Moore, G. (2021). A separation-of-function ZIP4 wheat mutant allows crossover between related chromosomes and is meiotically stable. *Scientific Reports*, *11*(1). https://doi.org/10.1038/s41598-021-01379-z

Martinez-Perez, E., Schvarzstein, M., Barroso, C., Lightfoot, J., Dernburg, A. F., & Villeneuve, A. M. (2008). Crossovers trigger a remodeling of meiotic chromosome axis composition that is linked to two-step loss of sister chromatid cohesion. *Genes and Development*, *22*(20), 2886–2901. https://doi.org/10.1101/gad.1694108

Mayer, K. F. X., Waugh, R., Langridge, P., Close, T. J., Wise, R. P., Graner, A., Matsumoto, T., Sato, K., Schulman, A., Ariyadasa, R., Schulte, D., Poursarebani, N., Zhou, R., Steuernagel, B., Mascher, M., Scholz, U., Shi, B., Madishetty, K., Svensson, J. T., … Stein, N. (2012). A physical, genetic and functional sequence assembly of the barley genome. *Nature*, *491*(7426), 711–716. https://doi.org/10.1038/nature11543

Mercier, R., Jolivet, S., Vezon, D., Huppe, E., Chelysheva, L., Giovanni, M., Nogué, F., Doutriaux, M., Horlow, C., Grelon, M., Mézard, C., & Umr, C. (2005). *Two Meiotic Crossover Classes Cohabit in Arabidopsis: One Is Dependent on MER3 , whereas the Other One Is Not*. *15*, 692–701. https://doi.org/10.1016/j.cub.2005.02.056

Mercier, R., Mézard, C., Jenczewski, E., Macaisne, N., & Grelon, M. (2015). The Molecular Biology of Meiosis in Plants. *Annual Review of Plant Biology*, *66*(1), 297–327. https://doi.org/10.1146/annurev-arplant-050213-035923

Miao, C., Tang, D., Zhang, H., Wang, M., Li, Y., Tang, S., Yu, H., Gu, M., & Cheng, Z. (2013). Central region component1, a novel synaptonemal complex component, Is essential for meiotic recombination initiation in RiceC. *Plant Cell*, *25*(8), 2998–3009. https://doi.org/10.1105/tpc.113.113175

Mieulet, D., Aubert, G., Bres, C., Klein, A., Droc, G., Vieille, E., Rond-Coissieux, C., Sanchez, M., Dalmais, M., Mauxion, J.-P., Rothan, C., Guiderdoni, E., & Mercier, R. (2018). Unleashing meiotic crossovers in crops. *Nature Plants*, *4*(12), Article 12. https://doi.org/10.1038/s41477-018-0311-x

Modliszewski, J. L., Wang, H., Albright, A. R., Lewis, S. M., Bennett, A. R., Huang, J., Ma, H., Wang, Y., & Copenhaver, G. P. (2018). Elevated temperature increases meiotic crossover frequency via the interfering

(Type I) pathway in Arabidopsis thaliana. *PLoS Genetics*, *14*(5). https://doi.org/10.1371/journal.pgen.1007384

Morgan, C., Fozard, J. A., Hartley, M., Henderson, I. R., Bomblies, K., & Howard, M. (2021). Diffusion-mediated HEI10 coarsening can explain meiotic crossover positioning in Arabidopsis. *Nature Communications*, *12*(1). https://doi.org/10.1038/s41467-021-24827-w

Morgan, C., & Wegel, E. (2020). Cytological Characterization of Arabidopsis arenosa Polyploids by SIM. In M. Pradillo & S. Heckmann (Eds.), *Plant Meiosis: Methods and Protocols* (pp. 37–46). Springer. https://doi.org/10.1007/978-1-4939-9818-0_4

Morreale, F. E., & Walden, H. (2016). Types of Ubiquitin Ligases. *Cell*, *165*(1), 248-248.e1. https://doi.org/10.1016/j.cell.2016.03.003

Muyt, A. D., Zhang, L., Piolot, T., Kleckner, N., Espagne, E., & Zickler, D. (2014). E3 ligase Hei10: A multifaceted structure-based signaling molecule with roles within and beyond meiosis. *Genes and Development*, *28*(10), 1111–1123. https://doi.org/10.1101/gad.240408.114

Nageswaran, D. C., Kim, J., Lambing, C., Kim, J., Park, J., Kim, E. J., Cho, H. S., Kim, H., Byun, D., Park, Y. M., Kuo, P., Lee, S., Tock, A. J., Zhao, X., Hwang, I., Choi, K., & Henderson, I. R. (2021a). HIGH CROSSOVER RATE1 encodes PROTEIN PHOSPHATASE X1 and restricts meiotic crossovers in Arabidopsis. *Nature Plants*, *7*(4), 452–467. https://doi.org/10.1038/s41477-021-00889-y

Nageswaran, D. C., Kim, J., Lambing, C., Kim, J., Park, J., Kim, E.-J., Cho, H. S., Kim, H., Byun, D., Park, Y. M., Kuo, P., Lee, S., Tock, A. J., Zhao, X., Hwang, I., Choi, K., & Henderson, I. R. (2021b). HIGH CROSSOVER RATE1 encodes PROTEIN PHOSPHATASE X1 and restricts meiotic crossovers in Arabidopsis. *Nature Plants*, *7*(4), Article 4. https://doi.org/10.1038/s41477-021-00889-y

Neale, M. J., Pan, J., & Keeney, S. (2005). Endonucleolytic processing of covalent protein-linked DNA double-strand breaks. *Nature*, *436*(7053), 1053–1057. https://doi.org/10.1038/nature03872

Neff, M. M., Turk, E., & Kalishman, M. (2002). Web-based primer design for single nucleotide polymorphism analysis. *Trends in Genetics*, *18*(12), 613–615. https://doi.org/10.1016/S0168-9525(02)02820-2

Osman, K., Algopishi, U., Higgins, J. D., Henderson, I. R., Edwards, K. J., Franklin, F. C. H., & Sanchez-Moran, E. (2021). Distal Bias of Meiotic Crossovers in Hexaploid Bread Wheat Reflects Spatio-Temporal Asymmetry of the Meiotic Program. *Frontiers in Plant Science*, *12*. https://doi.org/10.3389/fpls.2021.631323

Padmore, R., Cao, L., & Kleckner, N. (1991). *Temporal Comparison of Recombination and Synaptonemal Complex Formation during Meiosis in S. cerevisiae*. *66*, 1239–1256.

Pan, J., Sasaki, M., Kniewel, R., Murakami, H., Blitzblau, H. G., Tischfield, S. E., Zhu, X., Neale, M. J., Jasin, M., Socci, N. D., Hochwagen, A., & Keeney, S. (2011). A hierarchical combination of factors shapes the genome-wide topography of yeast meiotic recombination initiation. *Cell*, *144*(5), 719–731. https://doi.org/10.1016/j.cell.2011.02.009

Panizza, S., Mendoza, M. A., Berlinger, M., Huang, L., Nicolas, A., Shirahige, K., & Klein, F. (2011). Spo11-accessory proteins link double-strand break sites to the chromosome axis in early meiotic recombination. *Cell*, *146*(3), 372–383. https://doi.org/10.1016/j.cell.2011.07.003

Phillips, D., Jenkins, G., Macaulay, M., Nibau, C., Wnetrzak, J., Fallding, D., Colas, I., Oakey, H., Waugh, R., & Ramsay, L. (2015). The effect of temperature on the male and female recombination landscape of barley. *New Phytologist*, *208*(2), 421–429. https://doi.org/10.1111/nph.13548

Phillips, D., Wnetrzak, J., Nibau, C., Barakate, A., Ramsay, L., Wright, F., Higgins, J. D., Perry, R. M., & Jenkins, G. (2013). Quantitative high resolution mapping of HvMLH3 foci in barley pachytene nuclei reveals a strong distal bias. *Journal of Experimental Botany*, *64*(8), 2139–2154. https://doi.org/10.1093/jxb/ert079

Qiao, H., Rao, H. B. D. P., Yang, Y., Fong, J. H., Cloutier, J. M., Deacon, D. C., Nagel, K. E., Swartz, R. K., Strong, E., Holloway, J. K., Cohen, P. E., Schimenti, J., Ward, J., & Hunter, N. (2014). Antagonistic roles of ubiquitin ligase HEI10 and SUMO ligase RNF212 regulate meiotic recombination. *Nature Genetics*, *46*(2), 194–199. https://doi.org/10.1038/ng.2858

Rao, H. B. D. P., Qiao, H., Bhatt, S. K., Bailey, L. R. J., Tran, H. D., Bourne, S. L., Qiu, W., Deshpande, A., Sharma, A. N., Beebout, C. J., Pezza, R. J., & Hunter, N. (2017). A SUMO-ubiquitin relay recruits proteasomes to chromosome axes to regulate meiotic recombination. *Science*, *355*(6323), 403–407.

Raz, A., Dahan-Meir, T., Melamed-Bessudo, C., Leshkowitz, D., & Levy, A. A. (2021). Redistribution of Meiotic Crossovers Along Wheat Chromosomes by Virus-Induced Gene Silencing. *Frontiers in Plant Science*, *11*. https://doi.org/10.3389/fpls.2020.635139

Reynolds, A., Qiao, H., Yang, Y., Chen, J. K., Jackson, N., Biswas, K., Holloway, J. K., Baudat, F., Massy, B. D., Wang, J., Höög, C., Cohen, P. E., & Hunter, N. (2013). RNF212 is a dosage-sensitive regulator of crossing-over during mammalian meiosis. *Nature Genetics*, *45*(3), 269–278. https://doi.org/10.1038/ng.2541

Robert, T., Nore, A., Brun, C., Maffre, C., Crimi, B., Guichard, V., Bourbon, H. M., & Massy, B. D. (2016). The TopoVIB-Like protein family is required for meiotic DNA double-strand break formation. *Science*, *351*(6276), 943–949.

Rockmill, B., Voelkel-Meiman, K., & Roeder, G. S. (2006). Centromere-proximal crossovers are associated with precocious separation of sister chromatids during meiosis in Saccharomyces cerevisiae. *Genetics*, *174*(4), 1745–1754. https://doi.org/10.1534/genetics.106.058933

Rog, O., Hler, S. K., & Dernburg, A. F. (2017). The synaptonemal complex has liquid crystalline properties and spatially regulates meiotic recombination factors. *ELife*, *6*. https://doi.org/10.7554/eLife.21455.001

Rogakou, E. P., Pilch, D. R., Orr, A. H., Ivanova, V. S., & Bonner, W. M. (1998). DNA Double-stranded Breaks Induce Histone H2AX Phosphorylation on Serine 139 *. *Journal of Biological Chemistry*, *273*(10), 5858–5868. https://doi.org/10.1074/jbc.273.10.5858

Salomé, P. A., Bomblies, K., Fitz, J., Laitinen, R. A. E., Warthmann, N., Yant, L., & Weigel, D. (2012). The recombination landscape in Arabidopsis thaliana F 2 populations. *Heredity*, *108*(4), 447–455. https://doi.org/10.1038/hdy.2011.95

Sanchez-Moran, E., Santos, J. L., Jones, G. H., & Franklin, F. C. H. (2007). ASY1 mediates AtDMC1-dependent interhomolog recombination during meiosis in Arabidopsis. *Genes and Development*, *21*(17), 2220–2233. https://doi.org/10.1101/gad.439007

Séguéla-Arnaud, M., Choinard, S., Larchevêque, C., Girard, C., Froger, N., Crismani, W., & Mercier, R. (2017). RMI1 and TOP3α limit meiotic CO formation through their C-terminal domains. *Nucleic Acids Research*, *45*(4), 1860–1871. https://doi.org/10.1093/nar/gkw1210

Séguéla-Arnaud, M., Crismani, W., Larchevêque, C., Mazel, J., Froger, N., Choinard, S., Lemhemdi, A., Macaisne, N., Leene, J. V., Gevaert, K., Jaeger, G. D., Chelysheva, L., & Mercier, R. (2015). Multiple mechanisms limit meiotic crossovers: TOP3α and two BLM homologs antagonize crossovers in parallel to FANCM. *Proceedings of the National Academy of Sciences of the United States of America*, *112*(15), 4713–4718. https://doi.org/10.1073/pnas.1423107112

Serra, H., Lambing, C., Griffin, C. H., Topp, S. D., Nageswaran, D. C., Underwood, C. J., Ziolkowski, P. A., Séguéla-Arnaud, M., Fernandes, J. B., Mercier, R., & Henderson, I. R. (2018). Massive crossover elevation via combination of HEI10 and recq4a recq4b during Arabidopsis meiosis. *Proceedings of the National Academy of Sciences of the United States of America*, *115*(10). https://doi.org/10.1073/pnas.1713071115

Shen, Y., Tang, D., Wang, K., Wang, M., Huang, J., Luo, W., Luo, Q., & Hong, L. (2012). *ZIP4 in homologous chromosome synapsis and crossover formation in rice meiosis*. *4*. https://doi.org/10.1242/jcs.090993

Sidhu, G. K., Fang, C., Olson, M. A., Falque, M., Martin, O. C., & Pawlowski, W. P. (2015). Recombination patterns in maize reveal limits to crossover homeostasis. *Proceedings of the National Academy of Sciences of the United States of America*, *112*(52), 15982–15987. https://doi.org/10.1073/pnas.1514265112

Stacey, N. J., Kuromori, T., Azumi, Y., Roberts, G., Breuer, C., Wada, T., Maxwell, A., Roberts, K., & Sugimoto-Shirasu, K. (2006). Arabidopsis SPO11-2 functions with SPO11-1 in meiotic recombination. *Plant Journal*, *48*(2), 206–216. https://doi.org/10.1111/j.1365-313X.2006.02867.x

Steckenborn, S., Cuacos, M., Ayoub, M. A., Feng, C., Schubert, V., Hoffie, I., Hensel, G., Kumlehn, J., & Heckmann, S. (2023). The meiotic topoisomerase VI B subunit (MTOPVIB) is essential for meiotic DNA double-strand break formation in barley (Hordeum vulgare L.). *Plant Reproduction*, *36*(1), 1–15. https://doi.org/10.1007/s00497-022-00444-5

Storlazzi, A., Tesse, S., Ruprich-Robert, G., Gargano, S., Pöggeler, S., Kleckner, N., & Zickler, D. (2008). Coupling meiotic chromosome axis integrity to recombination. *Genes and Development*, *22*(6), 796–809. https://doi.org/10.1101/gad.459308

Storme, N. D., & Geelen, D. (2020). High temperatures alter cross-over distribution and induce male meiotic restitution in Arabidopsis thaliana. *Communications Biology*, *3*(1). https://doi.org/10.1038/s42003-020-0897-1

Strong, E. R., & Schimenti, J. C. (2010). Evidence implicating CCNB1IP1, a RING domain-containing protein required for meiotic crossing over in mice, as an E3 SUMO ligase. *Genes*, *1*(3), 440–451. https://doi.org/10.3390/genes1030440

Sung, P., & Robberson, D. L. (1995). DNA Strand Exchange Mediated by a RAD51-ssDNA Nucleoprotein Filament with Polarity Opposite to That of RecA. In *Cell* (Vol. 82, pp. 453–461).

Toby, G. G., Gherraby, W., Coleman, T. R., & Golemis, E. A. (2003). A Novel RING Finger Protein, Human Enhancer of Invasion 10, Alters Mitotic Progression through Regulation of Cyclin B Levels. *Molecular and Cellular Biology*, *23*(6), 2109–2122. https://doi.org/10.1128/mcb.23.6.2109-2122.2003

Tock, A. J., & Henderson, I. R. (2018). Hotspots for Initiation of Meiotic Recombination. *Frontiers in Genetics*, *9*. https://www.frontiersin.org/article/10.3389/fgene.2018.00521

Tock, A. J., Holland, D. M., Jiang, W., Osman, K., James D. Eugenio Sanchez-Moran, H., Edwards, K. J., Uauy, C., Ian R. Franklin, F. C. H., & Henderson. (2021). Crossover-active regions of the wheat genome are distinguished by DMC1, the chromosome axis, H3K27me3, and signatures of adaptation. *Genome Research*, *31*(9).

Underwood, C. J., Choi, K., Lambing, C., Zhao, X., Serra, H., Borges, F., Simorowski, J., Ernst, E., Jacob, Y., Henderson, I. R., & Martienssen, R. A. (2018). Epigenetic activation of meiotic recombination near Arabidopsis thaliana centromeres via loss of H3K9me2 and non-CG DNA methylation. *Genome Research*, *28*(4), 519–531. https://doi.org/10.1101/gr.227116.117

Varas, J., Sánchez-Morán, E., Copenhaver, G. P., Santos, J. L., & Pradillo, M. (2015). Analysis of the Relationships between DNA Double-Strand Breaks, Synaptonemal Complex and Crossovers Using the Atfas1-4 Mutant. *PLoS Genetics*, *11*(7), 1–29. https://doi.org/10.1371/journal.pgen.1005301

Vrielynck, N., Chambon, A., Vezon, D., Pereira, L., Chelysheva, L., Muyt, A. D., Mézard, C., Mayer, C., & Grelon, M. (2016). A DNA topoisomerase VI-like complex initiates meiotic recombination. *Science*, *351*(6276), 939–943. https://doi.org/10.1126/science.aad5196

Vujin, A., & Zetka, M. (2017). The proteasome enters the meiotic prophase fray. *BioEssays*, *39*(7), 1700038. https://doi.org/10.1002/bies.201700038

Wang, K., Tang, D., Wang, M., Lu, J., Yu, H., Liu, J., Qian, B., Gong, Z., Wang, X., Chen, J., Gu, M., & Cheng, Z. (2009). MER3 is required for normal meiotic crossover formation, but not for presynaptic alignment in rice. *Journal of Cell Science*, *122*(12), 2055–2063. https://doi.org/10.1242/jcs.049080

Wang, K., Wang, M., Tang, D., Shen, Y., Miao, C., Hu, Q., Lu, T., & Cheng, Z. (2012). The role of rice HEI10 in the formation of meiotic crossovers. *PLoS Genetics*, *8*(7). https://doi.org/10.1371/journal.pgen.1002809

Wang, M., Wang, K., Tang, D., Wei, C., Li, M., Shen, Y., Chi, Z., Gu, M., & Cheng, Z. (2010). *The Central Element Protein ZEP1 of the Synaptonemal Complex Regulates the Number of Crossovers during Meiosis in Rice*. *22*(February), 417–430. https://doi.org/10.1105/tpc.109.070789

Ward, J. O., Reinholdt, L. G., Motley, W. W., Niswander, L. M., Deacon, D. C., Griffin, L. B., Langlais, K. K., Backus, V. L., Schimenti, K. J., O'Brien, M. J., Eppig, J. J., & Schimenti, J. C. (2007). Mutation in mouse Hei10, an E3 ubiquitin ligase, disrupts meiotic crossing over. *PLoS Genetics*, *3*(8), 1550–1563. https://doi.org/10.1371/journal.pgen.0030139

Wei, X., Liu, Q., Sun, T., Jiao, X., Liu, C., Hua, Y., Chen, X., & Wang, K. (2023). Manipulation of genetic recombination by editing the transcriptional regulatory regions of a meiotic gene in hybrid rice. *Plant Communications*, *4*(2), 100474. https://doi.org/10.1016/j.xplc.2022.100474

Weisshart, K., Fuchs, J., & Schubert, V. (2016). Structured Illumination Microscopy (SIM) and Photoactivated Localization Microscopy (PALM) to Analyze the Abundance and Distribution of RNA Polymerase II Molecules on Flow-sorted Arabidopsis Nuclei. *Bio-Protocol*, *6*(3), e1725. https://doi.org/10.21769/BioProtoc.1725

Wicker, T., Schulman, A. H., Tanskanen, J., Spannagl, M., Twardziok, S., Mascher, M., Springer, N. M., Li, Q., Waugh, R., Li, C., Zhang, G., Stein, N., Mayer, K. F. X., & Gundlach, H. (2017). The repetitive landscape of the 5100 Mbp barley genome. *Mobile DNA*, *8*(1). https://doi.org/10.1186/s13100-017-0102-3

Wijeratne, A. J., Chen, C., Zhang, W., Timofejeva, L., & Ma, H. (2006). *The Arabidopsis thaliana PARTING DANCERS Gene Encoding a Novel Protein Is Required for Normal Meiotic Homologous Recombination □*. *17*(March), 1331–1343. https://doi.org/10.1091/mbc.E05

Xue, M., Wang, J., Jiang, L., Wang, M., Wolfe, S., Pawlowski, W. P., Wang, Y., & He, Y. (2018). The number of meiotic double-strand breaks influencecrossover distribution in arabidopsis[open]. *Plant Cell*, *30*(10), 2628–2638. https://doi.org/10.1105/tpc.18.00531

Xue, Z., Li, Y., Zhang, L., Shi, W., Zhang, C., Feng, M., Zhang, F., Tang, D., Yu, H., Gu, M., & Cheng, Z. (2016). OsMTOPVIB Promotes Meiotic DNA Double-Strand Break Formation in Rice. *Molecular Plant*, *9*(11), 1535–1538. https://doi.org/10.1016/j.molp.2016.07.005

Yelina, N. E., Lambing, C., Hardcastle, T. J., Zhao, X., Santos, B., & Henderson, I. R. (2015). *DNA methylation epigenetically silences crossover hot spots and controls chromosomal domains of meiotic recombination in Arabidopsis*. https://doi.org/10.1101/gad.270876

Yokoo, R., Zawadzki, K. A., Nabeshima, K., Drake, M., Arur, S., & Villeneuve, A. M. (2012). COSA-1 reveals robust homeostasis and separable licensing and reinforcement steps governing meiotic crossovers. *Cell*, *149*(1), 75–87. https://doi.org/10.1016/j.cell.2012.01.052

Zhang, C., Song, Y., Cheng, Z., Wang, Y., Zhu, J., Ma, H., Xu, L., & Yang, Z.-N. (2012). The Arabidopsis thaliana DSB formation (AtDFO) gene is required for meiotic double-strand break formation. *The Plant Journal*, *72*(2), 271–281. https://doi.org/10.1111/j.1365-313X.2012.05075.x

Zhang, J., Wang, C., Higgins, J. D., Kim, Y.-J., Moon, S., Jung, K.-H., Qu, S., & Liang, W. (2019). A Multiprotein Complex Regulates Interference-Sensitive Crossover Formation in Rice1 [OPEN]. *Plant Physiology*, *181*(1), 221–235. https://doi.org/10.1104/pp.19.00082

Zhang, L., Espagne, E., Muyt, A. D., Zickler, D., & Kleckner, N. E. (2014). Interference-mediated synaptonemal complex formation with embedded crossover designation. *Proceedings of the National Academy of Sciences of the United States of America*, *111*(47), E5059–E5068. https://doi.org/10.1073/pnas.1416411111

Zhang, P., Zhang, Y., Sun, L., Sinumporn, S., Yang, Z., Sun, B., Xuan, D., Li, Z., Yu, P., Wu, W., Wang, K., Cao, L., & Cheng, S. (2017). The Rice AAA-ATPase OsFIGNL1 Is Essential for Male Meiosis. *Frontiers in Plant Science*, *8*(September), 1–17. https://doi.org/10.3389/fpls.2017.01639

Zhu, L., Fernández-Jiménez, N., Szymanska-Lejman, M., Pelé, A., Underwood, C. J., Serra, H., Lambing, C., Dluzewska, J., Bieluszewski, T., Pradillo, M., Henderson, I. R., & Ziolkowski, P. A. (2021). Natural variation identifies SNI1, the SMC5/6 component, as a modifier of meiotic crossover in Arabidopsis. *Proceedings of the National Academy of Sciences*, *118*(33), 1–12. https://doi.org/10.1073/pnas.2021970118

Zickler, D., & Kleckner, N. (2015). Recombination, Pairing, and Synapsis of Homologs during Meiosis. *Cold Spring Harbor Laboratory Press*, 1,2. https://doi.org/10.1101/cshperspect.a016626

Ziolkowski, P. A., Underwood, C. J., Lambing, C., Martinez-Garcia, M., Lawrence, E. J., Ziolkowska, L., Griffin, C., Choi, K., Franklin, F. C. H., Martienssen, R. A., & Henderson, I. R. (2017). Natural variation and dosage of the HEI10 meiotic E3 ligase control Arabidopsis crossover recombination. *Genes and Development*, *31*(3), 306–317. https://doi.org/10.1101/gad.295501.116

11 Curriculum vitae

Name: Mohammad Abdelmordy Mohammad Ayoub

Education

Martin Luther University Halle-Wittenberg — Halle, Germany
Ph.D. candidate — (May 2017 – present)

Utrecht University — Utrecht, the Netherlands
Master of Science (MSc.) in biomedical sciences. — (Sep 2014 – Aug 2016)

Cairo University — Cairo, Egypt
Bachelor of Science (BSc.) in biotechnology. — (Sep 2007 – Jun 2011)

Professional Experience

Leibniz Institute of Plant Genetics and Crop Plant Research (IPK) Gatersleben, Germany
Advisor: Stefan Heckmann
Characterizing anti- and pro-crossover factors (RECQ4, FIGL1 and HEI10) in terms of modulating crossover landscape in barley. Null ***hei10, recq4 and figl1*** barley plants were generated. I have good experience in working with **transgenic barley & Arabidopsis** plants**.**
(May 2017 – Sep 2021)

Max-Planck-Institute of Biochemistry — Martinsried, Germany
Advisor: Wolfgang Zachariae
Worked on a research project to understand the differential regulation of centromeric cohesion protection
in meiosis I and meiosis II in yeast. (Jan 2016 – Aug 2016)

University Medical Center Utrecht — Utrecht, the Netherlands
Advisor: Geert Kops
Worked in a research project to investigate the regulation of $p31^{comet}$ and TRIP13 in spindle assembly checkpoint silencing in mammalian cells. (Oct 2014 – Dec 2015)

Leibniz Institute of Plant Genetics and Crop Plant Research (IPK) Gatersleben, Germany
Advisor: Thorsten Schnurbusch
Short internship in plant architecture research group, I worked on a map-based cloning project to identify row-type genes in barley. (Apr 2014 – Aug 2014)

Teaching Experience

Leibniz Institute of Plant Genetics and Crop Plant Research (IPK) Gatersleben, Germany
Supervised and instructed two master intern students (Giessen University) in cytological chromosome preparations and routine lab techniques including PCR, molecular cloning and sequencing. (May 2019 - Jan 2020)

Cairo University — Cairo, Egypt
Supervised and instructed students from the faculty of agriculture & faculty of vet. medicine in various courses such as genetics 101, cell biology, molecular genetics and introduction to genetic engineering. (01.2012 – 03.2014) and (09.2016 – 04.2017)

Publications

Steckenborn S., Cuacos M., **Ayoub MA.**, Feng C., Schubert V., Hoffie I., Hensel G., Kumlehn J., Heckmann S. The meiotic topoisomerase VI B subunit (MTOPVIB) is essential for meiotic DNA double-strand break formation in barley (*Hordeum vulgare* L.). *Plant Reprod.* 2023. doi:10.1007/s00497-022-00444-5

Randall RS.*, Jourdain C.*, Nowicka A.*, Kaduchová K.*, Kubová M.*, **Ayoub MA.***, Schubert V.*, Tatout C.*, Colas I.*, Kalyanikrishna, Desset S., Mermet S., Stevens A., Kubalova I., Mandáková T., Heckmann S., Lysak MA., Schubert D., Pecinka A., Baroux C. Image analysis workflows to reveal the spatial organisation of cell nuclei and chromosomes. *Nucleus* 2022. (*, co-first authorship) doi: 10.1080/19491034.2022.2144013.

Desjardins SD., Ogle DE., **Ayoub MA.**, Heckmann S., Henderson IR., Edwards KJ., Higgins JD. MutS homologue 4 and MutS homologue 5 maintain the obligate crossover in wheat despite stepwise gene loss following polyploidization. *Plant Physiol.* 2020; pp.00534.2020. doi:10.1104/pp.20.00534

Ahn YJ, Cuacos M, **Ayoub MA**, Kappermann J, Houben A, Heckmann S. In Planta Delivery of Chemical Compounds into Barley Meiocytes: EdU as Compound Example. *Methods Mol Biol.* 2020;2061:381-402. doi:10.1007/978-1-4939-9818-0_27

Youssef HM., Mascher M., **Ayoub MA.**, Stein N., Kilian B., Schnurbusch T. Natural diversity of inflorescence architecture traces cryptic domestication genes in barley (*Hordeum vulgare* L.).*Genet Resour Crop Evol* (2017) 64: 843. doi:10.1007/s10722-017-0504-6

Selected talks/ presentations (during PhD)

Ayoub MA, Steckenborn S., Lorenz J., Hartmann F., Hensel G., Kumlehn J., Schubert V., Heckmann S. Releasing the brakes and pushing the accelerator: studying anti- and pro-CO factors in barley. Invited speaker (interview) at EMBL, Heidelberg, Germany. 13.04.2022. [talk]

Ayoub MA, Steckenborn S., Lorenz J., Hartmann F., Hensel G., Kumlehn J., Schubert V., Heckmann S. The ZMM Member HEI10 Is Indispensable For Meiotic Class I Crossovers In Barley. PGSC EMBO workshop 2021, Leiden (Zoom), the Netherlands. 05-08.12.2021. [poster]

Ayoub MA, Lorenz J., Stein N., Kumlehn J., Heckmann S. HEI10 is critical for class I CO formation in barley. IPK Chromosome biology retreat, Gatersleben (Zoom), Germany. 19.11.2020. [talk]

Ayoub MA, Lorenz J., Barakate A., Waugh R., Stein N., Kumlehn J., Heckmann S. Can we manipulate the landscape of meiotic crossovers in barley? EMBO meiosis meeting, La Rochelle, France. 25-29.08.2019. [poster]

Ayoub MA, Lorenz J., Stein N., Kumlehn J., Heckmann S. Towards harnessing meiotic recombination in barley (*Hordeum vulgare*), International chromosome conference 2018, Prague, Czech Republic. 03.09.2018. [poster]

Ayoub MA, Lorenz J., Stein N., Kumlehn J., Heckmann S. Can we manipulate the meiotic recombination landscape in barley by depleting anti- and by overexpressing pro-CO factors? EMBO Plant Genome Stability and Change, IPK, Gatersleben, Germany. 05.06.2018. [poster]

Awards

Registration fees discount/travel grant for the EMBO PGSC workshop, Leiden.	(12.2021)
Travel grant (€400) to attend the ICC, Prague.	(09.2018)
Second public prize of U/SELECT presentation competition, Utrecht.	(09.2016)
Monthly stipend from MPI of Biochemistry, Martinsried.	(01-08.2016)
U/SELECT travel grant, Utrecht-Martinsried.	(01-08.2016)
Utrecht Excellence Scholarship, Utrecht.	(09.14-08.16)
Qualifying Scholarship from Misr El Kheir Foundation, Cairo.	(08.2013)
Faculty of Agriculture's award of excellence, Cairo.	(08.2011)
Cairo University's annual scholarship, Cairo.	(2009-2011)

Skills

Lab: DNA/RNA purification, (qRT-)PCR, cloning, immunostaining, microscopy, quantitative image analysis, western blot, IP and barley & Arabidopsis handling.
Coding: Basic knowledge of R and Python.

Bioinformatics: Primer design, gRNA design, CRISPR mutagenesis screening, multiple alignment and BLAST.
Software: ImageJ/Fiji, Graphpad, Adobe Illustrator and Excel.
Leadership: Supervised two master students at IPK Gatersleben and co-organized two departmental days and the plant science student conference 2018 at the IPK Gatersleben.

Courses (During PhD)

Biology meets programming: Introduction to Python.	Gatersleben	06.2022
3D Image Processing Training School.	Zurich/Zoom	12.2020
How to generate a paper? By Prof. Ingo Schubert.	Gatersleben.	10.2020
ImageJ/Fiji: Basics and advanced practices.	Halle	09.2019
Academic Writing.	Gatersleben	12.2018
Basic Bioinformatics training for Biologists.	Gatersleben	09.2017
Flow cytometric genome size estimation, sorting and high-throughput ploidy analysis.	Gatersleben	08.2017

References

Dr. Stefan Heckmann
Group leader of the Meiosis lab,
IPK Gatersleben,
Gatersleben 06466, Germany.
+49 (0)39482 608
heckmann@ipk-gatersleben.de

Prof. Dr. Andreas Houben
Group leader of the CSF lab,
IPK Gatersleben,
Gatersleben 06466, Germany.
+49 (0)39482 5486
houben@ipk-gatersleben.de

Prof. Dr. Geert Kops
Group leader of the chromosome segregation lab, Hubrecht Institute,
Utrecht 3584 CT, Utrecht, the Netherlands
+31 (0)30251 06464
g.kops@hubrecht.eu

12 Eidesstattliche Erklärung / Declaration under Oath

Ich erkläre an Eides statt, dass ich die Arbeit selbstständig und ohne fremde Hilfe verfasst, keine anderen als die von mir angegebenen Quellen und Hilfsmittel benutzt und die den benutzten Werken wörtlich oder inhaltlich entnommenen Stellen als solche kenntlich gemacht habe.

I declare under penalty of perjury that this thesis is my own work entirely and has been written without any help from other people. I used only the sources mentioned and included all the citations correctly both in word or content.

_____ _____

Datum / Date Unterschrift des Antragstellers / Signature of the applicant

13 Appendix

Supplementary table 1: gRNA sequences in *HvHEI10*, *HvRECQ4* and *HvFIGL1*

Name	Sequence	Targeted gene
gRNA1	AAACTTGACAAGGGATAAGC	*HvHEI10*
gRNA2	GCTGAGAAACGAGTATGAGT	
gRNA3	ATGCCTAACATATTGGACAG	
gRNA1	GGATGATGACGAGATTCTGG	*HvRECQ4*
gRNA2	GTTTTGATGCCAACTGGTGG	
gRNA1	ATTATGGTGTGAGGCCAAGC	*HvFIGL1*
gRNA2	ATTGCGTCCAGACATCTTTC	

Supplementary table 2: Primers used in this thesis

Name	Sequence	Annealing temp. [°C] / extension time / amplicon size (bp)	Purpose
SH-21	5'-ATGAAGTGCAACGCTTGCTGG-3'	63 / 40 sec / ~910	Amplifying and sequencing *HvHEI10* CDS
SH-24	5'-CTATAACGTGAACATTTGTGGACG-3'		
Bie475	5'-TTTAGCCCTGCCTTCATACG-3'	55 / 45 sec / ~700	Genotyping positive transformants of *hei10*
GH-zCas9-R1	5'-TTAATCATGTGGGCCAGAGC-3'		
35S F2 Catrin	5'-CATGGTGGAGCACGACACTCTC-3'	55 / 80 sec / ~900 + ~1200	Genotyping for both 35S promoter and *Hygromycin R* gene
GH-HYG-R5	5'-GATTCCTTGCGGTCCGAATG-3'		
pJET1.2-fwd	5'-CGACTCACTATAGGGAGAGCGGC-3'	65 / proper extension time* /	Sequencing insertions in pJET1.2 vector to confirm cloning
pJET1.2-rev	5'-AAGAACATCGATTTTCCATGGCAG-3'		
M13_fwd	5'-TGTAAAACGACGGCCAGT-3'	58 / proper extension time* /	Sequencing insertions in p35SBAM vector
M13_rev	5'-CAGGAAACAGCTATGACC-3'		
MA-285	5'-CGGACAAAAGGACCTGGAGA-3'	64 / 1 min / ~760	Amplifying and sequencing gRNA-flanking region in *HvHEI10*. Also used to amplify flanking region of BCC54 of *HvHEI10*
MA-284	5'-CGCAGCGTTGAGAGAGAGA-3'		
MA-428	5'-AAGAGCGCATACAGAAGTGT-3'	55 / 30 sec / ~400	Common forward primer
MA-427	5'-CTGAACGTTTCACCGACTC-3'		*HvHEI10-1*-specific reverse primer
MA-426	5-CTGAACGTTTCACCGACTTC-3'		*Hvhei10-1* specific reverse primer
MA-431	5'-CGGACAAAAGGACCTGGAGATGC-3'	67 / 20 sec / ~460	Common forward primer
MA-429	5'-AGTGGGTCACCGCTGTCCA-3'		*HvHEI10-2*-specific reverse primer
MA-430	5'-AGTGGGTCACCGCTGCA-3'		*Hvhei10-2* specific reverse primer
MA-58	5'-GGTAGGTGCTTCCATCCCATA-3'	59 / 90 sec / ~1360	Searching for a SNP within *HvRECQ4* area one
MA-57	5'-CCACTTGGTCAGTAGCATCA-3'		
MA-365	5'-CCAGTGTATCGCTTTGCTGA-3'	61 / 80 sec / ~1870	Together with MA-57, amplifying and sequencing gRNA target positions within *HvRECQ4*
MA-94	5'-TTTGAACTACTGACCCGCCT-3'	57 / 90 sec / ~1040	Searching for a SNP within *HvRECQ4* area two
MA-95	5'-AGAACTTGAACATGGCTGCC-3'		
MA-142	5'-TTGTTTGGTGGGTGCCTCTT-3'	59 / 90 sec / ~1300	Searching for a SNP within *HvFIGL1* area one, and for sequencing gRNA target positions
MA-143	5'-TTGCTCGTGAGTGAACTTGC-3'		
MA-102	5'-ACTAACCATGGACAGAGGGG-3'	59 / 90 sec / ~1360	Searching for a SNP within *HvFIGL1* area two
MA-103	5'-CGCACATCCTCCTTGTTGAG-3'		
MA-449	5'-CTGGTCCATTTGAGCTCTCTG-3'	64 / 60 sec / ~160	Measuring *HEI10* expression by qRT-PCR
MA-450	5'-CTGAGGACGCTTCACTGG-3'		
MA-463	5'-TCCGGTTGATGCTGAGGAAA-3'	64 / 60 sec / ~90	Measuring *DMC1* expression by qRT-PCR
MA-464	5'-AAAACAGCTTCTCCCTCGGG-3'		

MA-341	5’-aataGGATCCTAGGACCGCCAAGTGTATTT-3’	61 / 2 min 40 sec / ~3960	Amplifying *HvHEI10* promoter
MA-372	5’-ataaGTCGACAAGCGTTGCACTTCATTTTG-3’		
MA-373	5’-ataaGTCGACAGTTTGAAGAGCCGAGGAG-3’	59 / 50 sec / ~1150	Amplifying *HvHEI10* terminator part one
MA-381	5’-TTTGGAGAAGAATACGTCATC-3’		
MA-382	5’-TGCCATCAACCTACACTGACA-3’	64 / 30 sec / ~800	Amplifying *HvHEI10* terminator part two
MA-393	5’-aataCCATGGCCACCCTTGAATCAGAACCG-3’		
MA-334	5’-AGCGAGAGCCTGACCTATT-3’	57 / 10 sec / 160	Amplifying *hygromycin R* gene
MA-335	5’-GTCCGAATGGGCCGAAC-3’		
SH-183	5’-TATCTGGCCATGGCGGCCCTTCCTGCTGCTACTCCCATC-3’	61°C for 10 initial cycles, followed by 72°C for 28 cycles / 4 min / ~6300	Amplifying *AtHEI10* to enable cloning in p35sBAM vector via an overlap PCR
SH-184	5’-GCAATGGCCCTTAAGGCCGATGATGAACTTCGCCACCG-3’		
MA-277	5’-GTCACACTAACTGAAGAAGGCA-3’	64 / 40 sec / ~980	Amplifying flanking region of SNP in accessions HID80, HID101, and FT272 of *HvHEI10*.
MA-278	5’-CCAGCAGCAGACCAACTTTT-3’		
MA-289	5’-CGCACTCGTCCCAATACTTT-3’	64 / 40 sec / ~960	Amplifying flanking region of SNP in accessions FT507 of *HvHEI10*
MA-290	5’-AACCTTTCGTGTGACAACCA-3’		
MA-225	5’-CCATTCGTATCATAAAACTGCGATC-3’	54 / 20 sec / ~190	dCAPS primers to genotype *recq4-1*
MA-227	5’-TGCAGTGCACATCTAAATAA-3’		
MA-204	5’-AGTCAGATGGTGAACATGACTCGA-3’	54 / 20 sec / ~190	dCAPS primers to genotype *figl1-2*
MA-205	5’-TAGAGACTTTGTTGGTGCC-3’		
MA-206	5’-CAATGGTGGAGCTTACCAACAC-3’	54 / 20 sec / ~260	dCAPS primers to genotype *figl1-3*
MA-207	5’-GCCTGCGTGCTGCTTCATCGAATT-3’		
MA-437	5’-TGGATGATGACGAGATTCTGG-3’	57 / 30 sec / ~510	To genotype *RECQ4-2*
MA-438	5’-TTGAGGACTGAGTTCCCCA-3’		
MA-440	5’-TGGATGATGACGAGATTCGC-3’	53 / 30 sec / ~500	To genotype *recq4-2*
MA-441	5’-ACCATCAAGAAGTTTATTGG-3’		
MA-448	5’-TTGCGGAATTTGGAACCTC-3’	59 / 20 sec / ~240	To genotype *FIGL1-4*
MA-445	5’-CACGAAAGATGTCTGGACGCA-3’		
MA-447	5’-CACGAAAGATGTCTGGACAA-3’	57 / 20 sec / ~240	To genotype *figl1-4* (together with MA-448)
MA-427	5’-CTGAACGTTTCACCGACTC-3’	55 / 30 sec / ~400	To genotype *HEI10-1* (MA-427 & MA-428) or *hei10-1* (MA426 & MA-428)
MA-428	5’-AAGAGCGCATACAGAAGTGT-3’		
MA-426	5’-CTGAACGTTTCACCGACTTC-3’		
MA-429	5’-AGTGGGTCACCGCTGTCCA-3’	67 / 20 sec / ~450	To genotype *HEI10-2* (MA-429 & MA-431) or *hei10-2* (MA430 & MA-431)
MA-431	5’-CGGACAAAAGGACCTGGAGATGC-3’		
MA-430	5’-AGTGGGTCACCGCTGCA-3’		
SA_1H_F	5’-AGGGCCGTCCAAAAGAAA-3’	60 / 1 min / 547 (Barke) or 512 (GP)	To genotype hyrbid mutants in *HvRECQ4* or *HvFIGL1* on chromosome 1H
SA_1H_R	5’-ATGTGGGATGGGGAGAGAG-3’		
SA_3H_F	5’-CCCGAGGTAGCCCTCCAC-3’	60 / 1 min / 416 (Barke) or 565 (GP)	To genotype hyrbid mutants in *HvRECQ4* or *HvFIGL1* on chromosome 3H
SA_3H_R	5’-CATAGAGATGTTTCGGTCCTGT-3’		
IK-70	5’-GCTCACATGTTCTTTCCTGCG-3’	60 / 30 sec / ~750	To check sequence of cloned expression units of gRNAs targeting either *HvHEI10*, H*vRECQ4* or *HvFIGL1*.
IK-71	5’- CACCTGACGTCTAAGAAACC-3’		

* Extension times were calculated 40 sec / 1 kb.

Supplementary table 3: Vectors used in this thesis

Plasmid name	Backbone	Insert	Selective marker (host)
pJET1.2-HvHEI10_promoter	pJET1.2	Promoter of *HvHEI10*	Ampicillin (bacteria)
pNOS-HEI10_promoter	pNOS	Promoter of *HvHEI10*	Ampicillin (bacteria)
pJET1.2-HvHEI10_terminator	pJET1.2	Terminator of *HvHEI10*	Ampicillin (bacteria)

pNOS-HvHEI10_terminator	pNOS	Terminator of *HvHEI10*	Ampicillin (bacteria)
pNOS-HvHEI10_P_T	pNOS-HEI10_promoter	Terminator of *HvHEI10*	Ampicillin (bacteria)
p6i-2x35S-TE9_HvHEI10_P_T	p6i-2x35S-TE9	Promoter and terminator of HvHEI10	Hygromycin (plant), spectinomycin (bacteria)
p6i-2x35S-TE9_HvHEI10	p6i-2x35S-TE9_HvHEI10_P_T	*HvHEI10* open reading frame	Hygromycin (plant), spectinomycin (bacteria)
pJET1.2-HvHEI10-CDS	pJET1.2	*HvHEI10-CDS*	Ampicillin (bacteria)
pJET1.2-RECQ4	pJET1.2	RECQ4	Ampicillin (bacteria)
pGH565-1	pIK5	gRNA1 *HEI10*	Ampicillin (bacteria)
pGH567-2	pIK6	gRNA2 *HEI10*	Ampicillin (bacteria)
pGH568-1	pIK7	gRNA3 *HEI10*	Ampicillin (bacteria)
pGH578	pIK19	gRNA1-3 *HEI10*	spectinomycin (bacteria)
pGH589	pIK84	gRNA1-3 *HEI10*	Ampicillin (bacteria)
pGH619-2	p6i-2x35S-TE9	gRNA1-3 *HEI10*	Hygromycin (plant), spectinomycin (bacteria)
pGH569-2	pIK5	gRNA1 *RECQ4*	Ampicillin (bacteria)
pGH570-1	pIK6	gRNA2 *RECQ4*	Ampicillin (bacteria)
pGH579	pIK60	gRNA1-2 *RECQ4*	spectinomycin (bacteria)
pGH585	pIK84	gRNA1-2 *RECQ4*	Ampicillin (bacteria)
pGH616-2	p6i-2x35S-TE9	gRNA1-2 *RECQ4*	Hygromycin (plant), spectinomycin (bacteria)
pGH571-2	pIK7	gRNA1 *FIGL1*	Ampicillin (bacteria)
pGH576-8	pIK8	gRNA2 *FIGL1*	Ampicillin (bacteria)
pGH581	pIK19	gRNA1-2 *RECQ4* + gRNA1-2 *FIGL1*	spectinomycin (bacteria)
pGH594	pIK84	gRNA1-2 *RECQ4* + gRNA1-2 *FIGL1*	Ampicillin (bacteria)
pGH622-1	p6i-2x35S-TE9	gRNA1-2 FIGL1 + gRNA1-2 RECQ4	Hygromycin (plant), spectinomycin (bacteria)

Supplementary table 4: Antibiotics used in this thesis

Antibiotic name	Final concentration
Ampicillin	100 µg/mL
Hygromycin	100 mg/L
Spectinomycin	100 µg/mL
PPT	30 µg/mL
Rifampicin	100 µg/mL
Gentamicin	50 µg/mL